Spray Drying of Soybean Oleosomes

vorgelegt von

Dipl.-Ing.

Sania Maurer

geb. in Berlin

von der Fakultät III - Prozesswissenschaften der

Technischen Universität Berlin

zur Erlangung des akademischen Grades

Doktor der Ingenieurwissenschaften

- Dr.-Ing. -

genehmigte Dissertation

Promotionsausschuss:	
Vorsitzende der Prüfungskomission:	Prof. Dr.-Ing. Cornelia Rauh
Erstgutachter:	Prof. Dr. Dipl.-Ing. Dietrich Knorr
Zweitgutachter:	Prof. Dr. Thomas A. Vilgis
Tag der wissenschaftlichen Aussprache:	24.06.2014

Berlin, 2014

TO MY BROTHERS

Abstract

The continuous growth of the global market for functional foods has significantly increased the demand for new materials and products. The food industry discovered oleosomes as beneficial as pre-emulsified additives or carriers of bioactive ingredients. Plant seeds are rich in oleosomes, which are small subcellular oil droplets expressed during seed development and maturation. Within seeds, they exist as pre-emulsified oil high in unsaturated fatty acids, stabilised by a monolayer of phospholipids and proteins, called oleosins. Oleosins are anchored into the oil core with a hydrophobic domain, while the hydrophilic domains remain on the oleosome surface. The oleosins play a major role in the stability and function of oleosomes. To preserve the nutritional value of the oil and the function of oleosomes, spray drying is a promising technique. Soybean oleosomes have been spray dried for the first time. For the microencapsulation of oleosomes, maltodextrin was used. To achieve a high oil encapsulation efficiency, optimal process parameters needed to be established. Prior to spray drying, stability tests were performed to evaluate the applicability of oleosomes for spray drying. In addition, the importance of the oleosins for the physicochemical properties and stability of oleosomes was investigated. The application of enzymatic digestion and various characterisation techniques made it possible to correlate molecular changes of the oleosin structure with changing macroscopic properties of oleosomes. The results helped to better understand mechanisms of drying behind powder formation and the associated powder properties. Studies on the stability of oleosomes revealed that they are stable to temperatures up to 100 °C but only to a limited extent to shear stresses. After enzymatic digestion, oleosins lost their ability to stabilise oil-water and air-water interfaces and the macroscopic properties of oleosomes have changed. Measurements revealed that oleosomes rupture at the air-water interface and spread their constituents on the surface layer. This effect, as well as the low load of encapsulating agents in oleosomes might have lead to the poor spray drying efficiency of pure oleosome emulsions,

resulting in excessive amounts of free oil. With the addition of maltodextrin, the oil encapsulation efficiency was significantly improved.

Kurzfassung

Mit stetigem Wachstum des Weltmarktes für funktionale Lebensmittel, ist auch die Nachfrage nach neuen Materialien und Produkten gestiegen. In der Lebensmittelindustrie wurden Oleosome bereits als vorteilhaft als voremulgierte Zusatzstoffe oder Träger von bioaktiven Inhaltsstoffen entdeckt. Pflanzensamen sind reich an Oleosomen, die als kleine subzellulare Öltröpfchen während der Keimung entstehen. Innerhalb der Samen liegen sie als voremulgiertes Öl vor, das reich an ungesättigten Fettsäuren und von einer Monoschicht aus Phospholipiden und Proteinen, dem Oleosin, umschlossen ist. Die Oleosine sind mit einer hydrophoben Peptidsequenz in dem Ölkern verankert, während die hydrophilen Sequenzen an der Oberfläche der Oleosome bleiben. Das Oleosin spielt eine entscheidende Rolle für die Stabilität und Funktion der Oleosome. Um die Nährwerte des Öls und die Funktion der Oleosome zu bewahren, ist Sprühtrocknung eine vielversprechende Technik. Oleosome aus Sojabohnen wurden in dieser Arbeit zum ersten Mal sprühgetrocknet. Für die Mikroverkapselung der Oleosome wurde Maltodextrin verwendet. Um eine hohe Effizienz der Ölverkapselung zu erreichen, mussten optimale Prozessparameter gefunden werden. Vor der Sprühtrocknung wurden Stabilitätstests durchgeführt, um die Sprühfähigkeit der Oleosome feststellen zu können. Zusätzlich wurde die Relevanz des Oleosins für die physikochemischen Eigenschaften und die Stabilität der Oleosome untersucht. Die Anwendung enzymatischer Verdauung und zahlreicher Charakterisierungsmethodiken ermöglichten es, die molekularen Veränderungen der Oleosinstruktur mit den veränderten makroskopischen Eigenschaften der Oleosome in Verbindung zu setzen. Die Erkenntnisse aus den Messungen lieferten eine Verbesserung des Verständnisses der Mechanismen, die hinter der Pulverentstehung und den damit verbundenen Pulvereigenschaften stehen. Versuchsreihen zeigten, dass Oleosome bis 100 °C temperaturstabil, aber nur begrenzt scherstabil sind. Die enzymatische Verdauung zerstörte die Fähigkeit des Oleosins, Öl-Wasser- und Luft-Wasser-Grenzflächen zu stabilisieren und veränderte die Eigenschaften der Oleosome.

Messungen zeigten, dass Oleosome an der Luft-Wasser-Grenzfläche aufplatzen und sich ihr Inhalt auf der Oberfläche verteilt. Sowohl dieser Effekt, als auch die geringe Menge an Verkapselungsstoffen in den Oleosomen, könnten zu der niedrigen Ausbeute bei der Sprühtrocknung von reinen Oleosom-Emulsionen und damit großen Mengen an freiem Öl geführt haben. Mit der Zugabe von Maltodextrin konnte die Verkapselungseffizienz wesentlich verbessert werden.

Acknowledgements

First of all, I would like to express my special appreciation and thanks to my supervisor Professor Dr. Thomas Vilgis from the Max Planck Institute for Polymer Research (MPIP) for encouraging my research. His expertise and understanding added considerably to my graduate experience and he inspired me to look on foods from another perspective. Special thanks go to Professor Dr. Kurt Kremer who allowed for doing my research within his department of Polymer Theory at the MPIP. Many thanks to Professor Dr. Dipl.-Ing. Dietrich Knorr from the Technical University of Berlin for his encouragement, supervision and support in the progress of this project. I want to also thank the other member of my committee, Professor Dr.-Ing. Cornelia Rauh for taking over the chair of my defense.

Generous support from Dr. Birgitta Zielbauer, whose insightful comments and suggestions helped me enormously. I am also grateful for her provided assistance in acquiring the CLSM and SEM micrographs. Special thanks to Dr. Gustav Waschatko, for his valuable advice and support.

The application of diverse experimental techniques in this research project would not have been possible with the generous support of

- Prof. Dr. Tobias Reich from the Johannes Gutenberg University Mainz, who gave me the opportunity to do ESCA measurements and his research assistant Dipl.-Ing. Jakob Drebert, who conducted the experiments

- Dr. Andrew Jackson from the European Spallation Source ESS AB, who supervised the SANS measurements and was a great support in the data analysis

- Prof. Dr. Stephan Drusch from the Technical University of Berlin, who provided the pendant drop tensiometer for the surface tension measurements and Frederic Tamm, who gave me valuable advices for the measurements

- Prof. Dr.-Ing. Heike P. Schuchmann from the Karlsruhe Institute of Technology (KIT), who allowed me to use the laser diffractometer Horiba LA-950 for the particle size measurements and Dipl.-Ing. Philipp Stähle, who was always supportive

- Dr. Kaloian Koynov from the department of Physics at Interfaces at the MPIP, who provided the confocal laser scanning microscope

I would like to offer my special thanks to all of them.

Advices and comments given by Dr. Denise Schach, Dr. Michael Schleeger and Walter Scholdei have been a great help in the FTIR measurements. I would like to also thank Dr. Tobias Weidner for his advice regarding the ESCA spectra analysis. Many thanks to Dr. Ann Junghans from the Lujan Neutron Scattering Center for the fruitfull discussions about the SANS data analysis.

I am particularly grateful for the assistance in the preparation of the experiments given by Marta Ghebremedhin, Sarah Gindra and Edyta Bobra. A special thanks goes out to Natalie Russ, Steffen Beccard and all the other (former) Food Group members for their support and pleasant working atmosphere.

A very special thank to my family. Words cannot express how grateful I am to my mother and father for all of the sacrifices that they have made on my behalf.

At the end I would like to express my appreciation to my beloved husband and best friend Karsten, who was always there when I needed him. Thank you for your warmth, patience and love.

Contents

List of Figures

List of Tables

Nomenclature

Elemental Formula

D_2O deuterated water

NaN_3 sodium acid

Na_2CO_3 sodium carbonate

NH_4Cl ammonium chloride

NaCl sodium chloride

NaOH sodium hydroxide

Abbreviations

AA amino acid

ADSA axisymmetrical drop shape analysis

BP band pass

CAS-number chemical abstracts service-number

CD circular dichroism

cDNA complementary deoxyribonulceic acid

CLSM confocal laser scanning microscopy

DE dextrose equivalent

DLS dynamic light scattering

DMSO dimethylsulfoxid

DNA deoxyribonucleic acid

ESCA elemental spectroscopy for chemical analysis

FFA free fatty acid

FITC fluorescin isothiocyanate

FSD Fourier self-deconvolution

FTIR Fourier-transform infrared

FWHM full width at half maximum

LDA laser doppler anemometry

LDL low density lipoprotein

LP long pass

MD maltodextrin

MES 2-(N-Morpholino)-ethansulfonsäure

MWCO molecular weight cut-off

pI isoelectric point

PIDS polarisation intensity differential scattering

PL phospholipid

PSD particle size distribution

PUFA poly-unsaturated fatty acids

SANS small angle neutron scattering

SAXS small angle X-ray scattering

SDS-PAGE sodium dodecyl sulfate polyacrylamide gel electrophoresis

SEM scanning electron microscopy

SFG sum frequency generation

SLS static light scattering

SNR signal-to-noise ratio

TAG triacylglyceride

Tris tris(hydroxymethyl)-aminomethan

XPS X-ray photoelectron spectroscopy

Greek Symbols

α constant involving nozzle design parameters

β constant involving liquid properties

ϵ dielectric constant

η shear viscosity ..... [Pa·s]

λ inelastic mean free path (ESCA) ..... [nm]

λ wavelength

λ_{em} emission wavelength ..... [nm]

λ_{ex} excitation wavelength ..... [nm]

λ_e latent heat of evaporation ..... [kJ/kg]

μ_a dynamic viscosity of the air ..... [kg/sm]

Φ instrumental work function

π surface pressure ..... [mN/m]

ψ power ..... [$kg \cdot m^2/s^3$]

ρ scattering length density

ρ_{air} density of air ..... [kg/m^3]

σ cross section

σ surface tension ..... [mN/m]

σ_0 surface tension of water ..... [mN/m]

Θ take-off angle ..... [°]

θ scattering angle ..... [°]

$\tilde{\nu}$ wavenumber ..... [cm^{-1}]

ζ zeta-potential

Roman Symbols

ΔT_{LMTD} log mean temperature difference ..... [K]

$\dot{m}_{\mathrm{air}}$ mass flow rate of air ..... [kg/s]

$\dot{m}_{\mathrm{liq}}$ mass flow rate of liquid ..... [kg/s]

$\frac{\mathrm{d}X}{\mathrm{d}t}$ average rate of moisture removal ..... [kg/s]

$\mathrm{K_c}$ cut-off coefficient factor

$\vec{k}$ wavevector

$\vec{q}$ scattering vector

$\vec{x}$ trajectory of neutron

A absorbance

b scattering length

D droplet diameter ..... [μm]

D(v, 0.1) volume mean diameter where 10 % of the distribution is below this diameter ..... [μm]

D(v, 0.5) volume mean diameter where 50 % of the distribution is below or above of this diameter ..... [μm]

D(v, 0.5) volume mean diameter where 90 % of the distribution is below of this diameter ..... [μm]

D[3,2] equivalent surface area mean diameter ..... [μm]

D[4,3] equivalent volume weighted mean diameter ..... [μm]

d_{50} cut-off point

E_{b} binding energy ..... [eV]

E_{K} kinetic energy ..... [eV]

I_0 intensity of emitted electrons ..... [CPS]

k_{d} thermal conductivity of drying gas ..... [$\mathrm{W/(m \cdot K)}$]

N number of molecules/unit volume

n complex refractive index

n_i	imaginary part or attenuation coefficient	
n_r	real refractive index	
Q	volume flow rate through the cyclone	[L/h]
Q_3	cumulative volume distribution	[vol%]
q_3	volume frequency distribution	[%/μm]
T_in	inlet temperature	[°C]
t_c	average drying time	[s]
V	molecular volume	
v_in	cyclone inlet velocity	[m/s]
v_rel	relative velocity between air and liquid mass flow	[m/s]
z	distance	[nm]
Z_0	outer vortex length	[m]
E	electric field	[V/m]

1. Introduction

Over the last two decades, the demand for functional food that provides health benefits over standard nutrition has significantly increased. The global market for functional foods is still continuously growing, promoting significant research in the development of processes, new materials and products that can deal with the increasing demands of today. Since most of the ingredients used in the production of functional foods such as vitamins, probiotics, fats and flavours, are prone to degradation, the food industry utilises microencapsulation technologies to embed sensitive components into a protective matrix, isolating them from their surrounding environment.[157] Thereby, undesirable interactions with, *e.g.* temperature, oxygen, mechanical stress and other food components can be avoided and changes in sensory properties or general appearance induced by chemical reactions be reduced. In food processing, there exists several methods for microencapsulation. One of the most widely adopted ones is spray drying. Spray drying involves the conversion of liquids into powders and is in comparison to the most other drying techniques more appropriate for the drying of heat sensitive components.[67, 66]

A prominent example for the microencapsulation of a sensitive food ingredient using spray drying is the encapsulation of fat and oil, containing high amounts of polyunsaturated fatty acids.[7, 25, 49, 51, 89] The main purpose of fat and oil encapsulation is to achieve a preferably high encapsulation efficiency in order to avoid contact with the ambient oxygen and thus to prevent fat oxidation. Proteins such as milk and soy proteins [66, 90, 185] are preferentially used as oil encapsulant due to their excellent emulsifying and film-forming properties and good solubility in water. The highest oil encapsulation efficiencies were obtained in combination with carbohydrates, compared to when only protein was used.[48, 157] However, fat oxidation can occur as soon as the oil is extracted from its natural protective environment, the plant seed. Thus, the best protection of fat and oil against oxidation is achieved when avoiding contact to oxygen well in advance, that

is when still being embedded in its natural environment.

The seeds of oleaginous plants contain naturally pre-emulsified oil provided in oil bodies, also referred to as oleosomes. Oleosomes are small subcellular organelles that serve as energy source for plant growth and metabolism. By partitioning neutral lipids, mainly triacylglycerides, into lipid droplets, the lipids and thus the plant's energy source are preserved. These droplets are stabilised by a phospholipid monolayer and an integral protein, called oleosin. The oleosins play a major role in the oleosome stability and exhibit a unique structure. They are anchored into the oil matrix with their hydrophobic domains, while their hydrophilic domains completely cover the oleosome surface.[81, 181] Thus, by extracting the oleosomes from seeds, a naturally protein-stabilised oil-in-water emulsion is obtained, which exhibits a relatively good oxidative stability.[98] However, the oxidative stability decreases with increasing storage time [98] and the oleosome emulsion is prone to microbial spoilage due to the high water content. Therefore, microencapsulation is an appropriate technique to improve the long term stability of oleosomes. Moreover, oleosomes can be used as capsules for lipid-soluble food ingredients, thus providing a new promising functional ingredient.

The aim of this thesis was to investigate the impact of spray drying on the oleosome's integrity, meaning physicochemical properties and stability. Maintaining the original structure of the oleosomes upon spray drying is a pre-requisite to obtain a high oil encapsulation efficiency. Thus, the main objective of this work was to establish a spray drying method yielding well encapsulated and intact oleosomes. The oleosomes used for spray drying were extracted from soybean seeds. Soybeans are an important agricultural commodity and its global annual production and consumption in 2013 were about 260 million tons, which is more than for wheat.[9] This shows that oleosomes can be economically produced from an easy accessible and widely available source. However, in order to design rational structure-based oleosome products and to understand the mechanisms behind powder formation and microencapsulation, a detailed knowledge about the link between micro- and macroscopic properties of oleosomes based on their molecular structure is required.

Therefore, the role of the oleosin for the stability and function of oleosomes was investigated by means of biophysical and spectroscopic methods. The results have been published under the title "The Role of Intact Oleosin for Stabiliszation and Function of Oleosomes" in *The Journal of Physical Chem-*

istry B in 2013. Therefore, the content of this paper is reproduced in the first part of **Chapter 6** in brief, with special emphasis on the particle size and ζ-potential measurements, as well as the drop shape analysis. Particle size and ζ-potential measurements allow to evaluate the stability of the oleosome emulsion, which is crucial for the oil encapsulation efficiency.[40, 89] Stability tests were performed by changing the emulsion's pH-value and by analysing the impact of heat and shear stress on the integrity of the oleosomes. The two latter are typical stress factors that occur during spray drying. By means of drop shape analysis, information about the interfacial behaviour of oleosomes at the air-water interface were gathered. Their adsorption kinetics and the composition of oleosome constituents determine the formation of the surface composition of the final powder upon spray drying.[51]

Spray drying of soybean oleosomes was done for the first time. Therefore, **Chapter 7** starts with the evaluation of the appropriate process parameters and their impact on the macroscopic properties of oleosome powders. In order to improve oil encapsulation efficiency, maltodextrin was introduced as encapsulating agent. Powder morphology and composition of characteristic powder samples of non-encapsulated oleosomes and oleosomes encapsulated with maltodextrin spray dried at different temperatures were analysed by scanning electron microscopy and confocal laser scanning microscopy. Electron spectroscopy for chemical analysis was used to quantify the chemical composition of the powder surface and thus to determine the oil encapsulation efficiency. This gained knowledge is helpful in order to better understand the mechanisms behind powder formation.

The powder samples were redispersed and their particle size distribution and ζ-potential were compared to those of crude oleosome emulsions. Whether these properties are conserved is an indicator for the oil encapsulation efficiency and stability of oleosomes during spray drying. Since the oleosin is crucial for the function and stability of the oleosomes, Fourier-transform infrared spectroscopy was applied to investigate the impact of spray drying on the secondary structure of the oleosin.

In **Chapter 8**, different methods for the determination of the average particle size of soybean oleosomes are briefly discussed. Since the optical parameters of oleosomes are not yet known and difficult to determine, particle size measurements using light scattering involves some experimental uncertainties. Therefore, nuclear magnetic resonance and small angle neutron scattering measurements were also performed in order to obtain more

precise information about the average diameter of oleosomes. Small angle neutron scattering measurements allow also to determine the structure of oleosomes in a non-invasively and non-destructively manner. However, it was not possible within the time frame of this study to acquire a reasonable amount of measurements to gather a comprehensive picture about the oleosome size and structure. Thus, **Chapter 9** contains a brief overview of the first small angle neutron scattering measurements and an outlook about future work.

To begin with, a brief overview about the current research of oleosomes (**Chapter 2**) is given followed by an explanation about the general principle of spray drying and the relevance of microencapsulation in food processing (**Chapter 3**). Subsequently, some analytical methods used for the oleosome and powder characterisation are presented with emphasis on the particle sizing method based on light scattering and Fourier-transform infrared spectroscopy (**Chapter 4**). Materials and methodologies are explained in **Chapter 5**.

2. Soybean oleosomes

Oleaginous plants require a high energy input for germination, seedling establishment and biosynthesis. For their energy supply, neutral lipids are accumulated in plant tissue cells in form of subcellular, micellar-like organelles, also referred to as **oleosomes** or oil bodies. Some unique integral proteins and phospholipids (PL), which form an intermediate monolayer between protein and lipid matrix, encapsulate the oleosomes. Proteins and PL serve as surfactants thus emulsifying the abundant hydrophobic lipids, mainly triacylglycerides (TAG) and sterol esters into small hydrophilic oil droplets, exhibiting sizes in the nano or micron range.[60] DNA cloning tests revealed one major integral protein, the oleosin, which is unique to oleosomes and only found in plant species so far.[81]

Oleosins are supposed to play a major role in the oleosome stabilisation, as well as in mobilisation and degradation of oleosomes during active plant metabolism. Their amphiphilic N- and C-terminal domains anchored by a hydrophobic domain in the oil matrix completely cover the oleosome surface. Thereby, oleosins partition water-insoluble TAG into spherical individual entities with a high surface-to-volume ratio, prevent thus droplets from coalescence and act as lipase receptor during TAG hydrolysis. Partitioning of TAG into highly stable oil droplets helps plants to withstand periods of drought, coldness, rehydration and heating for months or years before the stored oleosomes are mobilised and degraded for the plant growth.[82, 60, 151]

The size of oleosomes varies from 0.2 to 2 µm, depending on the oleosin to oil ratio that is mainly influenced by synthesis of oleosin in the respective plant species, as well as by environmental and nutritional conditions.[166, 177, 181] Tzen (1993) correlated the analysis of the oleosome constituents with the size determination of oleosomes and reported that the amount of oleosin decreases with increasing oleosome size. Oleosomes of sesame seeds, for example, possess 0.57 % protein and 97.37 % oil at an average size of 2 µm, while rape seed oleosomes are composed of 3.46 % pro-

tein and 94.21 % oil at a size of 0.65 µm. The oleosome size modulation by the oleosin level and thus the variation in the surface-to-volume ratio of the oleosomes is supposed to correlate with the physiological state of oleosomes during seed maturation and germination and plays an important role in seed resistance to environmental stress factors.[92, 151, 165, 166] Desiccation-sensitive oil seeds, exhibiting oleosin-deficient oleosomes of relatively large size, appeared to be unstable to drying and rehydration in vivo and susceptible to coalescence due to a decreased surface-to-volume ratio of the oleosomes.[110, 151] Maintaining a high surface-to-volume ratio proved to be favourable in matters of stress resistance during the dehydration/rehydration cycle of desiccation that seeds are undergoing. Additionally, TAG mobilisation and thus germination are accelerated due to more available lipase binding sites.[110, 166] To date, comparative studies of how the oleosome's physiological states during seed development and the subsequent plant growth correlate with the oleosin level are still lacking. Specific time-dependent accumulation pattern of oleosins at the oleosome surface are suggested [110, 166], resulting in different oleosome sizes that are favourable for the respective developing state.

Soybean seeds in specific are rich in oil (12-30 %) with a high content of unsaturated fatty acids, and in proteins (30-40 %). They contain all the essential amino acids (AA) in almost such an amount as is required by humans and animals (Table 2.1). The oil is entirely included within the oleosomes and thus protected from lipid oxidation in vivo. Besides the TAG, the lipid core of oleosomes contains also other constituents, such as phytochemicals, vitamins, and hydroperoxides. It is assumed that minor amounts of tocochromanols and isoflavones, although present in relatively low concentrations, can increase the oxidative stability of oil. The association of such phytochemicals with oleosomes, typically at the oleosome interface due to their amphiphilic character, is differently strong in vivo and thus, isolation of oleosomes from soybeans can result in partial loss.[58] Corresponding studies [58] revealed that isoflavones content in isolated oleosomes was with 430 mg/kg dwb significantly lower than the 2300 mg/kg dwb measured for soybean seeds, indicating a significant loss of isoflavones during the isolation process. In contrast to isoflavones, tocopherol, in particular its isoform δ-tocopherol, appeared to be strongly associated with oil bodies, as similar amounts to that of soybean seeds (270-340 mg/kg dwb) were found in isolated oleosomes. Significantly losses were obtained for both isoflavones

and tocopherols when the oleosomes were washed with urea after isolation. Thus, the extraction method and solvents used for the oleosome isolation are crucial for oxidative stability of the lipidic content during storage.[58]

Table 2.1.: Composition of compounds in soybeans [102]

Component	**Range**	**Typical**
Protein (%)	**30-50**	**40**
Amino acid composition (g/100 g seed)		
*Non-essential**		
Arginine	2.45-3.49	2.90
Aspartic acid	3.87-4.98	4.48
Glutamic acid	6.10-8.72	7.26
*Essential**		
Isoleucine	1.46-2.12	1.76
Leucine	2.71-3.20	3.03
Lysine	2.35-2.86	2.58
Oil (g/100 g seed)	**12-30**	**20**
Fatty acid composition (% relative to the total oil)*		
Oleic acid	25-86	25
Linoleic acid	25-60	53
Linolenic acid	1-15	7
Palmitic acid	4-23	11
Stearic acid	3-30	4
Carbohydrates* (%)	**26-38**	**34**
Sucrose	2.5-8.2	5.5
Stachyose	1.4-4.1	5.0

*only the most present amino acids/fatty acids/carbohydrates are listed

1-4 % of oleosins are present in isolated oleosomes, that is 0.4-1.6 % of the seed weight and 2-20 % of the total seed proteins, depending on the plant species.[23, 26, 82, 151, 181] Proteomic analysis yielded alanine (A), threonine (T), and valine (V) as in the oleosins most present AA, whereof the last two are essential.[36, 64] The content of PL in oleosomes is with 1-4 % similar to that of proteins, with 45-52 % of phosphatidylcholine, 20-25 % phosphatidylethanolamine and 25-30 % phosphatidylinositol. On the

one hand, precise quantities can vary because of soybean cultivation under different conditions, and, on the other hand, that is particularly the case for proteins, depend on the oleosome extraction process.

2.1. Extraction of oleosomes

In general, oleosomes are extracted by two to three cycles of flotation, following centrifugation of ground, filtered and homogenised seeds.[31, 85, 198] The degree of purification, which is in particular the removal of non-oleosome associated proteins, is affected by the solvent and its conditions. Determining parameters are the pH-value, amount of added sugar and use of aqueous or organic solvents. Aqueous extraction at high alkaline regions (pH-value of 11) revealed oleosomes entirely free of any storage proteins, *i.e.* β-conglycinin, glycinin and allergenic proteins like *gly* m dB 30K.[31] The recovery of oleosomes conducted at lower pH-values (*e.g.* pH 7.5) proved to result in higher contaminations of non-oleosome proteins [35, 85], whereas it was reported that washing oleosomes with urea improved the purification [58, 108, 195]. This is regarded controversial, as the use of chaotropic agents might lead to oleosin denaturation.[132] Nature and amount of residual soy proteins at the oleosome surface directly correlate with the physicochemical properties and stability of oleosomes subjected to different environmental conditions, *e.g.* pH-value, ionic strength and temperature.[98, 140] In addition, the viscosity of the isolation medium influences the yield of oleosome recovery. Therefore sucrose of up to 20 % is added to provide an appropriate density gradient, allowing oleosomes to form a removable floating cream layer.[8, 31] Depending on the oleosin-to-oil ratio, the size and thus the density of oleosome droplets differ and some oleosomes may sediment or remain in the supernatant fluid during centrifugation.[8, 64]

Most of these extraction processes are conducted on a lab-scale basis with limited yields of oleosomes that are, indeed, sufficient for biochemical analysis but by far to low to be practicable for food processing. Kapchie et al. (2011) developed a pilot-plant scale process where almost 91 % of intact soybean oleosomes could be extracted by aqueous flotation from 75 kg soy flour applying continuous centrifugation in a three-phase decanter and several steps of slurry recirculation.[97] This renders oleosomes attractive for processing in food formulas at larger scales although further process optimisation is still required.

2.2. Sequence and structure of oleosins

Most of the oleosome characteristics are attributed to the molecular structure of oleosins, which are alkaline proteins of low molecular mass (15-30 kDa). Oleosins are expected to play a major role in the remarkable stability of oleosomes, in their synthesis and in the TAG metabolism during seed germination and plant growth. In the last three decades, the interest in exploring the structure of oleosins has risen, aiming to better understand the link between the molecular oleosin structure and the physicochemical properties of oleosomes in vivo and ex vivo. A. H. C. Huang (1992) did pioneering work by modelling a whole maize germ oleosome and its oleosin, which has, in comparison to other proteins found in nature, an unusual structure (Fig. 2.1).

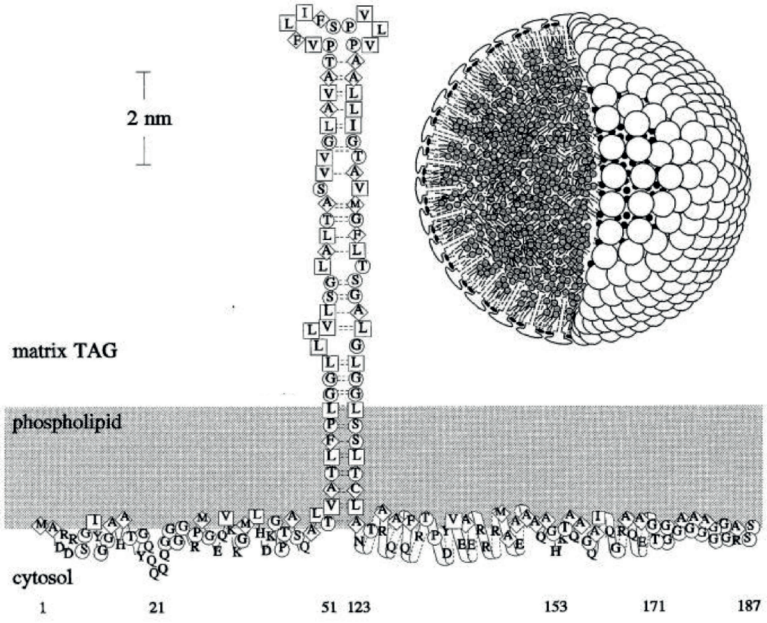

Figure 2.1.: Model of a maize oleosome and a detailed description of its oleosin primary sequence firstly described by [81].

The oleosin structure model by Huang et al. (1992) is mainly based on theoretical assumptions supported by microscopic observations and preliminary sequence analysis by cDNA cloning tests. However, the model, first rather preliminary, could be approved by more profound proteomic analysis

of *e.g.* rice oleosins [35] and peanut oleosins [23].

Primary structure In general, the oleosin is regarded as triblock copolymer. A long hydrophobic strand of 72 AA is anchored in the lipid core of oleosomes. Amphiphatic N- and C-terminal domains flank the central part and completely cover the surface of oleosomes. While the hydrophobic domain is highly conserved, the AA sequence of the N- and C-terminal domains is different in composition and length among plant species. In Fig. 2.2, the primary structure of a maize and a soybean oleosin isoform is shown in comparison, with their hydrophobic, positively and negatively charged AA residues being highlighted. The total length is 187 AA for the maize and 226 AA residues for the soybean oleosin, whereby the differences in length arise from shorter N- and C-terminal domains for the maize oleosin in contrast to the soybean oleosin. Purple coloured letters highlight the hydrophobic AA residues (77-130), mainly alanine (A), glycine (G), leucine (L) and threonine (T). These AA residues form the longest, continuous hydrophobic sequence found in nature. Three proline (P) and one serine (S) residues form a hairpin at the end of the penetrating hydrophobic domain, also referred to as "proline-knot". Polar residues are only located in the N- and C-terminal domains. Positively charged groups (green coloured letters) are orientated towards the interior of oleosomes, interacting there with charged PL groups and small amounts of free fatty acids (FFA). In contrast, negatively charged groups (red coloured letters) are arranged towards the cytosol.[82, 151, 182] It is assumed that not only the hydrophilic groups of the oleosin contribute to the hydrophilic oleosome surface but also that of PL and FFA [81]. However, cleavage of the N- and C-terminal domains by protease digestion yielded unstable oleosomes prone to coalescence. This pointed out that emulsifying and stabilising properties are rather relatable to the peripheral amphiphatic than to the hydrophobic domains.[108] Accordingly, stabilisation of oleosomes by oleosins occurs via steric hindrance and electrostatic repulsion.[26, 165]

Secondary structure Despite many attempts to explore the secondary structure of oleosins, contents of α-helical, β-sheet and random coil structures reported to date within the proposed models [162, 81, 86, 108, 132, 181] are inconsistent. Various oleosome, respectively oleosin isolation procedures from different plant species and a diversity of analytical strategies to ap-

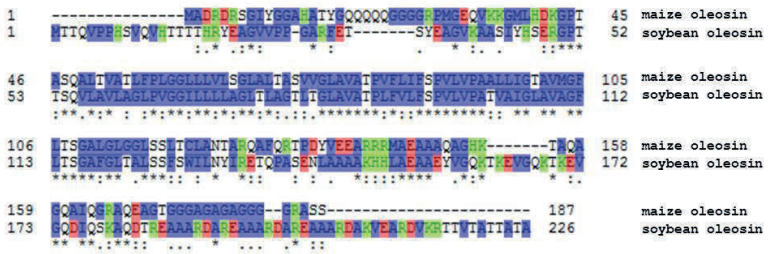

Figure 2.2.: AA sequence of maize oleosin in comparison with that of soybeans. Hydrophobic AA are purple, negatively and positively charged AA residues are coloured red or green, respectively.[36]

proach this issue mainly contribute to this controversy.

According to the model shown in Fig. 2.1, an anti-parallel β-sheet structure penetrating into the TAG matrix stabilised by inter-strand hydrogen bonding between adjacent, pairing AA residues is suggested. This information is derived from circular dichroism (CD) and conventional secondary structure predictions based on the primary sequence. Here, the formation into anti-parallel β-sheets is attributed to the "proline-knot" motif that acts as a loop that folds back the β-strand. A relatively short sequence of 30-60 AA residues on the site of the C-terminus and close to the central domain is assigned to be α-helical. The secondary structure of the N-terminal domain could not be specified due to insufficient information about its sequence.[81, 182] Results from CD and Fourier-transform infrared spectroscopy (FTIR) measurements of oleosins from rape seeds [112] and peanuts [86] were consistent with this secondary structure prediction.

To facilitate a more refined secondary structure analysis, other researchers analysed only the hydrophobic domain from rape seed oleosin isolated by SDS-PAGE and enzymatic digestion. Resulting from this, they reported that parallel intermolecular β-sheet (51 %) dominate with minor amounts of anti-parallel structure (12 %) as revealed by CD and FTIR.[113] A contribution of the "proline-knot" to the topology of the oleosin structure is not assumed but rather its function in targeting oleosins into oleosomes during synthesis. Similar measurements were done with the N-terminal domain expressed in *Escherichia coli* as a recombinant fusion protein.[112] Reconstituted in liposomes, regarded here as closest approximation to the oleosin situation in vivo, the N-terminal domain contains little α-helical, some ran-

dom coil and mostly β-sheet structural elements. Comparative analysis of purified and reconstituted N-terminal domains demonstrated that structural changes occur by embedding them in the respective environment.

Secondary structure analysis is recommended to be best performed in the natural environment of oleosins, respectively their domains, where N- and C-terminal domains of different origin are expected to adopt similar structures. This, however, is probably not the case under other conditions due to variations in AA sequences among species.[112] Secondary structure analysis by Lacey et al. (1998) also considered a higher content of β-sheet structures in the N-terminal domain as likely but disagreed with the fact that the hydrophobic domain is predominantly consistent of β-sheet, neither parallel nor anti-parallel. Instead, protease treatment of oleosins, both of sunflower and safflower, revealed distinct contents of α-helical structures, which is consistent with previous studies by Millichip et al. (1996).

2.2.1. Interfacial behaviour

Lipid droplets like oleosomes, fat milk globules and animal lipoproteins particles are found ubiquitous in biological organisms, from prokaryotes to mammals and plants. All these droplets have something in common: The very hydrophobic lipid core is surrounded by a layer or layers of emulsifiers that keep lipid droplets suspended and stable against aggregation and coalescence. The emulsifiers are PL and proteins or peptides.[167] A major difference between oleosomes and other lipid droplets is the unique structure of oleosins which is a structurally reminiscent of a chain surfactant.[184]

In general, physicochemical properties of emulsifiers are unique and adjusted to requirements of the respective metabolism of organisms. Functions of proteins are particularly ascribed to assembly, mobilisation and hydrolysis of fat droplets during metabolism. However, the precise role of proteins in the biosynthesis of lipid droplets and particularly their binding to them are still unclear. The increasing interest in fat droplets, particularly with regard to fat digestion in humans and animals, optimised oil extraction and biofuel productions and usage of them in new food or pharmaceutical formulas, has stimulated new research on the interfacial behaviour and adsorption kinetics of lipid-body associated proteins.[167] Although oleosomes are abundant in plant tissues, particularly in plant seeds, research on them has started late and yet little is known about interfacial properties of the oleosin and

its interactions with PL at the interface between oleosomes and aqueous medium.

Experimental approaches reported in literature are diverse and controversially debated. Research on the interfacial behaviour of oleosins is critical as the oleosin is strongly associated with the oleosome and its isolation can result in structural conformation changes and in the formation of insoluble aggregates.[162, 156] Although the isolation of oleosin is linked to difficulties, it is of high interest to understand the interfacial behaviour of pure oleosins in order to clarify its role in the stability and biological function of oleosomes. Furthermore, solutions of pure oleosins allow to assess the emulsifying properties of oleosins in comparison to other, commonly used proteins. Deleu et al. (2012) focused on the emulsifying and oleosome stabilisation properties of oleosins and PL, both isolated from rape seeds, in relation to competing effects of both with regard to their adsorption kinetics and interfacial rheological properties at the oil-water interface. Nikiforidis et al. (2013) investigated the foaming properties of isolated maize germ oleosins by analysing their surface activity and viscoelasticity at the air-water interface. In both studies, organic solvents are used for oleosin, respectively PL isolation. Since organic solvents are considered to be detrimental for the oleosin structure, Roux et al. (2004) analysed the interfacial properties of bacterially expressed oleosins from *Arabidopsis thaliana* at the oil-water interface of recombined oleosomes.

The challenging task with which all researchers had to deal with was the poor solubility of oleosins in aqueous solutions due to their long hydrophobic domain. However, to best mimic the oleosin's natural environment, the oleosome, the analysis of emulsifying and stabilising properties of oleosins in aqueous solutions is indispensable. Despite the constraints with regard to oleosin's solubilisation, the studies came to the following conclusions: Oleosin adsorption is highly essential for the oleosome's stability and excesses of PL at surfaces lead to droplet coalescence due to reduced steric repulsion forces provided by oleosins.[43] The reduction in surface tension and the formation of relatively high viscoelastic surface films are mainly based on synergistic effects between oleosins and PL.[156, 43] In general, oleosins are considered to have very good emulsifying properties equal to or better than other proteins like milk proteins. Adsorption of oleosins to the drop surface of a rape seed oil model occurred faster than it was observed for lactoglobulin and casein, presumably to due the less globular and thus less

compact, as well as smaller structure of oleosins.[43] However, 0.8 g/m^2 of oleosin are required to effectively stabilise the surface, which is significantly higher than the value reported for casein (1 mg/m^2).[57]

A first schematic model of the adsorption behaviour of soybean oleosomes to the air-water interface was suggested by Waschatko et al. (Fig. 2.3). In this study [192], changes in surface pressure over time (exemplary shown in Fig. 2.3) and by compressing the surface area using a film balance were correlated with Brewster angle micrographs that visualised oleosome constituents at the surface layer. The adsorption mechanism of oleosomes to the air-water interface is comparable with that of animal apolipoproteins. Particularly the low-density lipidprotein (LDL) particles, found for example in egg yolk, have been extensively investigated and their interfacial behaviour is well characterised.[5, 41] However, it is expected that oleosomes are much more stable than LDL-particles due to the different arrangement of their stabilising proteins at the oil-water interface. The apolipoprotein is located peripheral on the lipid droplet and the oleosin is additionally integrated into the oil core via its long hydrophobic domain.[78, 91]

Oleosomes immersed in the aqueous subphase diffuse to the air-water interface due to their amphiphilic nature and buoyancy forces (Fig. 2.3, 1.). Since it is energetically unfavourable for the hydrophilic protein groups to be in contact with hydrophobic air molecules (2.), oleosomes rupture (3.) and a 2D-surface film of spread TAG, PL, FFA and oleosins is formed at the interface (4. and 5.). Conformation, orientation and arrangement of oleosins within the 2D-film depend on subphase conditions, the interfacial behaviour of thermodynamically competing constituents and the oleosome concentration inserted (5.). Four different scenarios (a-d) are assumed: First, the oleosin structure unfolds with the hydrophilic domains remaining in the aqueous phase whilst the hydrophobic domains reach out into the air. Second, oleosins desorb from the interface with their hydrophobic domains joined to micellar, dense structures enclosed by hydrophilic domains. Third and fourth, the hydrophobic domains of oleosins interact either with PL or PL and TAG film patches and the hydrophilic domains are exposed to the subphase. Changes in subphase conditions like the pH-value and the ionic strength revealed that the charge distribution along the oleosin structure is the driving force in the interfacial behaviour of oleosomes at air-water interfaces. At a pH-value of 5, which is close to the oleosins' isoelectric point (pI $\approx$ 5.3), electrostatic repulsive interactions between adjacent oleosome

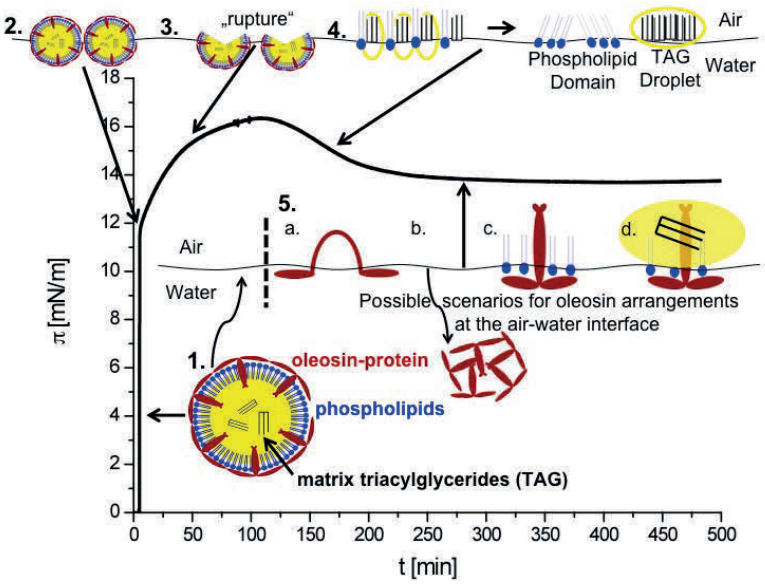

Figure 2.3.: Film balance measurement of the surface pressure as a function of time and corresponding scenarios at the air-water interface. The schematically illustrated scenarios (1-5) describe the rupture of oleosomes and the formation of a 2D-film of spread oleosome constituents upon adsorption. Different possibilities for orientation, conformation and arrangement of oleosins within the 2D-film are considered (a-d).[193]

diminish as charged oleosin groups exposed to aqueous medium become neutral. Thus, short ranged van der Waals and hydrophobic forces dominate, allowing oleosomes to pack more densely at the air-water interface. This results in a higher surface pressure than that of for more alkaline or acidic subphase conditions. A similar effect is observed at high ionic strength ($I = 100$ mM) where the charge of oleosin groups is screened and thus the oleosome net surface charge becomes neutral.[193]

2.2.2. Physicochemical stability of isolated oleosomes and their application

Stability tests revealed that the stability of emulsions composed of oleosomes is comparable to technically prepared emulsions.[28] Therefore, usage of oleosomes in industrial manufacturing, being either food, cosmetics or pharmaceutical products, can offer many benefits towards commonly produced

emulsions. High-energy consuming processes like homogenisation involved in the production of sufficiently stable oil-in-water emulsions become negligible as oleosomes already provide a well-stabilised pre-emulsified oil. Commonly emulsions are prepared of compounds which were afore thoroughly extracted, often under environmentally unfriendly and unhealthy conditions. Moreover, the recovery of oleosomes occurs from renewable and environmentally more friendly sources, which are exclusively plants.[18] Plant oil is assumed to be due to its high content of unsaturated fatty acids healthier than animal fats. Additionally, oleosomes can act as carrier system for bioactive ingredients such as vitamins [58], flavour, aroma [59] and drug agents [180] to protect them against degradation during processing and storage and to deliver them to the desired host.

To date, oleosomes are predominantly utilised in pharmaceutical and cosmetic products, for example in drug delivery [34] and skin care products [42]. Their usage in food products is still rather rare. However, particularly with regard to the steadily increasing demand for vegetarian or vegan products, oleosomes and its constituents are suitable replacements for ingredients of animal origin, like egg yolk or milk-based additives. Applications are conceivable in ice creams, mayonnaise, salad dressings, juices, vinaigrettes, pet food etc.[18] In concern to food-relevant quality criteria, a detailed knowledge about the physicochemical stability of oleosomes against various environmental stresses that oleosomes encounter during processing and storage, is crucial. Lipid oxidation imparts undesirable odours and flavour.[28, 58] High temperatures and dehydration during preservation processing and freeze-thaw cycles can result in phase separation following oil droplet aggregation, which in turn changes texture and other rheological properties.[197] Furthermore, interactions between oleosomes and other food ingredients can influence oleosome's stability and function.[28]

An ensemble of isolated oleosomes forms a predominantly protein-stabilised emulsion. Its stability depends on colloidal interactions between the surfactant-stabilised droplets which in turn are determined by the interfacial composition. Changes in the electrolyte concentration and pH-value can have a tremendous impact on emulsion stability.[72] When the pH-value of the continuous phase is far enough from the protein's isoelectric point, either in the alkaline or acidic regime, electrostatic repulsive interactions dominate, thus preventing coalescence or flocculation. Close to or directly at the pI, short ranged interactions such as van der Waals or hydrophobic

interactions presumably result in droplet aggregation and subsequent phase separation. With regard to ionic influences, four different scenarios might occur: 1) Droplet repulsion is reduced due to electrostatic screening, 2) ions bind to emulsions droplets thereby weakening electrostatic repulsion, 3) the structural organisation of water molecules is altered, resulting in an increased hydration repulsion between droplets, 4) hydrophobic interactions between non-polar groups are changed.[83, 124] Apart from the interfacial composition, also the volume fraction of the dispersed phase, as well as the droplet size and distribution can have an influence on the emulsion stability.[195]

Various studies have shown that the interfacial composition of oleosomes is crucial for their physicochemical stability and depends significantly on the extraction procedure of oleosomes. [28, 32, 84, 98, 140] Extraction conditions, particular the pH-value and usage of organic solvent, determine the type of protein that remains associated with oleosomes after washing and centrifugation.[31, 140] Comparative studies of maize germ and sunflower oleosomes revealed that the same procedure applied yields different results: Whilst maize germ oleosomes are free of any non-oleosome associated proteins after extensive washing with sucrose at mild alkaline pH-value, residual seed proteins are detected on sunflower oleosomes. However, long-term stability, *i.e.* no changes in average particle size, charge distribution on droplet surface and intermolecular droplet interactions over 15 days, only applies for oleosomes, in this case from maize germs and sunflower seeds, with an additional surface layer of extraneous proteins.[140] Soybean oleosomes, extracted at pH 8.6, remain stable after temperature treatment at 90 °C or lower for 30 minutes and at additions of NaCl not higher than 50 mM. However, the presence of extraneous proteins is not excluded.[85] At pH-values close to the pI of proteins, depending on the protein type between 4.5 to 5.5, flocculation or coalescence between oleosomes occurs. To improve the stability in low acidic environments, often encountered in foods such as juices and salad dressings, hydrocolloids like xanthan gum [139], citrus peel pectin [84] and carrageenan [198] are added. Coatings of pectin or carrageenan and the presence of sucrose yield oleosome solutions that are stable to freeze-thaw cycles.[84, 197]

3. Spray drying

Spray drying is a common unit operation to convert a liquid, pumpable material into a free flowing powder. By intense water evaporation, preservation, cost reduction in transport and storage, as well as ease in handling are achieved. In 1872, Samuel Perry first described the basic concept of spray drying in his patent. More than one hundred years later, large-scale set-ups have been established for commercial purposes. Today, for various industries such as food, (agri-)chemical, pharmaceutical, biotechnological and material, spray drying is common practice. In the field of food manufacturing, the dairy sector is the largest among all others that employs spray drying as main technology for producing milk-based powders. Compared to other drying technologies, spray drying offers many advantages:

- drying of heat-sensitive substances is feasible,
- minimal thermal-induced degradation due to quick water evaporation and thus reduced exposure to heat
- continuous operation is possible and constant powder quality is maintainable throughout the entire production run

A non-negligible disadvantage of spray driers is the high energy consumption. For the evaporation of one kilogram water an energy of 5,000 kJ is required. This is among all dehydration processes the second largest, only that of freeze drying is higher.[17]

Final product quality depends on spray dryer equipment design and material, drying parameters and feed stock properties. Additionally, each of these factors comprises numerous parameters that interact among themselves. The change in any parameter imparts direct consequences on the drying process and thus final product properties. Fig. 3.1 gives an overview of summarised cause-and-effect relationships influencing the powder quality. Owing to complex relationships and the diversity of feed solution characteristics, no standard procedure for spray drying exists. Required spray

dryer design, set-up, processing parameters and feed solution conditions are determined empirically. Moreover, set-ups evolved in lab-scale or pilot plant-scale trails are often not directly transferable to larger production scales.[29]

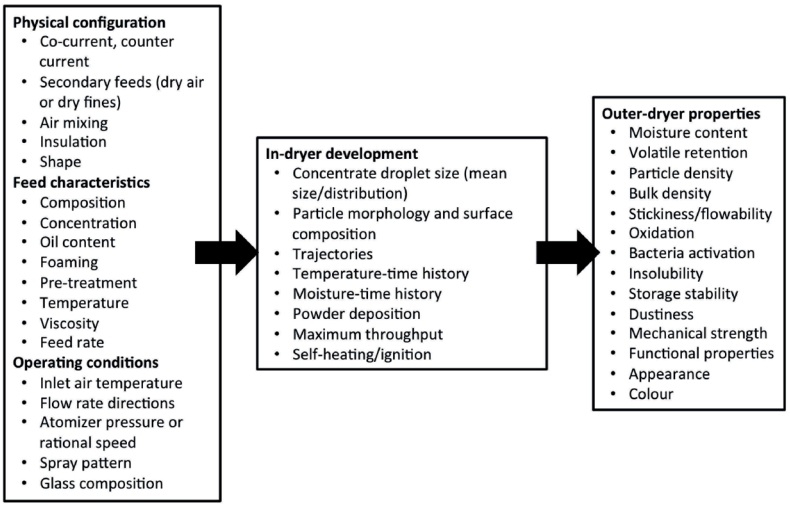

Figure 3.1.: Cause-and-effect relationship between process parameters and powder characteristics. Modified according to [29].

3.1. Principle set-up

The basic concept of spray drying involves the transformation of a liquid bulk solution into numerous droplets of large surface and the evaporation of moisture from liquid droplets. A liquid solution of a specific viscosity and defined solid material content is fed via a pump to the atomizer (Fig. 3.2). The feed solution encounters inside or outside of the atomizer a stream of low-humidity hot gas, being either heated ambient air or inert nitrogen gas, depending on the atomizer used. The drying medium disrupts the liquid into individual droplets and produces a spray released into the drying chamber. Fast heat and mass transfer processes occur simultaneously between the hot air and the droplets, thus evaporation of moisture occurs within milliseconds due to the increased surface-to-volume ratio of droplets. Contact of liquid and air stream takes place either in a co-current or counter-current manner, where liquid and air flow have the same or contrary direction, respectively. Former is for heat sensitive materials more feasible, as the

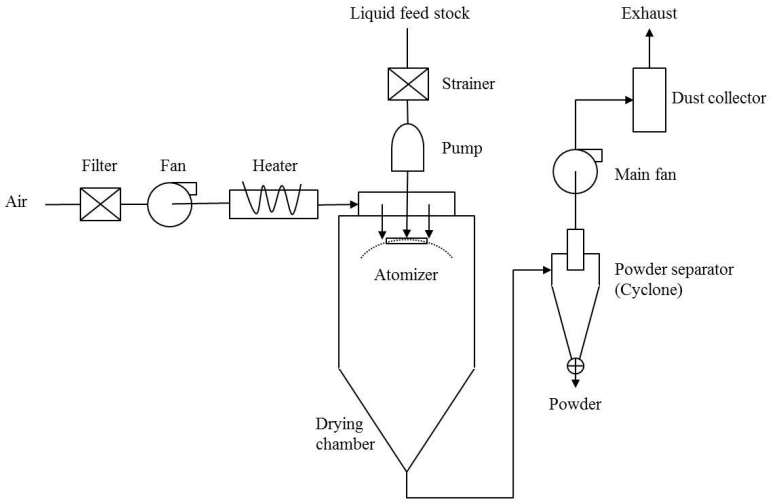

Figure 3.2.: Basic concept of a single-stage spray dryer. Redrawn from [29].

hottest air flow encounters the liquid flow when it exhibits the maximum moisture content. Dimensions of the drying chamber are adjusted in order to satisfy specific requirements regarding the heat sensitivity of liquids or to the desired powder quality. Gravity forces and suction powers transport the aerosol to the cyclone where dried particles are separated from the hot air, which is exhausted to ambience or recycled following filtration of dust particles. The final powder particles are recovered at the bottom of the cyclone and are ready for packaging.[29]

3.1.1. Atomization

Efficiency of the atomization process is the most decisive factor for achieving an economic spray drying process of a top quality product. Different atomizer types classified according to the energy supplied for droplet disintegration, operation mode, shape and number of orifices and geometry are used depending on the characteristics and volumes of feed solutions. In food industries, pneumatic nozzles (pressure energy), rotary wheels (centrifugal energy) and two-fluid nozzles (pressure and gas energy) are implemented in spray drying processes. Recently, the usage of ultrasonic horns (sonic energy) has advanced, but test trials for verifying their practicability have not been accomplished yet. For small size spray dryers as used for lab-scale

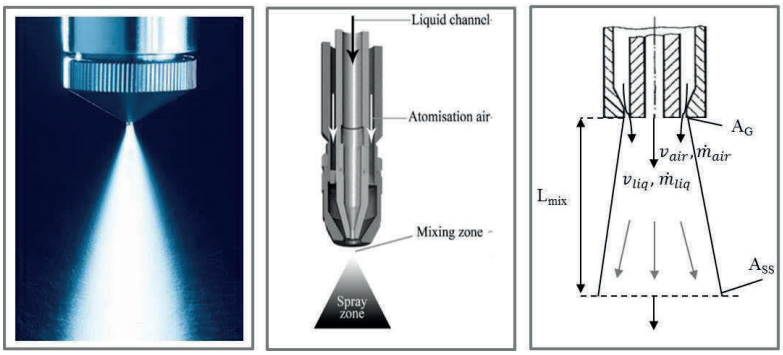

Figure 3.3.: External mixing, two-fluid nozzle. A) Nozzle in process [1]. B) Cross-section. C) The air velocity ν_{air} at the nozzle orifice is significantly higher than the liquid velocity ν_{liq}. The same average velocity ν_{mr} is reached by the air and liquid flow after passing the mixing length L_{mix} (equal to a few millimetres of the liquid orifice diameter). Figure c) is redrawn from [75].

processes, often external mixing, two-fluid nozzles are used (Fig. 3.3). Gas and liquid flow are discharged in axial direction, whereby the former flows concentrically and the latter centric through the nozzle. The kinetic energy of the gas is given by a certain pre-defined pressure whereas a pressure drop may occur at access to the drying chamber. To compensate this, the exhaust fan usually operates at higher power than the air fan (Fig. 3.2). The nozzle acts as a tool that changes the internal and kinetic energy of the liquid by reducing the cross-sectional area available for the liquid flow.[17, 75]

The primary purpose of atomization is to disintegrate a bulk solution into dispersed droplets with large surfaces sufficient for efficient heat and mass transfer to and from liquid droplets. The creation of large surfaces facilitates quick drying as the rate of evaporation directly correlates with the droplet surface. The disintegration itself depends on several factors: Relative velocity differences between the contacting air and liquid mass streams have to be sufficient for the supply of kinetic energy to disrupt the liquid feed into dispersed droplets. At high liquid-to-air mass flow rates or high liquid densities, the gas insufficiently penetrates into the liquid sheet, which is then poorly disintegrated, causing a spray of large droplets. Same happens to feeds of high viscosity and high surface tension. The natural stability of the liquid impedes the creation of a turbulence flow within the liquid stream as less power can be transferred by the gas to the liquid.[75]

The ratio of power (ψ) in Watts transferred by the air ($\dot{m}_{air}$) mass flow to the liquid ($\dot{m}_{liq}$) mass flow is quantified, here using the example of an external two-fluid nozzle (Fig. 3.3), by the following equation:

$$\frac{\psi_{\mathrm{air/liquid}}}{\psi_{\mathrm{air}}} = \frac{\dot{m}_{\mathrm{liq}}/\dot{m}_{\mathrm{air}}}{\left((\dot{m}_{\mathrm{liq}}/\dot{m}_{\mathrm{air}}) + 1\right)^2} \tag{3.1}$$

The equation shows that the maximum of atomization efficiency is limited to $\dot{m}_{\mathrm{liq}}/\dot{m}_{\mathrm{air}} = 1$. The lowest droplet size is obtained when $\dot{m}_{\mathrm{liq}}/\dot{m}_{\mathrm{air}} \rightarrow 0$.[189] Taking all afore mentioned factors into account, the droplet size (D) is a function of liquid surface tension, viscosity and density, as well as of the relative velocity (v_{rel}) and mass flow rate ratio between the air and liquid at the orifice outlet, the air density (ρ_{air}) and the constant α and β (involving nozzle design parameters and liquid properties), as described by Eq. 3.2.[120]

$$D = \frac{\alpha}{v_{\mathrm{rel}}^2 \rho_{\mathrm{air}}} + \beta \left(\frac{\dot{m}_{\mathrm{air}}}{\dot{m}_{\mathrm{liq}}}\right) \tag{3.2}$$

To summarise, the performance of the atomizer determines the spray pattern that in turn influences the droplet size and distribution, trajectory and velocity, chamber dimensions required, wall material deposition and mixing efficiency of drying medium and dispersed liquid. These factors again have a distinct influence on the drying efficiency, powder properties and the powder collection efficiency.

3.1.2. Droplet drying

During spray drying, thermal energy of the hot air stream is transferred to the (colder) liquid droplets by convection. Convection is regarded as a combination of diffusion and bulk motions of molecules. Whether which of the two becomes the dominating influence depends on the distance of the moving fluid to the droplets surface. Close to the surface, diffusion takes place while bulk motion influences dominate the further away from the surface of the droplets. Furthermore, convection is classified in natural and forced convection. Former is caused by buoyancy forces induced by density differences between two fluids of varying temperature. Latter occurs when external devices induce fluid flows of specific velocities as it happens by the liquid feed pump or air pressure release during spray drying. Due to the relative velocity difference between the air and liquid flow, the fluids are

constantly replaced by the hot air stream which results in a heat transfer higher than for natural convection.[29]

Heat and mass transfers simultaneously initialise the drying process of droplets when these are exposed to hot air. Modelling the heat and mass transfer of a pure solvent droplet is complicated, since various factors, such as fluid physical properties (dynamic viscosity, thermal conductivity, specific heat at constant pressure, thermal expansion etc.) and fluid circulation motions must be known. Droplets with dispersed or dissolved solids potentise these problems even more, particularly, as mass concentration and composition and thus thermodynamic properties of droplets and drying mechanisms change with progressing drying. To approach this complexity, kinetics and mechanisms of droplet drying are schematically explained by illustrations as shown in Fig. 3.4.[29, 96]

The droplet drying process is divided into two stages, when hygroscopic substances are involved even into three stages. At the beginning of the drying process, free moisture evaporates from the droplet's surface and the drying rate is comparable to that of pure water evaporation. Diffusional and capillary forces draw moisture from within the droplet to maintain saturated conditions at the droplet surface. In the first stage of drying, droplet volume and average rate of moisture removal ($\frac{\mathrm{d}X}{\mathrm{d}t}$) remain constant. The latter and the average drying time (t_c) can be expressed as shown in Eq. 3.3 and Eq. 3.4:

$$\frac{\mathrm{d}X}{\mathrm{d}t} = \frac{2\pi D_\mathrm{av} k_\mathrm{d}}{\lambda_\mathrm{e}} \Delta T_\mathrm{LMTD} \tag{3.3}$$

$$t_\mathrm{c} = \frac{\lambda_\mathrm{e}}{8\mathrm{k_b}\Delta T_\mathrm{LMTD}} \rho_0 D_0^2 - \rho_1 D_1^2 \tag{3.4}$$

The average droplet diameter is described by D_av, D_0 and D_1 represent the droplet diameter at the beginning and the end of drying, considering droplet shrinkage with progressing drying. The thermal conductivity of the drying gas is expressed by k_d, the latent heat of evaporation is given by λ_e, the log mean temperature difference (LMTD) between the air and droplet temperature by ΔT_LMTD. $\rho_{0,1}$ are the droplet densities at the beginning and the end of drying.[119] During the constant rate period, the surface temperature of the droplet subjected to evaporation remains constant at the wet-bulb temperature of a pure water droplet following an initial slight increase (Fig. 3.4, 0-1).

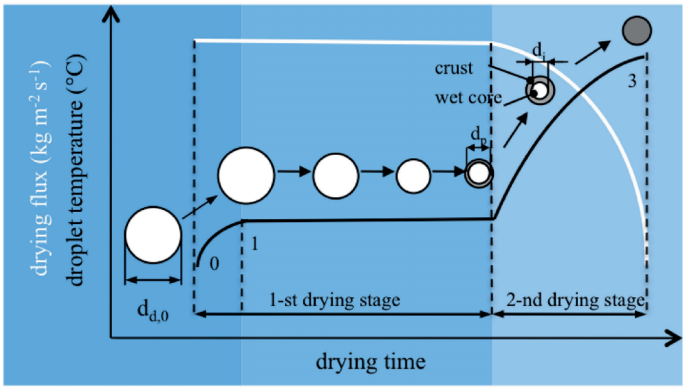

Figure 3.4.: Drying flux and droplet temperature of a drying droplet as a function of time with corresponding changes in droplet volume and morphology. Droplet drying is divided into to the first drying stage and the second drying stage or "falling-rate"-period. Redrawn from [29, 96].

With progressing drying, saturation of the moisture film at the droplet surface is not maintainable. Loss of liquid mass and concentration of solid mass occur, reflected by the reduction in droplet volume (Fig. 3.4: 1-2). Crust formation is induced by the radial orientated mass transfer of solids to the droplet surface, here represented by the sharp inflection point or critical point (Fig. 3.4: 2), which initiates the second drying stage. Various factors such as drying conditions (humidity, temperature, relative fluid flow velocities), physical properties of the liquid solvent (vapour pressure, surface tension, density, viscosity) and of the dispersed and dissolved solid particles (chemical composition, interfacial behaviour, concentration) determine the crust formation.

The second drying stage is also called "falling-rate"-period as the rate of moisture removal gradually decreases with increasing drying time. During this period, the dry-bulb temperature of the droplet rises to the outlet temperature of the drying medium. The volume of the drying droplet remains more or less constant. The average moisture removal rate ($\frac{\mathrm{d}X'}{\mathrm{d}t}$) is determined by the following equation [119]:

$$\frac{\mathrm{d}X'}{\mathrm{d}t} = \frac{-12k_\mathrm{d}}{\lambda_\mathrm{e} d_1^2 \rho_\mathrm{s}} \Delta T_\mathrm{LMTD} \tag{3.5}$$

Here, ρ_s is the density of particles. A precise expression of the drying time

is difficult as it depends on the nature of dissolved and dispersed solids.

In general, the moisture transfer mechanism during the drying stages is regarded as the limiting factor of the drying rate. As long as the droplet surface is sufficiently saturated, drying is diffusion controlled due to the diffusion density difference between the drying fluid and the droplets. Other drying mechanisms are taking place with the start of the falling-rate period and when the free water is completely removed. The morphology of the crust influences significantly the ongoing mass transfer mechanisms during this stage and thus the drying time, efficiency and quality. Porous solids exhibit a network of interconnecting pores and channels in which capillary flow due to capillary forces takes place. This mechanism is often accompanied by moisture transport-assisted evaporation and condensation between liquid-bridges inside the pores. Liquid and vapour diffusion occur in non-porous solids due to density gradients. The higher the solid content of a droplet, the shorter the constant rate period, if not negligible. Accordingly, the time of the falling-rate period is longer. For heat-sensitive materials it might be also reasonable to reduce the inlet temperature, as at very high drying temperatures, the droplet temperature might exceed the evaporation temperature when the wet-bulb temperature is higher than the temperature at the droplet surface. Depending on the porosity of the crust formed during drying, vapour pressure is built up within the particle and its temperature-controlled expansion can lead to particle disruption, rupture, expansion and fractures.[29]

3.1.3. Particle separation

For powder recovery, either filter bag systems, electrostatic precipitators or cyclones are used. Latter is favourably used due to its simple design, easiness to clean and the absence of moving elements. The cyclone (Fig. 3.2) is composed of a cylindrical part and a conical part at its bottom. Powder recovery is achieved by gravity. The air stream carrying the dried particles enters the cyclone tangentially. Sufficiently large particles are forced by centrifugal forces to the cyclone's walls and channeled into a vortex-like path down to the bottom of the cyclone.[32] Small particles tend to exhibit higher radial velocities and are captured by the exhaust air stream. Thus, the powder separation efficiency is usually below 100 % and determined by the cut-off point (d_{50}) expressed by Eq. 3.6:

$$d_{50} = \mathrm{K_c}\sqrt{\frac{9\mu_\mathrm{a}Q}{\pi\rho_\mathrm{p}Z_0 v_\mathrm{in}^2}} \tag{3.6}$$

where ρ_p is the particle density, $\mathrm{K_c}$ the cut-off coefficient factor depending on the cyclone geometries, Q the volume flow rate through the cyclone, Z_0 the outer vortex length, respectively the cyclones' effective length, μ_a the air dynamic viscosity and v_in the cyclone inlet velocity.[13, 190] Efficiency of cyclones can be optimised by a higher velocity of the inlet volume flow, larger particles (for example by a higher solid content in the feed solution or a higher pumping rate), reduction in cyclone radius and a sufficient residence time of particles. To minimise air pollution by exhausting dust particles, air filtration is applied following powder separation.[29]

3.2. Microencapsulation

Various food additives are sensitive to degradation during processing and storage that might result in undesirable off-flavours, odours, colour changes and losses. This concerns especially components of high nutritional value like vitamins, unsaturated fatty acids, flavonoids, aroma and flavour components in general. Often the need for efficient food preservation counteracts the ambition for the maximum retention of bioactive ingredients during processing. By embedding or encapsulating sensitive, volatile and reactive compounds in biopolymeric matrices, a suitable protection against environmental stress can be achieved. For capsules in the submicron range, this procedure is referred to as microencapsulation. Microencapsulation involves not only the protection of valuable ingredients but also utilises easier handling of solidified materials and preservation. The controlled release of compounds at desired site, time and release rate, masking of undesired aroma and flavours and the separation of compounds that would otherwise react with each other, are important aspects of microencapsulation.[89] Recent accomplishments by food industries are the encapsulation of microorganisms, so-called probiotics, for implementation in milk products to provide a functional product that has a beneficial impact on the consumers' digestion.[117]

Microencapsulation can be achieved by the following techniques: spray drying, spray cooling, coacervation, centrifugal extrusion, rotational suspension separation, liposome entrapment, fluidised-bed coating, freeze drying and inclusion complexation. Among all these techniques, spray drying is

the one most widely used as it is economical, allows quick and uncomplicated changeovers between different products without extensive technical alteration works, produces particles of good quality and is low in cost. In principle, two different capsule designs can be produced, either capsules of a single-core surrounded by a shell or multiple-cores embedded in a continuous wall matrix.[66] Physical properties of the wall material mainly influence the encapsulation efficiency and the (long-term) stability of capsules against environmental stresses during processing, storage and consumption. When microcapsules are produced, aiming for the controlled release of the core material in a specific host, the wall material determines the stimulus that is required to trigger the release. Mechanisms that trigger the release are changes of pH-values, temperature and osmotic pressure, as well as enzymatic reactions and application of mechanical stresses.[69] In general, the chosen wall material should be chemically inert with respect to the encapsulated material, completely soluble in food-relevant solvents (water, ethanol), impermeable for volatile compounds, inexpensive and of food-grade. Furthermore, the wall material should facilitate complete dispersion and emulsification of the core material and provide a permanent and stable barrier against environmental stresses. By all means, the wall material should not compromise the sensory properties of food.[6, 67, 89]

3.2.1. Wall materials for oil encapsulation

Numerous wall materials are available for the microencapsulation of fats and oils, as well as lipophilic, volatile bioactive compounds. Choosing a feasible wall material is crucial for spray drying, as the physical properties of the encapsulating compound influences diverse characteristics. For example, they determine the emulsion properties before drying, the droplet drying mechanism and the volatile retention during drying. The long-term stability of the encapsulated core material within powder particles after drying is another critical point.[66]

The encapsulation of oils or fats rich in poly-unsaturated fatty acids (PUFA) requires wall materials that provide an excellent barrier against oxygen permeability and volatile retention to prevent lipid oxidation and loss of aromas and flavours. Owing to the low odour threshold of aromatic compounds evolved from lipid oxidation, already low amounts of free surface oil result in unacceptable off-flavours and odours. Simple spray drying

of an oil-in-water emulsion is usually not sufficient to obtain microcapsules suitable for usage in food formulas. Additional encapsulation, if not double encapsulation, by using blends of wall materials and consecutively running encapsulation processes is required.[48]

Commonly, carbohydrates, like hydrolysed and modified starch products, gums, cyclodextrins and cellulose derivates, and proteins such as whey proteins, gelatine, soy proteins and caseinates are used as wall materials. Substances obtained from Maillard reaction processes represent a new class of emerging biopolymers usable for microencapsulation.[89] In the following, the preferential application of carbohydrates and proteins as wall material for the encapsulation of oil by spray drying is explained in more detail.

Carbohydrates Gum arabic has been the most popular and most widely used encapsulation agent among all available carbohydrates. Owing to its complex mixture of glycoproteins and polysaccharides, gum arabic provides excellent emulsifying, as well as flavour and aroma retention properties. However, high levels of impurities resulting from its recovery, as well as extensive seasonal variations in crop yields that result in high cost prices, demanded a gradual replacement of gum arabic by other wall materials. The emphasis is nowadays on hydrolysed and modified starches. Hydrolysation and thus depolymerisation of starch molecules occur by the addition of enzymes or acids. Depending on the depolymerisation degree, also referred to as dextrose equivalent (DE), starches are classified according to their functional properties. Higher DE-values indicate products that have a low impact on solution viscosity at high solid content, lower permeability to oxygen and better encapsulation efficiency. Particularly maltodextrin, a mixture of higher saccharides, glucose dimers (maltose) and monomers (dextrose), is favourably used in microencapsulation processes as it is inexpensive, exhibits low sweetness and is tasteless.[89, 66]

Despite the favourable attributes, these ingredients are inferior to the exceptional capabilities of gum arabic due to the lack of emulsifying properties and poor flavour retention during spray drying. Chemical modification of starches by introducing side chains of lipophilic succinic acid yields starches with satisfying emulsifying properties. In comparison to their native counterparts, flavour retention capabilities and encapsulation efficiency are improved.[49, 176] Excellent protection against oxygen diffusional intrusion can be achieved by using cyclodextrins as encapsulation agent. Cyclo-

dextrins are composed of cyclic arranged monomers of glucose (six to eight), forming relatively rigid and hollow ring structures that allow the inclusion of substances.[164, 200]

Also low molecular weight sugars such as sucrose, fructose, lactose and trehalose or blends of such are used as encapsulation agents. Solutions containing a very high sugar content result in powder with pronounced, undesirable stickiness upon spray drying. Due to the rapid removal of the dispersing medium during drying, amorphous powders are formed. Low molecular weight sugars exhibit high hygroscopicity and solubility in the amorphous state. The sticky behaviour of amorphous powders depends on physical properties of the sugars like solubility, hygroscopicity, melting point and glass-transition temperature, sugar content and drying temperatures. Comparing the sugars relatively to each other, it can be stated that the higher the melting point and glass-transition temperature and the lower the solubility and hygroscopicity of the used sugar, the less sticky is the powder. This accounts particularly for lactose that is favourably used for encapsulation and as naturally given encapsulation agent in milk powder.[54, 90, 185]

Proteins While the oil encapsulation by using carbohydrates is mainly driven by surface film solidification due to phase transitions upon drying, proteins are primarily used for stabilising the infeed emulsion prior to spray drying. A highly stabilised emulsion of properly homogenised, small droplets of narrow distribution is crucial for drying efficiency. Some proteins exhibit excellent emulsifying properties, high solubility and film formation properties owing to their amphiphilic character.[142]

The native structure of proteins is based on complex interactions between forces, involving hydrogen bonding, van der Waals forces, electrostatic forces, hydrophobic interactions and conformational entropy.[144, 150, 154] The protein's physical properties and functions are determined by its structural conformation. Sequences of amino acids form the protein's primary structure that determines the folding of structural units into the secondary conformation, as well as the association of structural units into the tertiary and quaternary domains. Particularly short ranged interactions, such as van der Waals, hydrogen bonding and hydrophobic interactions, are involved in the stabilisation of folded proteins. Polar (charged or non-charged) and apolar AA residues distributed along the peptide chain further contribute to the folding of proteins in polar or non-polar solvents and thus determine their

solubility. Environmental conditions such as pH-value, type and strength of ions present, temperature and shear stress can influence the protein properties like structural conformation, interfacial behaviour and charge distribution. Long ranged electrostatic repulsion forces, acting between oppositely charged emulsion droplets, and steric interactions mainly contribute to the stability of protein-stabilised emulsions. Charge neutralisation due to screening effects or solution pH-values close to the protein's pI results in a reduction of repulsive forces and an increase of short ranged attraction forces followed by droplet aggregation and phase separation.[142] However, it is assumed that aggregation does not automatically involve major conformation changes of the protein.[175]

Upon formation of new interfaces, either liquid/liquid or air/liquid interfaces, induced for example by homogenisation, adsorption of and droplet stabilisation by the protein take place. By approaching the proximity of the newly formed interface, the protein unfolds, which is accompanied by a shift between forces that stabilise and destabilise its structure. The unfolding upon adsorption is regarded as an entropically favoured process.[141] What kind of conformational states are adopted by unfolded proteins depends on interactions between proteins and lipids, between proteins and other surfactants present, as well as on the geometries of the formed interfaces.[142]

Among all proteins, gelatine has been the most preferably used wall material for encapsulation of oil. Also milk proteins such as whey proteins and caseinates, as well as egg proteins are widely applied in spray drying processes. However, the increasing demand for food free of animal-originated additives stimulated investigations to find replacements of equivalent properties. Moreover, protein isolates and concentrates isolated from soybeans are widely used as encapsulating agents.[185]

4. Characterisation methodologies

The functionality and stability of a powder are directly linked to its chemical composition and physical characteristics. Processing history, type of used raw materials, interactions among powder compounds and their environment, packaging, storage and transport conditions influence the powder characteristics.[63, 136] A precise knowledge of the influences on the powder characteristics is crucial for the production of a powder whose quality meets the manufacturers and consumers expectations. However, quality is a differently perceived property. From the consumers' point of view, aspects such as convenience, taste, flavour and appearance are regarded as good quality parameters. For food manufacturers, the emphasis is strongly on processing conditions that raw materials, intermediate and final products encounter with the primary aim of achieving a high safety level in terms of a long shelf-life. Such ambitious safety constraints often involve severe losses in nutritional content and sensory quality. Food powders are complex systems composed of proteins, lipids, carbohydrates, vitamins, aromas and so on. Chemical composition and physical properties induced by all these compounds can vary during processing and subsequent storage and need to be controlled. During drying, factors such as water content, heat and mass transfer conditions, temperature and humidity conditions, sticking and crystallisation phenomena linked to glass transition temperatures, chemical reactions induced by environmental influences and changes in shape, porosity, size and mechanical properties have to be considered.[20] Figure 4.1 gives a rough overview of the links between the powder physical and chemical properties, both of the particle core and surface, and the powder functionality related to mechanical, thermal and hydration constraints. Besides the bulk properties, special attention is given to the surface composition as it strongly affects the powder's reconstitution characteristics and handling properties such as redispersibility, flowability, wettability, stickiness and

agglomeration.[136]

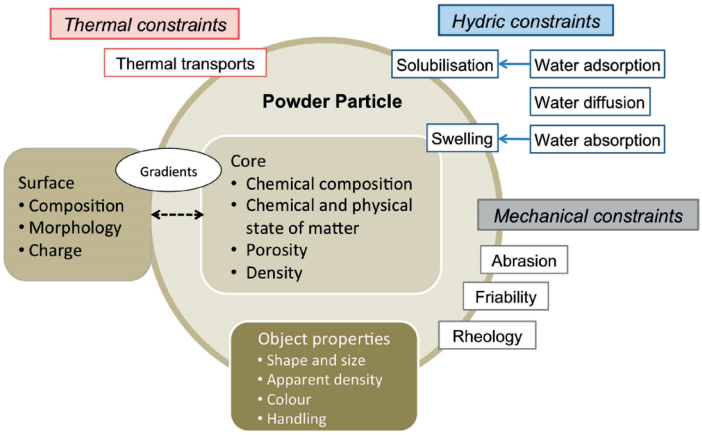

Figure 4.1.: Links between the matter properties, object properties and constraints (mechanical, thermal and hydric) of a powder particle (modified according to [136]).

In order to investigate and understand the influences of diverse and numerous factors on powder properties, a multi-scale approach involving various analytical methods is required (Fig. 4.2). By coupling macroscopic approaches in scale ranges of µm to nm to microscopic (nm - µm), molecular (Å - nm) and atomistic approaches (Å), physical and chemical phenomena during drying originating from the physicochemical nature of compounds and interactions among them are best explainable.[136]

In case of oil encapsulation by spray drying [7, 15, 25, 40, 53, 79, 145, 185], quality control parameters for the evaluation of the drying efficiency are, *e.g.*, the emulsion droplet size distribution before spray drying, the interfacial behaviour of the used emulsifiers, impact of process parameters on structural composition of dried compounds, the powder morphology and its surface composition. Droplet or particle size measurements are applicable before, during or after spray drying. Before, to investigate the emulsion stability of the liquid feed and during or after to detect the droplet size distribution of the spray pattern or of the reconstituted powder. The droplets and particles can exhibit sizes ranging from nanometre to millimetre. Thus, the physical principle of instrumentation for particle analysis is chosen according to the droplet size distribution expected, whereupon the droplet physical properties like optical and bulk properties are to be considered. Such microscopic properties are governed, amongst others, by the molecular properties

of the used emulsifier, *i.e.* chemical structure, polarity and interfacial behaviour. Tensiometric measurements linked with vibrational spectroscopic measurements correlate macroscopic observations like interfacial behaviour with changes in chemical structure on molecular level. Techniques such as scanning electron microscopy (SEM) and X-ray photoelectron spectroscopy (XPS) are used for investigating the surface morphology and surface composition, respectively. In the latter case, information obtained by the atomistic approach, *i.e.* quantification of relative atomic surface concentration, is related to macroscopic powder characteristics. Thereby, the amount of free surface oil is determinable which affects the reconstitution properties of particles, the powder quality and the encapsulation efficiency.[54]

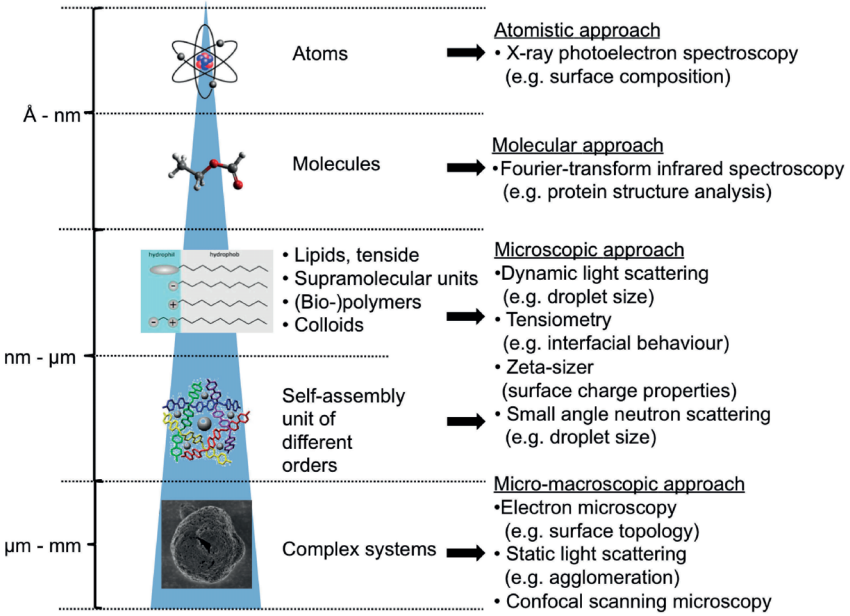

Figure 4.2.: Multi-scale approach for the analysis of powder characteristics (modified according to [136]).

4.1. Particle sizing

The particle size influences numerous properties and the overall functionality of food powders. Nowadays, elaborate techniques utilise quick, if not instantaneous, measurements after or during processing, so that particle sizes are regarded as a valuable indicator for product quality and performance.

Size and shape of powders influence flowability, compaction and reconstitution properties. For many products, the particle or droplet size distribution is critical for texture, sensory and stability properties. Often, controlling and measuring particle size distributions are required throughout the lifetime of products, starting from processing to consumption.[80]

Powder particles are 3-dimensional objects of varying volume, different surfaces, length and width. They exhibit different density, colour, opacity, conductivity and refractive indices which depend on the chemical composition of the powders. The principles that are responsible for behaviour and appearance of particles during particle characterisation are affected by these different properties.[129] As manifold as the powder properties are the analytical techniques available to determine the particle size, namely, microscopy, light interaction, electrical property, sedimentation and classification methods.[194]

However, the linear dimensions of an arbitrary particle are not describable by a single dimension like the diameter that complicates the description of particle size distributions (PSD). Therefore, the concept of equivalent sphere is introduced in order to make particle size measurements simpler and more convenient (Fig. 4.3). By relating a non-spherical particle and its equivalent sphere exhibiting the same property (*e.g.* weight, surface area, volume or length) to a given principle, the particle can be characterised by a single size parameter - the equivalent sphere diameter.[129]

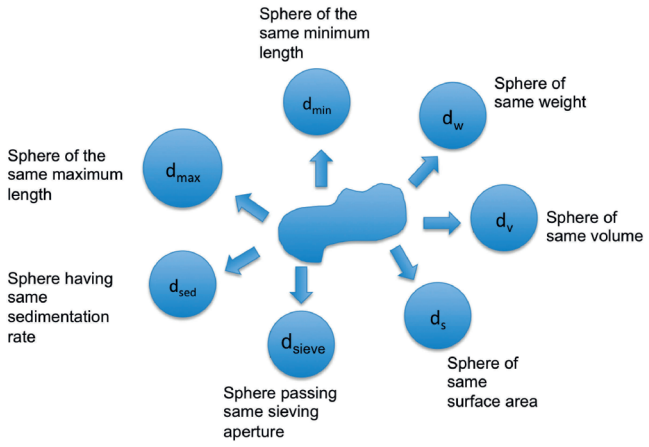

Figure 4.3.: Model of equivalent sphere (modified according to [153]).

In practice, particle generation processes create a collection of particles

with a certain PSD. The information derived from the particle size measurement technique indicates the quantity of particles within each size class. The narrower the width of size classes, the more precise is the classification of differently sized particles. Instrumental resolution properties and measurement range, as well as the polydispersity of particles are decisive for the degree of particle size classification. PSD are expressed by normalised frequency distribution (q_x) and cumulative distribution (Q_x) curves. The former describes the amount of fractions within a defined interval of particle sizes. The latter indicates the quantity of particles larger or smaller than an ascertained size. According to the principle of used sizing technique, PSD are weighted by either number, volume or intensity, denoted by the subscript x, *i.e.* 0 for number and 3 for volume weighted PSD. For example, microscopic measurements yield numbers of particles of a certain size whereas light scattering or sieving measurements deliver information about volume, respectively mass.[129]

Statistical parameters such as means, modes, percentiles and standard deviations can be derived from PSD and used for comparative tests in product specifications. In order to relate PSD with the product performance, weighted mean diameters are commonly used.[129] Weighted mean diameters are the result of particle property (*e.g.* size, volume) and weighting factor (*e.g.* number, area) as shown by the following examples:

$$D\,[3,2] = \frac{\left(\sum n_i D_i^3\right)}{\left(\sum n_i D_i^2\right)} \tag{4.1}$$

$$D\,[4,3] = \frac{\left(\sum n_i D_i^4\right)}{\left(\sum n_i D_i^3\right)} \tag{4.2}$$

Equation 4.1 is the surface weighted mean diameter or Sauter mean diameter and Eq. 4.2 the volume weighted mean diameter, where n_i is the amount of particles contained in class i, having a mean diameter D_i. In general, the relation of particle parameter and weighting factor should be oriented towards the information of interest with regard to the application of particulate systems in processing. For example, the Sauter diameter is reasonable to consider in applications where the surface area of particles is the decisive factor in process efficiency.

Measurement technologies The choice of the appropriate measurement technology depends on several factors: Instrumentation resolution, polydis-

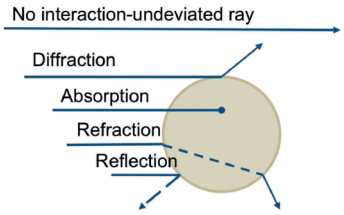

Figure 4.4.: Light scattering phenomena upon matter interaction (modified according to [194]).

persity of the sample, sample physical properties such as optical parameters and density, dispersion of the sample in dry or wet form, in-line measurements required and sample stability preparation procedures.

Some imaging techniques such as microscopy or electron sensing allow a direct look at both the particle shape and size. While with former only relatively few particles are examined and thus unrepresentative sampling is likely, this problem is circumvented by the latter. However, both techniques are not or conditionally suitable for the analysis of emulsions or dispersions.[153]

Most laboratories operate light scattering techniques as standardised particle characterisation method. The use of light as analysing tool allows non-destructive, non-invasive and time-dependent characterisation of particles in situ and ex situ. When an incident beam of light of a certain wavelength (photon energy) and intensity (photon flux) strikes solution particles, fractions of the light interact with particle matter and are reflected, diffracted, refracted and/or absorbed by particles depending on the particle physical properties (Fig. 4.4). However, the fundamental definition of light scattering only comprises the first three incidences and states: light scattering is the alteration of direction and intensity of a light beam upon material interaction without any changes in energy, respectively absorption. From the angular distribution of intensity of the scattered light, particle characteristics such as size, shape, orientation, structure and composition can be derived.[93]

Commonly used scattering techniques are static light scattering (SLS) and dynamic light scattering (DLS). With SLS, particle sizes are detectable in a range of several hundred nanometers to a few millimetres. Particle sizes are derived from scattering pattern intensities of light recorded at various angles. Different to the optical approach by SLS, with DLS, the particle size

is determined by correlating light intensity fluctuations with hydrodynamic motions of the particles. The application of DLS is limited to particle sizes ranging from the lower nanometre to lower sub-micron region and factors such as sample condition, sample concentration and environmental conditions can significantly influence the generation of data.[10]

Particle size determination is also feasible by small angle neutron scattering (SANS) or small angle X-ray scattering (SAXS) based on the same principle as light scattering though no light but neutrons or electrons are scattered upon matter interaction.[114] High operation costs, low availability and relatively long measurement periods render such techniques unfavourable as standard methods.

4.1.1. Laser diffraction analysis

Laser diffraction analysis has become a popular and widely used technique by the food industry to measure particle sizes. Instrumentation is compact, no time-consuming set-ups or calibration are required, operation is easy and fast and high reproducibility can be achieved. However, the most compelling advantages of laser diffraction are the broad dynamic size range ranging from nanometers to millimeters and its applicability to diverse food types including sprayed liquids, powders and suspensions. The measurement principle corresponds to static light scattering; scattering intensities as a function of incident wavelength (λ) and scattering angle (θ) are mathematically related to the particle properties on basis of theoretical models of light scattering. However, such a characterisation requires an accurate relation between particle properties and physical models often involving non-negligible constraints. Disregards or misuse of such constraints can result in questionable, unrealistic or even false measurements.[100, 194, 199]

Fundamentals of models or theories approaching the phenomenon of light scattering are based on Maxwell's electromagnetic theory of light and have been first summarised among others by Rayleigh, Fraunhofer and Mie. Each model is valid in a particular size range and a specific light propagation by particles governed by relative refractive indices of scatterer and its surrounding medium.[199] When a coherent wave of laser light beam encounters an object, scattering in all directions occurs and evolves in characteristic scattering-angle-dependent intensity pattern (Fig. 4.5). Alterations are a combined effect of reflection, refraction and diffraction.[194]

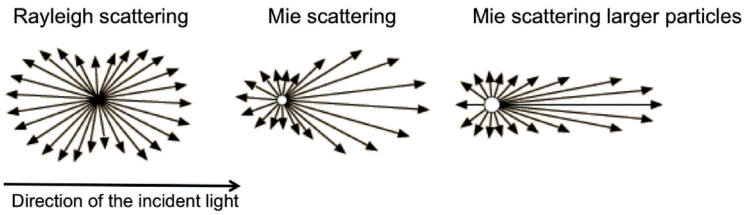

Figure 4.5.: Scattering pattern by Rayleigh and Mie.[143]

The scattering or interference pattern of spherical particles are represented in form of alternating bright and dark rings centred around a dark spot. The intensity is a function of scattering-angle, wavelength, particle size and relative refractive index of the particle and the medium. With increasing distance from the central spot, the intensity decreases and the distance between two rings becomes smaller. Simplified, small particles scatter light with small intensity at broad angles while large particles scatter light with high intensity at narrow angles.[171, 199]

Classification of scattering pattern is based on the wavelength (λ) ratio between the incident light and the particle size (D). Small particles of a few tens of nanometers that are significantly smaller than the wavelength ($D < 0.1\lambda$) show Rayleigh scattering, which is a symmetric pattern of equally forward and backward scattered light intensity (see Fig. 4.5). As no angular information can be derived from it, the Rayleigh model is irrelevant to laser diffractometry. Particle of sizes within an order of the incident wavelength ($0.1\lambda < D < 10\lambda$) show Mie scattering (Fig. 4.5). Most laser diffraction analysers generate information about the particle size by deconvolution of scattering pattern based on the Fraunhofer diffraction theory or the Mie theory.[131] The Fraunhofer diffraction theory is commonly used for large particles ($D > 20$ µm) and assumes that light is scattered by particles, regarded as circular and opaque disks, at narrow angles. In principle, information about the optical properties of the particles is not required. However, for particles smaller than 2 µm, this theory becomes incorrect. Thus, the Mie theory is applied for measuring particles that are smaller than the wavelength of the incident wave. In most cases, the application of the Mie model is related to particle sizes larger than 120 nm though it applies to spheres with diameters being very small or infinitesimal large. To derive particle sizes from intensity pattern, computational extensive and complex numerical calculations and diffraction approximations are

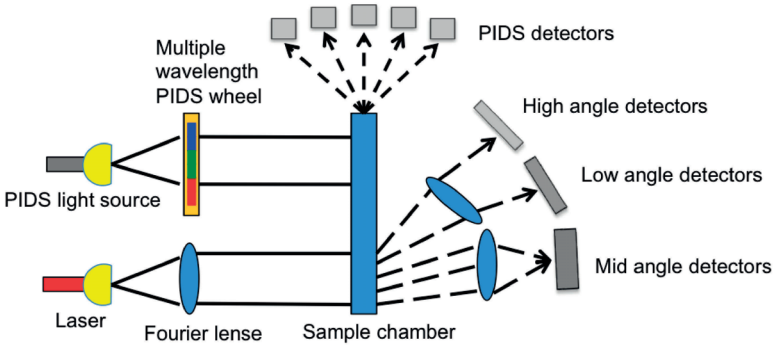

Figure 4.6.: Schematic principle of a laser diffractometer with PIDS-technology after [21].

performed. For an accurate performance of such calculations, the following constraints are to be considered: Avoidance of multi-scattering effects by particles, knowledge of relative refractive indices, all particles exhibit the same optical properties and are spherical and isotropic.[171, 194]

Problems arise when analysing emulsions commonly constituted of multiple compounds. Each of the compounds has specific optical properties that contribute differently to scattering of light. Precise determination of refractive indices of emulsions by common techniques [128] is not possible and only conditionally achieved by theoretical approaches [99]. Thus, the used relative refractive indices during particle analysis have to be regarded as rough approximation of real values and obtained particle sizes to be taken with care.[128] Moreover, emulsions subjected to conditions causing instability may exhibit irregular shaped, non-spherical particles. Measurements performed under such circumstances are critical as constraints of Mie theory are not valid any more.[194]

4.1.2. Polarisation Intensity Differential Scattering

In Fig. 4.6 a schematic set-up of a laser diffractometer as it is implemented in the LS 13320 of Beckmann-Coulter is illustrated. In order to achieve high accuracy of particle size measurements in a large dynamic size range (40 nm - 2,000 µm), the standard diffractometer set-up is upgraded by an additional Fourier lens and a specific measurement principle, called polarisation intensity differential scattering (PIDS).[21]

Standard diffractometers are composed of a light source, a collimator,

sample cell, one Fourier lens and a series of detectors. A laser-light beam of specific wavelength is collimated to completely illuminates all particles within the sample cell. The Fourier lens consecutively arranged to the sample cell bundles light diffracted from randomly distributed particles and directs it to the detectors at different angles. There, the flux defined as light intensity per detector area is measured and applied as raw material to further, software-based numerical calculations yielding particle sizes.[194, 199]

Since scattering pattern are governed by the ratio between wavelength of light and particle size, laser diffractometers with single light sources, respectively wavelength, usually utilise relatively narrow measurement ranges of particle sizes. Moreover, most detector constructions and detection surface areas are not feasible to distinguish between scattering pattern generated by large and small particles. Consequently, the detectable angular range and therefore the measurable particle size range are limited.[21]

To broaden the restricted angular range and thus the dynamic particle size range, a second Fourier lens is implemented. The advantages of this procedure are twofold: First, light scattered at very large angles is bundled and brought into focus of specifically arranged detectors and second, measurement artefacts such as chromatic or colour aberration are avoided. The characterisation of particles in the sub-micron range is often subjected to resolution problems resulting in poor information extraction out of scattering pattern. Bott and Hart (1991) developed therefore the PIDS technology, an alternative procedure that allows characterisation of particle sizes in the sub-micron range. The measurement principle utilises the polarisation sensitivity of particles, which are smaller than the wavelength of the incident light.[21]

PIDS is based upon the transverse, electromagnetic wave nature of light; the oscillation of its electric and magnetic field propagate in the same direction, which is perpendicular to the direction of the incident light beam. When the beam encounters a small particle, an oscillation dipole moment within the particle is induced by the oscillating electric field. As a result of this, the oscillating dipole of the particle scatters light in all directions except in that of the propagating light. The scattering pattern of the particles is sensitive to light polarisation, either vertical or horizontal, and depends on the ratio between particle size and wavelength. Thus, the measurement of the PIDS-signal is performed at three different wavelengths (450, 600 and

900 nm) and alternating polarisation of 90°, respectively. The resulting differences in the light-intensities scattered perpendicular or parallel to the scattering plane are recorded as a function of scattering angle. Detectors are appropriately arranged to the scattering direction of light. Information obtained from the PIDS-intensities is then applied to the standard algorithm of the data generated by the primary laser. From this, a continuous PSD is computed.[21]

4.2. Protein secondary structure analysis

Proteins are ubiquitous in nature and highly relevant for the life-sustaining metabolism of organisms. The biological function of proteins is directly related to their structure, which is unique for each protein. Despite the diversity, all proteins feature the same basic structural elements. The primary structure comprises amino acids linearly linked through peptide bonds to a polypeptide chain. Such chains fold to three-dimensional structures referred to as secondary structure. Different secondary structural elements stabilised via intra- and intermolecular interactions between amino acids in the backbone sequence can evolve: α-helices, β-strands, reverse turns or loops. Proteins that lack secondary structure form irregular structural elements, like random coil conformation. The tertiary structure is a superior spacial arrangement of proteins and is composed of several secondary structure units. Hydrogen bonds, van der Waals forces and Coulomb interactions between tertiary structure units form the superior quaternary structure.[22]

In food processing, the functional properties of proteins such as stabilisation, emulsification and gelatinisation are crucial for final product quality. However, the conditions that proteins encounter during processing can cause aggregation or denaturation of the protein resulting in structural alterations and consequently changes or losses of functionality. During spray drying, proteins are subjected to a variety of stress factors like temperature, shear forces and dehydration. Lee et al. (2002) observed that already low drying or inlet temperatures caused denaturation.[109] Upon atomization, proteins are exposed to very large air-liquid interfaces provoking protein unfolding due to entropic forces and thus alterations in their biological activity.[179, 186] The impact of severe shear stresses during spray drying is rather unknown. However, it is assumed that combined effects of shear forces and large air/liquid interfaces can result in protein denatura-

tion or aggregation due to constant renewal of air-liquid interfaces.[10, 115] In general, the native protein structure is usually maintained in its natural environment. In aqueous solution, proteins interact with surrounding water molecules via hydrogen bonding. Water removal upon dehydration can result in structural changes and loss in functionality.[3] The integrity of the protein functionality is crucial for the spray drying efficiency. Purely stabilised emulsion droplets can result in powder particles exhibiting a high free surface content upon lypophilisation.

Vibrational spectroscopies such as FTIR or CD proved to be reliable techniques to analyse semi-quantitatively conformational changes in protein secondary structure and for studying protein adsorption dynamics.[106] Alternatively, X-ray crystallography and nuclear magnetic resonance spectroscopy are applicable though former is limited to proteins capable of crystal formation and latter involves complex, time-consuming spectra interpretation for proteins larger than 20 kDa. With FTIR, the protein secondary structure can be examined in aqueous-based solutions, dried states and in deuterated forms.[172]

4.2.1. Fourier-transform infrared spectroscopy

Infrared spectroscopy is a widely used optical technique to identify and quantify organic and inorganic substances in diverse types of matter as it is fast, simple, non-destructive and non-invasive. It is a reliable method for structure determination of small molecules like carbon dioxide in greenhouse chambers but also of rather larger, more complex molecules such as membrane proteins.[12] Food industries exploit infrared spectroscopic measurements for monitoring of, *e.g.* enzyme reaction and sugar metabolic processes and for quality evaluation and control of food, both during cultivation of raw material and sensory trials of final products. Among all available infrared spectrometers, FTIR spectrometers are the ones most used.[73]

Qualitatively and quantitatively analysis of numerous molecules are based on vibrational and rotational transitions of molecules induced by absorption of electromagnetic radiation of light in the infrared region. The spectral region of infrared radiation ranges from wavelengths of 0.75 µm to 1,000 µm divided into three sub-regions: near-infrared (0.78 - 2.5 µm), mid-infrared (2.5 - 50 µm) and far-infrared (50 - 1,000 µm) region. In FTIR-spectra, the absorption is commonly plotted against the wavenumber, which is the

reciprocal of the wavelength. A pre-requisite of infrared light absorption is that the frequency of light coincides with that of the vibration and an oscillating dipole moment of the molecule exists. The probability of absorption and the frequency of vibration depend on chemical properties of the molecule groups such as masses, electron density and binding angle, strength and polarity of vibrating bonds, as well as on intra- and intermolecular interactions. Molecules vibrate in different principial vibrational modes: Stretching, bending and torsional vibration. The first two involve either a change in bond length or bond angle. Since different forces are required to cause the respective vibration, each vibrational mode results in a specific resonant frequency that matches the transition energy of the vibrating bond or group. Any alteration in intra- and intermolecular bond strength is reflected in the vibrational spectrum.[12, 27]

Conventional spectrometer such as dispersive instruments are of limited use as only qualitative results are obtained, particularly for rather complex molecules like proteins, and aqueous solutions are not measurable. Such limitations are overcome by FTIR spectrometer. In contrast to dispersive techniques, FTIR provides a higher resolution, sensitivity, signal-to-noise ratio (SNR) and frequency accuracy. This is explained by the different construction and operation of FTIR spectrometers.[173]

In conventional spectrometers, spectra are obtained by measuring the intensity of light of a single wavelength that has been filtered out from light passing through a monochromator. A complete spectrum is scanned upon variation of the monochromator's wavelength settings so that one spectral resolution element at a time is obtained. FTIR spectrometers are equipped with an interferometer that facilitates to generate data from the whole spectral range simultaneously. Nowadays, different types of interferometer are implemented in FTIR spectrometer though the principle features of an interferometer are commonly explained by referring to the Michealson interferometer. A typical Michelson interferometer is well explained in [173]. Interferometers produce a considerable amount of raw data that has to be transformed into the desired result, which is the amount of light emitted at each wavelength. By computational processing, the detected light intensities for each interferometer set-up are related to the measured spectrum by Fourier transformation.[12]

4.2.2. Protein FTIR spectra analysis

The improved SNR, sensitivity, resolution and frequency accuracy of FTIR spectrometers contributed to their increased popularity for fast and ease protein secondary structure analysis and acquisition of high-quality spectra from low protein sample amounts.[172] The good SNR and high wavenumber precision facilitate computational data manipulation, which is often essential for understanding spectra-structure correlations of complex proteins. Valuable spectral information can be obtained upon mathematical data treatment such as interactive spectral subtraction, Fourier self-deconvolution, curve fitting, second derivative calculations and precise measurement of band maxima.[173]

When the mid-infrared light wave interacts with the protein's polypeptide chains, nine characteristic vibrational modes can be recognised, namely, amide A, B, and I-VII. The characteristic infrared bands of peptide linkage are described in Table 4.1.[106] Due to the high conformational sensitivity to small variations in the molecular geometry and hydrogen bonding pattern, the amide I proved to be the most suitable vibrational mode to indicate changes in the composition and conformation of protein secondary structure.[45, 173] Stretching vibrations of C=O bonds of the amid group coupled to the in-phase bending of the N-H bond and the stretching of C-N bond are responsible for infrared bands in the region between 1,600 and 1,700 cm^{-1}.[172] However, proteins consist of a variety of polypeptide segments folded into complex three-dimensional secondary structural elements. Since each of the segments contributes to the infrared spectral signal, extensive band overlapping of thus indistinguishable absorption maxima occurs resulting in a featureless, instrumentally unresolvable amide I band. By mathematical-supported resolution-enhancement methodologies, individual band components can be resolved. Therefore, it is possible to quantify the relative contribution of secondary structural elements to the band features.[173]

With regard to the quantification of secondary structure elements, it is assumed that any protein is a linear sum of a few fundamental structure elements. The amide I band assignment to α-helical, β-sheet, β-turn, random coil and irregular shaped elements of the secondary structure by mathematical procedures mainly based on band narrowing for better visualisation involves many, non-negligible critical aspects. Susi and Byler (1986) did

Table 4.1.: Characteristic vibrational modes of peptide linkage induced by mid-infrared light [106]

Vibrational mode	**Approximate frequency (cm^{-1})**	**Description**
Amide A	3,300	NH stretching
Amide B	3,100	NH stretching
Amide I	1,600-1,690	C=O stretching
Amide II	1,480-1,575	CN stretching, NH bending
Amide III	1,229-1,301	CN stretching, NH bending
Amide IV	625-767	OCN bending
Amide V	640-800	Out-of-plane NH bending
Amide VI	537-606	Out-of-plane C=O bending
Amide VII	200	Skeletal torsion

pioneering work on data manipulation in [173] and explained in detail the resolution-enhancement methods with emphasis on second derivative calculations and Fourier self-deconvolution (FSD).

Briefly, second derivative calculations are performed to enhance the spectra resolution by removing baseline offsets and slopes from the spectrum. To avoid an increase in noise, derivatives are calculated by using the Savitzky-Golay algorithm as smoothing function.[159] FSD involves the deconvolution of the line shape of the spectrum, which is of Lorentzian-shape in case of the amide I band, resulting in a time-domain function or interferogram. Thereby, spectral bands are narrowed by simultaneously maintaining the integral intensities and frequencies of each band. In order to deconvolve spectra properly, two constants have to be applied to the calculations, the half-width at half-height of unresolved bands, σ, and the resolution efficiency factor, K. Both constants depend on the substance analysed. Improper selection of these two constants results in serious errors and artefacts such as unreal side slopes, distorted spectra and high noise.[173]

In general, FSD and second derivative calculations have to be performed with care as both enhance water vapour bands, interference fringes and impurity bands. According to the resolved bands, here by considering both deviated and deconvoluted spectra, secondary structure elements are assigned and the exact peak position, widths, heights and areas of overlapping bands are determined by iterative, non-linear curve fitting procedures.[106]

Band assignment is further complicated by protein secondary analysis in aqueous solutions. Water absorption occurs among others around 1645 cm^{-1}, which is, due to H-O-H bending vibrations, in the same frequency range of the amide I band. Since the intensity of water absorbance is of one magnitude larger than that of the amide I band, the resulting overlap impedes spectral analysis of the amide I band. Elaborate sample techniques and the high sensitivity of FTIR spectrometer make it possible to digitally subtract water bands from protein spectra. However, precise and accurate measurement of frequency and intensity of the amide I band are a pre-requisite to avoid spectral artefacts. Measurements of protein solubilised in deuterated water (D_2O) provide a suitable alternative to avoid the "water-problem" since the absorption region of D_2O does not interfere with that of the amide I band. Limitations of this procedure are that an accurate protein secondary structure analysis implies a complete H-D-exchange, which is often not given or determinable. Additionally, it is not known how D_2O affects the protein structure and if the obtained results are comparable to the structure of proteins in their natural environment.[106]

5. Materials and Methods

5.1. Materials

Soybeans (Davert) for the oleosome production were bought from a local supermarket. Ultra pure water filtered with a Millipore device (Billerica, MA/USA) was used for all preparation steps. For oleosome digestion, trypsin NB from porcine pancreas (Cat. No. 37294, tryptic activity ≥50 µkat/ (Ph.Eur.), Serva, Germany) was used, which mainly contains trypsin but also minor contents of chymotrypsin and elastase.

For the preparation of the buffer solutions, the following chemicals were used: Phosphoric acid, ACS reagent (Sigma-Aldrich, Munich, Germany), acetic acid (≥99.8 %, Sigma-Aldrich, Munich, Germany), monosodium phosphate (≥99.0 %, Fluka, Munich, Germany), MES (≥99 %, Carl Roth, Karlsruhe, Germany) and Tris (≥99.9 %, Sigma-Aldrich, Munich, Germany).

5.1.1. Maltodextrin

For the encapsulation of oleosomes via spray drying, maltodextrin (MD) with a dextrose equivalent (DE) of 16.5-19.5 (CAS-number: 9050-36-6, Sigma-Aldrich, Saint Louis, USA) was used. Maltodextrin [$(C_6H_{10}O_5)_nH_2O$] is commonly obtained by acidic or enzymatic hydrolysis of starch and consists of α-D-glucose units linked primarily by (1→4) glycosidic linkages. The DE index expresses the relationship between the amount of reducing sugars and dextrose or glucose. For example, MD with a DE of 20 contains 0.8 % glucose, 5.5 % maltose, 11 % maltotriose and 82.7 % higher saccharides.[101] The properties and functionality of MD vary with the DE and the degree of polymerisation. MD, exhibiting a lower content of high molecular weight polysaccharides, are better soluble in water, than those with a higher content. In principle, they are virtually non-hygroscopic compared to corn syrups, in particular those with the lowest DE. The higher the level of high molecular weight saccharides, the higher the viscosity of MD solutions. Low

DE maltodextrins can effectively bind more fat, as their composition and thus their binding are comparable to starch. In the food industry, MD is widely used due to its multifaceted functions in food systems, particularly its contribution to a creamy and smooth mouthfeeling in many food products.[101]

5.2. Oleosome extraction

Oleosomes were extracted from soybeans by a modified aqueous flotation-centrifugation method proposed by Chen and Ono.[31] Dried soybeans were soaked in deionized water at 4 °C for at least 12 h. Subsequently, the excessive water was decanted and fresh water was added to the soaked beans to obtain a 10 % soybean-to-water ratio. The soybeans were then ground in a Vorwerk Thermomix TM31 at a speed of 10,200 rpm for 90 s. Raw soy milk was obtained by filtering the resulting slurry through two layers of Kimtech science precision wipes (21 × 11 cm^2, Kimberly Clark). To remove residual storage proteins, 25 wt% sucrose was added to the soy milk and the pH-value was adjusted to 11.0 with 1 $mol \cdot L^{-1}$ NaOH solution. The solution was divided into portions of 50 mL and centrifuged (15,000g, 4 °C) for at least 5 h. Due to the centrifugal forces and density gradients, the solution separated into three layers: 1) the cream layer containing the main portion of oleosomes, 2) the supernatant and 3) the sediment with precipitated storage proteins and residual soybean material. For further purification, the floating cream layer was taken off with a spoon, redispersed in a 20 wt% sucrose solution of pH 11.0 and centrifuged anew. This washing step was performed twice. The purified oleosome cream layers were collected and dispersed in 50 mL of deionized water. Subsequently, the oleosome solution was dialysed in a cellulose tube (MWCO 12,000−14,000, b = 45 mm, wall thickness = 20 µm) from ZelluTrans (Carl Roth, Karlsruhe, Germany) to remove the sucrose used for the extraction of oleosomes. Finally, an oil-in-water emulsion of intact soybean oleosomes was obtained. Until use, oleosomes were stored at 4 °C in the fridge for time periods shorter than 48 h. Otherwise, 0.01 wt% sodium acid (NaN_3) was additionally added to prevent microbial spoilage. The oleosome concentration appropriate for analysis was adjusted by dilution with buffer solutions or by concentration via centrifugation. A halogen moisture analyser (Mettler Toledo HR73, Giessen, Germany) was used to determine the water content of oleosome

emulsions.

5.3. Enzymatic digestion

One milligram of trypsin from porcine pancreas was added to 1 mL of dialysed, isolated, intact oleosomes ($c = 15$ wt%). The digestion was performed at 25 °C for 1 h at 500 rpm in a HLC ThermoMixer MKR 13 (Digital Biomedical Imaging Systems AG, Pforzheim, Germany).

5.4. Oleosin and soy oil extraction

The isolation of oleosins from soybean oleosomes was performed by a modified method developed by [140]. First, oleosomes were centrifuged at 5,000g for 3 h to obtain a cream layer of approximately 45 % oleosomes. Subsequently, 1 volume of oleosome cream layer was properly mixed in 5 volumes of diethylether to extract the soy oil. After stirring for 20 min, the mixture was centrifuged at 5,000g for 15 min. The upper organic phase was discarded and the washing step was performed another two times. Chloroform-methanol and water (4:2:1) were added to the residual cream layer constituents and centrifuged anew at 5,000g for 15 min. A layer of white material, formed at the interface between the upper chloroform and lower methanol-water layer, was collected and again redispersed in chloroform-methanol-water to remove residual lipid fractions. After centrifugation and evaporation of organic solvents, the washed cream layer was freeze-dried and redispersed in acetone followed by centrifugation. By using small amounts of water, the precipitate was collected and freeze-dried again. This step was performed twice. Subsequently, the oleosin powder was stored at a dry and dark place until further analysis.

5.5. Particle sizing methods

5.5.1. Laser diffractometry

Laser diffractometers yield volume-weighted particle/droplet size distributions. For the measurements, two different laser diffractometer instruments were used, one from Retsch Technology, Germany, (Horiba LA-950) and one from Beckmann-Coulter, Germany, (LS 13320), whereas most of the

measurements were performed by using the LS 13320. The measurement range of the LA-950 is 0.01 - 3,000 µm and that of the LS 13320 is 0.04 - 2,000 µm. While the Horiba LA-950 covers the complete measurement range with two LED-light sources (blue and red) of different wavelengths (405 and 650 nm), the LS 13320 utilises three different wavelengths (450, 600 and 900 nm). The measurement principle of laser diffractometry has been already explained in detail in Subsec. 4.1. In order to avoid multi-scattering effects, the samples were diluted as appropriate prior to measurement. In the LA-950, the sample was measured in a rectangular cuvette (15 mL) and stirred continuously with a magnetic stir bar during measurement. In the LS 13320, the sample was circulated via pumping in a sample cell to pass the incident light.

For evaluation of the particle/droplet size distribution of native and trypsin-digested oleosomes, the cumulative volume distribution, Q_3 (vol%), the volume frequency distribution, q_3 (%/µm), and characteristic diameters were measured. Cumulative volume distribution is defined as the average volume of particles/droplets that are equal to or smaller than a specific particle/droplet size, D. Volume frequency distribution describes the amount of particles/droplets within a certain class of volume fraction. Following parameters were derived from the particle/droplet size distribution: $D[4,3]$, $D[3,2]$, $D(\mathrm{v}, 0.1)$, $D(\mathrm{v}, 0.5)$ and $D(\mathrm{v}, 0.9)$. $D(\mathrm{v}, 0.1)$, $D(\mathrm{v}, 0.5)$ and $D(\mathrm{v}, 0.9)$ express the volume diameter where 10, 50 and 90 % of the distribution are below this diameter.

Evaluation of complex refractive index According to the Mie theory [131], the complex refractive index, n, (Eq. 5.1), which depends on the wavelength of incident light and the temperature of the medium, is required for a precise characterisation of the particle size distribution of oleosomes.

$$n = n_\mathrm{r} + i n_\mathrm{i} \tag{5.1}$$

where n_r is the real part of the refractive index that typically describes the bending of an incident light ray at the surface of an object. The imaginary part of the complex refractive index is denoted by n_i, also referred to as attenuation coefficient that quantitatively describes the turbidity of a sample. Here, the loss of directed beam of light per unit length of propagation through a medium due to scattering and/or absorption is measured.[24, 128]

For highly turbid and heterogeneous media like oleosome emulsions, a meaningful and simultaneously determination of the real and imaginary part of the complex refractive index is critical. Particularly multi-scattering effects, relatively pronounced polydispersity and the chemical composition of the dispersed emulsion droplets, that exhibit different optical properties, complicate a direct and accurate measurement.[46]

The diffractive data was calculated using a predefined optical model for liquid disperse formulations of small droplets (≤10 µm) according to Mie theory. However, the refractive index of oleosomes is not yet known and could not be readily determined due to the constituents' inhomogeneity. A detailed evaluation of methodologies that are appropriate for the determination of the complex refractive index of oleosomes would go beyond the scope of this thesis. Instead, the real parts of the refractive indices (n_r) were estimated according to literature values. These are 1.47 for soybean oil [201] and range from 1.594 to 1.630 for common proteins (*e.g.*, casein, lactoglobulin, lysozyme) [126]. The refractive index of phospholipids is assumed to be identical to soybean oil. For the attenuation coefficient, either 0 (Horiba LA-950), 0.01 or 0.1 (LS 13320) is used, which corresponds to the guidelines of the laser diffractometer manufacturer for lightly coloured translucent materials. Test trials, where the measured scattering intensities were compared with the calculated ones (variance $\chi 2 = 0.45$), verified appropriate indices of 1.6 (real part) and 0, respectively 0.01 (attenuation coefficient). The ionic strength of the oleosome-buffer solution was kept constant at 10 mM, and measurements were conducted at room temperature (21 °C). Particle/droplet size distributions were measured in triplicate using three different samples.

5.5.2. Light microscopy

A light microscope IX81 (Olympus, Japan) with an oil immersion objective (UPLFL 100xO, NA 1.3, W.D. 0.1 mm) was used to determine the particle size of native oleosomes dispersed in different buffer solutions (10 mM, NaCl, varying pH-value). Oleosome emulsions were diluted as appropriated, placed onto a specimen holder and covered with a cover slid. Sample preparation and image acquisition were performed at 21 °C. Particle sizes were measured using the ImageJ software package.

5.6. Methodologies for oleosome characterisation

5.6.1. ζ-potential measurements

The ζ-potential was measured on basis of the laser Doppler anemometry (LDA) and deduced from the electrophoretic mobility of droplets, having a charged surface, according to the Helmholtz-Smoluchowski equation (Eq. 5.2).

By application of an external field, the charged dispersed droplets move with different velocity detected by laser light scattering. Assuming that oleosomes are spherical with a smooth surface, the ζ-potential, ζ, is a function of the shear viscosity, η, the velocity of the particles, ν, the external electrical field, E, and the dielectric constant, ε.

$$\zeta = \frac{4\pi\eta\nu}{E\varepsilon} \tag{5.2}$$

Prior to measurement, native and trypsin-digested oleosomes were diluted using buffer solutions (10 mM NaCl, varying pH-value) to avoid multiscattering effects. Diluted oleosome emulsions were filled into a cuvette, which was then placed into the working chamber of a Zetasizer Nano ZS (Malvern, Herrenberg, Germany). Measurements were conducted in duplicate from two freshly prepared samples at 25 °C.

5.6.2. Drop shape analysis

Axisymmetric drop shape analysis (ADSA) was applied to investigate the dynamic properties of native and digested oleosome layers at the air-water interface. An automated drop tensiometer OCA20 (Dataphysics GmbH, Filderstadt, Germany) (Fig. 5.1) was used to determine the interfacial surface pressure of native and trypsin-digested oleosomes dispersed in a buffer solution of pH 2 and at constant ionic strength (10 mM, NaCl). The shape changes of the pendant drop were recorded with a high speed frame grabber (200 frames/s). Static measurements were conducted in a temperature-controlled chamber ($T = 22.8 \pm 0.2$ °C). The syringe placed in the automated dosing system was enclosed with a cuvette, which was filled with a few drops of distilled water and tightly sealed with Parafilm to prevent water evaporation and thus changes in the drop volume due to air cur-

rent. The drop was formed with a dosage rate of 5 µL/s at the tip of a stainless steel hydrophobized capillary. 15.6-1560 mg/L of native and trypsin-digested oleosomes were injected into the drop, having a volume of 15 ± 0.3 µL. Measurements were started after a waiting time of 30 s to ensure that the drop volume could equilibrate after the drop formation for each measurement equally. Changes in the drop shape were monitored for 600 s. A software belonging to the drop tensiometer OCA20 was used to fit the Gaussian-Laplace equation of capillary to the experimental drop shape coordinates and thus to be able to determine the interfacial tension.[33] The surface pressure was calculated according to $\pi = \sigma_o - \sigma$ and plotted against the time. Here, σ_0 is the surface tension of water (72.65 mN/m at 22.8 °C) and σ the measured surface tension. Measurements were performed at least in duplicate.

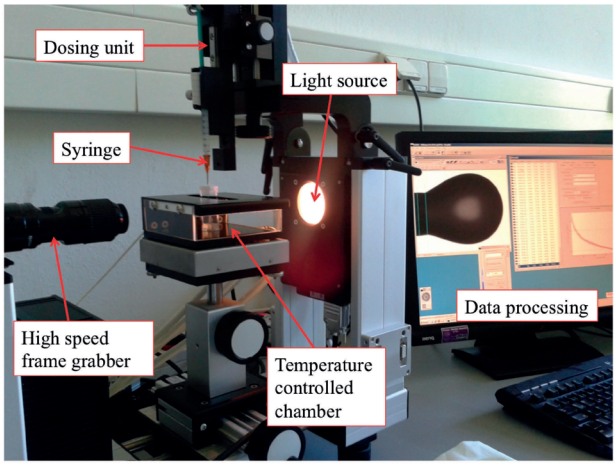

Figure 5.1.: Pendant drop tensiometer OCA20 from Dataphysics GmbH used for the analysis of the interfacial behaviour of native and trypsin-digested oleosomes. (This measurement system belongs to the Department of Food Technology and Food Material Science of the Technical University Berlin.)

5.6.3. Temperature treatment

Native oleosome emulsions with a concentration of 15 wt%, having a pH-value of either 3 or 7, were subjected to temperatures of 40, 60, 80, and 99 °C for 1 h while mixing at 700 rpm. Temperature treatment was performed using a HLC ThermoMixer MKR 13 (Digital Biomedical Imaging Systems

AG, Pforzheim, Germany). Before analysis, oleosome emulsions were allowed to cool down to room temperature. Particle size measurements, using the laser diffractometer Horiba LA-950, and ζ-potential measurements were performed as described previously. For dilution, buffer solutions of pH-values appropriate to the pH-value of the used oleosome emulsion, which is pH 3 or 7, were used.

5.6.4. Shear stress treatment

Native oleosome emulsions, having a concentration of 3.5 and 15 wt%, were subjected to shear stress using a T18 basic Ultra-Turrax (IKA, Staufen, Germany) at 3,500 or 7,000 rpm for 10 or 30 s, respectively. Particle size measurements employing the laser diffractometer LS 13320 were performed directly after shear stress treatment. In order to investigate shear stresses to which the liquid feed solution is subjected during spray drying, the Büchi B-290 Mini-Spray Dryer was used to atomize oleosome emulsions (3.5 and 15 wt%) by the spray nozzle at room temperature (21 °C). The atomized oleosome emulsion was collected right after the spray nozzle with a glass container. Different settings of spray air and liquid flow rates were applied as specified in Table 5.3.

5.7. Spray drying of oleosomes

5.7.1. Sample preparation

The oleosome (OB) emulsions were diluted as appropriate using a buffer solution of pH 7 and at an ionic strength of 10 mM (NaCl). Maltodextrin solutions were prepared by dissolving weighted amounts of powder into buffer of same pH-value and ionic strength as used for the emulsions. Emulsions containing MD were obtained by diluting oleosome emulsions with different ratios of buffer (pH 7, 10 mM NaCl) and MD solution to obtain samples with the same oleosome concentration (3.5 wt%) but different MD concentration (5 and 10 wt%). Table 5.1 and Table 5.2 specify the total content (wt%) and content on dry weight basis (wt%) of compounds included in the feed emulsions used for spray drying.

Table 5.1.: Total content (wt%) of compounds in feed emulsions used for spray drying

Sample	Solid content (wt%)	c_{OB} (wt%)	c_{MD} (wt%)	c_{oil} (wt%)	$c_{protein}$ (wt%)	c_{PL} (wt%)
OBc15	15.0	15.0	0	13.8	0.6	0.6
OBc30	30.0	30.0	0	27.6	1.2	1.2
OBc3.5_MDc5	8.5	3.5	5	3.2	0.14	0.14
OBc3.5_MDc10	13.5	3.5	10	3.2	0.14	0.14

Table 5.2.: Concentration of compounds on dry weight basis (wt%) in the feed emulsions used for spray drying

Sample	Solid content (wt%)	c_{OB} (wt%)	c_{MD} (wt%)	c_{oil} (wt%)	$c_{protein}$ (wt%)	c_{PL} (wt%)
OBc3.5_MDc5	8.5	41.2	48.8	37.6	1.6	1.6
OBc3.5_MDc10	13.5	26.0	74.0	23.8	1.1	1.1

5.7.2. Spray drying

The prepared feed emulsions of varying oleosome and MD concentration were spray dried using a Büchi B-290 Mini-Spray Dryer (Büchi Labortechnik, Flawil, Switzerland). The principle set-up of this spray dryer is shown in Fig. 5.2. In order to achieve an efficient powder separation, a high performance glass cyclone was used. For the evaluation of the process parameters, the samples were spray dried at three different inlet drying temperatures (T_{in}), which were set to 100, 130 and 180 °C and four different ratios of spray air and liquid feed flow rate (L/h), respectively. The different sets of spray air and liquid feed-flow rate are specified in Table 5.3. The outlet temperatures in terms of varying process parameters and different sample composition are shown in the appendix (Fig. B.1). The liquid samples were atomised using a two-fluid nozzle, having a cap-orifice diameter of 0.7 mm. Liquid feed was pumped to the nozzle via a peristaltic pump using a silicone tubing (d = 3 mm). Inert nitrogen gas from an in-house supply was used as spray air, which was heated to the appropriate drying temperature and controlled by a variable area flow meter.

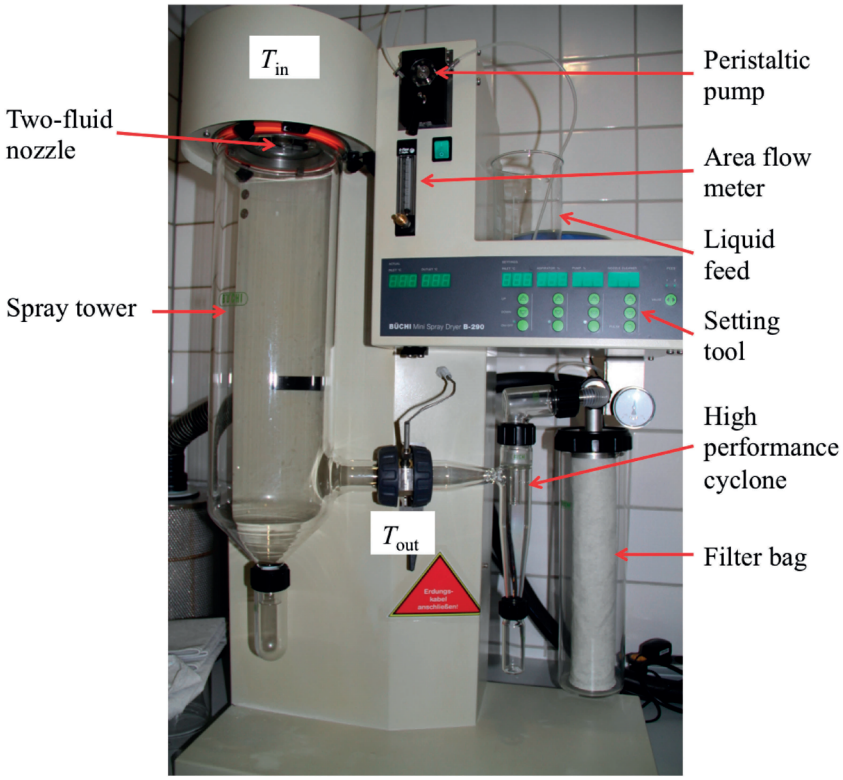

Figure 5.2.: Lab-scale Büchi B-290 Mini-Spray Dryer.

Drying air and liquid feed were sprayed in the same direction, thus contact of the liquid and the drying air occurred in a co-current manner. The aspirator speed was set to 100 % for all drying processes. All sample compositions as specified in Table 5.1 were spray dried at all differently combined process parameters as indicated in Table 5.3. Directly after drying, the powder samples were collected, weighted and transferred into small glass containers just by pouring to avoid mechanical stress. The glass containers were tightly sealed and stored at a dry place until further analysis. The yield (%) was calculated according to Yield $= \frac{\text{Dry weight}}{\text{Weighted sample}} \times 100$. Due to the limited amount of oleosomes that could be produced by the lab-scale extraction process, samples produced at all possible process parameters were only spray dried once.

Table 5.3.: Sets of varying spray air and liquid feed flow rates applied for spray drying oleosome emulsions of varying oleosome and MD concentration

air flow rate (L/h)	**liquid flow rate (L/h)**
439	0.3
	0.16
1052	0.3
	0.16

5.8. Methodologies for powder characterisation

5.8.1. Scanning electron microscopy

The microstructure of spray dried oleosome powders was analysed using a Leo Gemini 1530 (Zeiss, Oberkochen, Germany) scanning electron microscope (SEM). A few particles of the powder sample were dusted onto aluminium holder using double-adhesive conductive pads (d = 12 mm, Plano GmbH, Wetzlar, Germany). By directing a jet of dry air at the surface of the holder, excess particles were removed.

5.8.2. Confocal laser scanning microscopy

Confocal laser scanning microscopy (CLSM) is one of a few techniques that allows imaging of high-resolution optical sections through a thick specimen. Thereby, maximum resolved information about the microstructure of a bulk material, such as powder particles, can be obtained with a minimum of sample preparation. For image recording, a single, precisely point in the sample, the so-called focal point, is illuminated by a laser source focused on this point by the objective lens. The illuminated spot scatters and reflects laser light, and if the sample is fluorescent, it also emits fluorescent light, which are then re-collected by the objective lens. A beam splitter separates off some wavelengths of the (fluorescent) light. Out-of-focus light is suppressed by a pinhole to facilitate sharper images. This "filtered" light carries the information from the sample into a photodetector device, where its signal intensity is detected. Different focal planes of the image can be created by deflecting the beam in the x-y, x-z or the y-z dimension by a scanning device and thereby scanning the focused spot on the sample. By scanning on a defined line, information about the three-dimensional microstructure can be gained.[2, 19]

Sample preparation For the analysis of the spray dried oleosomes, oleosome emulsions were stained, prior to spray drying, with two different fluorescent dyes to be able to differentiate between oil and protein sections in the final powder. 1 mg of Nile red, a lipophilic fluorescent dye with maximum excitation at $\lambda_{ex} = 530\,nm$ and maximum emission at $\lambda_{em} = 635\,nm$, was used to stain the oil fraction in 1 mL of a 15 wt% oleosome emulsion. For protein labelling, fluorescin isothiocyanate (FITC) was used, which has a maximum excitation at $\lambda_{ex} = 492\,nm$ and maximum emission at λ_{em}=518 nm. The coupling procedure of the FITC isomer to the protein was performed according to the preparation instructions provided by the manufacturer (Sigma-Aldrich, Saint Louis, MO/USA). First, a stock solution of FITC was prepared by dissolving 5 mg FITC into 1 mL DMSO. The pH-value of the oleosome emulsion containing 6 mg/mL oleosin was adjusted to 9 using sodium carbonate (Na_2CO_3). While continuously stirring the oleosome emulsion, 50 µL of FITC-solution per 1 mL oleosome emulsion were slowly added in 5 µL aliquots. The reaction of the FITC with the oleosin was carried out in the dark for at least 8 h at 4 °C. Subsequently, 50 mM of NH_4Cl were added to stop the reaction. The emulsion was further incubated for

2 h at 4 °C. Excessive FITC was removed by dialysis in the dark for 12 h at 4 °C using Thermo Scientific Slide-A-Lyzer G2 Dialysis cassettes (20K MWCO). After the dialysis, the labelled pure oleosome emulsions (15 wt%) were spray dried at 100 and 180 °C. For the encapsulation with MD, the emulsions were diluted with buffer solution (pH 9, 10 mM) and MD was added as required to obtained an emulsion with 3.5 wt% oleosomes and 5 or 10 wt% MD. The drying temperatures were 100 and 180 °C.

CLSM imaging Few particles of powder samples were dusted into eight well-chambered borosilicate cover glass systems (Nunc, LabTek, Thermo Fisher Scientific, USA) and covered with immersion oil ($n = 1.515$). A commercial confocal laser scanning system FluoView 300 FV 300 (Olympus, Japan) in combination with an inverted microscope IX70 (Olympus, Japan) was used to analyse the microstructure of spray dried oleosome powders. An oil-immersion objective (PLAPON 60xO, NA 1.4, W.D. 0.15 mm, Olympus, Japan) was used and images were taken at 90 µm sample depth. Fluorescence of Nile red was excited by the blue laser at 543 nm. The emitted light was collected after passing through a LP 565 long band emission filter. An argon fibre laser (488 nm) was employed to excite the fluorescence of FITC. Emitted light thereof was filtered by a band pass (BP) of an emission wavelength of 510-540 nm before detection. By exciting the fluorescent probes consecutively, multi-image acquisition was possible to obtain a composite image of FITC- and Nile-red labelled powder sections. Lasers coupled to a scanning unit allowed to record images in the xy-plane at different z-positions. The obtained CLSM images were then stacked to three-dimensional images by using the ImageJ software package, including the LOCI plugin.

5.8.3. Electron spectroscopy for chemical analysis

Electron spectroscopy for chemical analysis (ESCA), also referred to as X-ray photoelectron spectroscopy, is a surface-sensitive analysis technique, which determines quantitatively the elemental composition of the outermost layer (2-10 nm) of solid surfaces. This technique is widely used for the quantification of free surface fat on milk powder and for the evaluation of fat encapsulation efficiency [53, 63, 104]. For analysis, the solid sample is exposed to an X-ray beam generated by either an aluminium Kα-X-ray

(1486.6 eV) or magnesium Kα-X-ray (1235.6 eV) source. Photons ($h\upsilon$) penetrate with varying penetration depth into the surface of the sample, there interacting with atomic and molecular orbital electrons (Fig. 5.3).

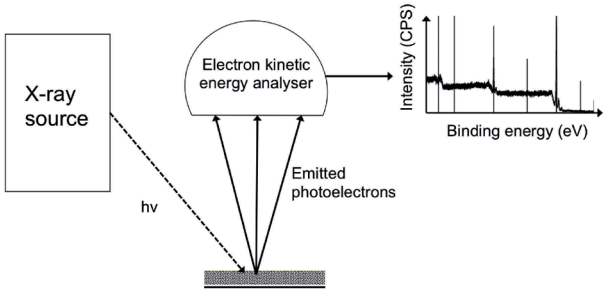

Figure 5.3.: Schematic setup of a X-ray photoelectron spectroscope used for electron spectroscopy for chemical analysis. Redrawn from [4].

As a result of this, photoelectrons, whose binding energy (E_b) is lower than the energy of the incident photons, are ejected from the sample atoms. The kinetic energy (E_K) of emitted electrons is approximately equal to the difference between the photon energy and the binding energy [4, 56] and is given by Eq. 5.3:

$$E_\mathrm{K} = h\upsilon - E_\mathrm{b} - \Phi \tag{5.3}$$

where Φ is the instrumental work function, which determines the energy required by the electron to free itself from the surface. Only electrons that do not suffer inelastic collision, which typically accounts for electrons that originate from distances far away from the surface, succeed to escape from the surface. Once being involved in inelastic collision with atoms of the solid, the electrons lose kinetic energy and only contribute to the background intensity. The distance, which an electron travels before it suffers from inelastic collision, depends on its kinetic energy and the density of the solid.[4] With increasing distance z from the surface of the material, the amount of electrons that contributes to the signal decay can be expressed by Eq. 5.4:

$$I_\mathrm{z} = I_0 e^{-z/\lambda \sin\theta} \tag{5.4}$$

where I_0 is the intensity of emitted electrons at z=0, λ is the inelastic mean free path and θ is the analysed take-off angle.[56] An electron kinetic

energy analyser detects the escaping photoelectrons. In principle, ESCA measurements are conducted under high vacuum (*e.g.* 10^{-8} mbar) to avoid scattering effects by air molecules. The recorded spectrum shows the number of detected electrons per energy interval as a function of their kinetic energy normally converted to binding energy. Each molecular element exhibits a unique spectra and it is assumed that the spectra of a mixture of elements are based on combined peaks of the individual elements.[4]

Spectra recording ESCA measurements were conducted with a SPECS (Surface Nano Analysis GmbH, Berlin Germany) at the University of Mainz, Germany. These measurements were utilised to measure the relative atomic concentration (at%) of carbon (C), oxygen (O), nitrogen (N) and phosphor (P) in spray dried oleosomes. A monochromatic magnesium Kα-X-ray (1235.6 eV) and a hemispherical capacitor analyser (PHOIBOS 100 MCD) were used for spectra recording. The instrument's work function was 4.25. The take-off angle of the electrons was 45°. Measurements were performed under high vacuum of $1.1 \cdot 10^{-8}$ to $5.5 \cdot 10^{-9}$ mbar. First, a survey spectrum from 53.6 eV to 1254.6 eV with a pass energy of 50 eV at a step size of 0.1 eV and a dwell time (time per step) of 0.1 s was recorded from the analysed sample. Thereby, an overview of the overall composition of the sample is obtained. For spectra recording of the element components, 10 scans were performed. High resolution spectra were obtained by lowering the pass energy to 13 eV and increasing the number of scans to 20. All other parameters remained the same. In general, the acquisition time of the spectra varied depending on the peak area.

The powder samples were dusted onto a double-sided adhesive carbon disc. Excessive, non-sticking particles were remove by shaking off. Spectra from oleosome constituents, such as lecithin (Serva, Heidelberg, Germany), isolated oleosin and soybean oil, as well as of MD (Sigma-Aldrich, Saint Louis, USA) were recorded to determine their elemental composition (C, O, N, P) relevant for the surface component analysis of the spray dried oleosomes. The soybean oil was placed into the working chamber 24 h prior to measurement in order to outgas the contained water by stepwise increasing the vacuum to the desired pressure. Characteristic samples of spray dried and encapsulated oleosome powders were chosen for the ESCA measurements. Thus, powders produced from emulsions of 15 wt% native oleosomes at drying temperatures of 100 and 180 °C, as well a powders of

encapsulated oleosomes (feed emulsion of 3.5 wt% oleosome and 10 wt% MD) spray dried at 100 and 180 °C were analysed. From all samples survey scans and high resolution scans were recorded and then processed using the CasaXPS software package.

Data processing First of all, the survey spectra (Fig. 5.4a) were calibrated by setting the binding energy of the C 1s peak at 285 eV. Peaks of the elements were identified by using the peak finder of the software. Relative atomic concentrations of the elements were calculated using peak areas. After a linear baseline correction, the peak areas were normalised according to the acquisition parameters and the transmission function provided by the instrument manufacturer, as well as to the sensitivity factors of the elements. Following sensitivity factors were used: 1 for C 1s, 2.85 for O 1s, 1.05 for P 2p and 1.8 for N 1s. The peaks were decomposed and the underlying profiles were fitted on basis of the Marquardt algorithm [118] with a 70 % Gaussian and 30 % Lorentzian shape function.

This procedure was applied to all spectra of pure molecular components (soybean oil, lecithin, oleosin and MD) present in the spray dried powder samples and of the spray dried powders composed of different amounts of these components. Each component in the powder is characterised by a specific ratio between the elements.[56] It is assumed that the elemental composition of the different molecular components in the powder samples can be linearly combined to obtain information about the elemental composition of the surface. Thus, the surface composition of the spray dried (encapsulated) oleosome powders can be estimated by taking into account the relative atomic concentrations (at%) of the different elements (C 1s, O 1s, P 2p, N 1s) in the pure components and in the powder. The quantification of the surface composition is then achieved by solving following matrix (Eq. 5.5):

$$\begin{pmatrix} I^1_{\text{comp.1}} & \cdot & \cdot & \cdot & \cdot & I^1_{\text{comp.}i} \\ \cdot & & & & & \cdot \\ \cdot & & & & & \cdot \\ \cdot & & & & & \cdot \\ \cdot & & & & & \cdot \\ I^n_{\text{comp.1}} & \cdot & \cdot & \cdot & \cdot & I^n_{\text{comp.}i} \end{pmatrix} \cdot \begin{pmatrix} \gamma_1 \\ \cdot \\ \cdot \\ \cdot \\ \cdot \\ \gamma_i \end{pmatrix} = \begin{pmatrix} I^1_{\text{sample}} \\ \cdot \\ \cdot \\ \cdot \\ \cdot \\ I^n_{\text{sample}} \end{pmatrix} \tag{5.5}$$

According to this matrix, the estimation of the relative surface coverage

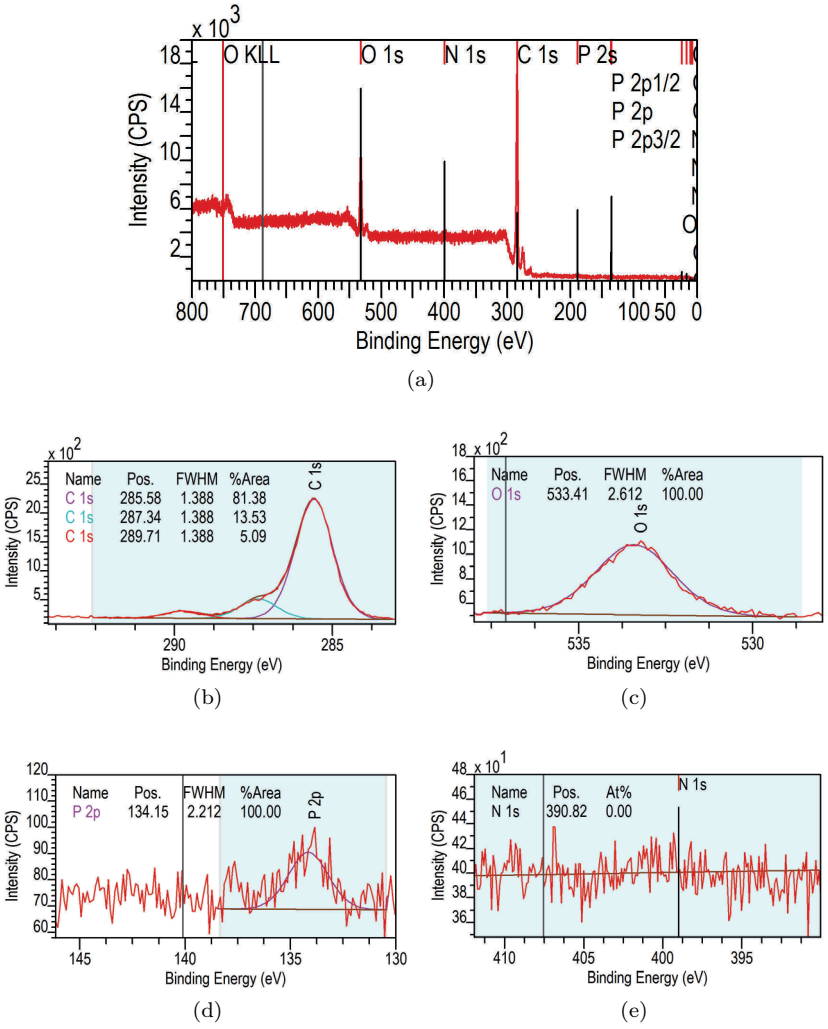

Figure 5.4.: Survey spectrum of a powder of non-encapsulated oleosomes (exemplary) and high resolution spectra thereof of the identified elements C 1s, O 1s and P 2p (N 1s not found) deconvoluted and fitted to resolve underlying peaks. (a) Survey spectrum. High resolution spectrum of (b) C 1s, (c) O 1s, (d) P 2p and (e) N 1s.

comprises i components of at least i elements (n) in the sample. $I^n_{\text{comp}.i}$ denotes the relative amount of the element (n) in the pure component (i) and I^n_{sample} the one in the sample. The relative coverage of component i is expressed as γ_i.[56]

Since oleosomes are composed of soybean oil, lecithin/PL and oleosin, it is considered that the oleosome powder samples contain C, O, P and N, whereas P exclusively originates from lecithin and N from oleosin, which was also shown by the reference measurements of the pure components. The relative atomic concentration of pure oleosome components and also of MD, here denoted by I^n_{comp}, derived from spectra processing are presented in Table 5.4.

Table 5.4.: Relative atomic concentration (at%) of oleosome components and MD, used here as encapsulating material, as measured by ESCA

Reference sample	**Relative atomic concentration (at%)**			
	C	**O**	**P**	**N**
Soybean oil	87.0	13.0	0	0
Soy lecithin	82.4	16.4	1.2	0
Oleosin	76.7	18.0	0	5.3
MD	56.0	44.0	0	0

Table 5.5.: Relative atomic concentration (at%) of powders of (encapsulated) oleosomes as measured by ESCA

Powder sample	**Relative atomic concentration (at%)**			
	C	**O**	**P**	**N**
OBc15_100 °C	85.5	12.7	1.9	0
OBc15_180 °C	84.1	14.8	1.1	0
OBc3.5_MDc10_100 °C	82.3	15.7	0	2.0
OBc3.5_MDc10_180 °C	83.1	14.4	0	2.4

Table 5.5 includes the relative amounts of C, O, P and N in the powder sample of spray dried oleosomes (I^n_{sample}) as measured by ESCA. In order to calculate the fraction (γ_i) of surface area covered with, for example soy oil

or protein, the matrix formula must be rewritten with regard to the elements measured in the analysed powder. Taking, for example the powder sample produced from 15 wt% oleosome emulsions at 100 °C (OBc15_100 °C), the system of equations (Eq. 5.6 - Eq. 5.9) to be solved is given by:

$$I^{C}_{\mathrm{OBc15,100°C}} = I^{C}_{\mathrm{oil}} \cdot \gamma_{\mathrm{oil}} + I^{C}_{\mathrm{oleosin}} \cdot \gamma_{\mathrm{oleosin}} + I^{C}_{\mathrm{lecithin}} \cdot \gamma_{\mathrm{lecithin}} \tag{5.6}$$

$$I^{O}_{\mathrm{OBc15,100°C}} = I^{O}_{\mathrm{oil}} \cdot \gamma_{\mathrm{oil}} + I^{O}_{\mathrm{oleosin}} \cdot \gamma_{\mathrm{oleosin}} + I^{O}_{\mathrm{lecithin}} \cdot \gamma_{\mathrm{lecithin}} \tag{5.7}$$

$$I^{P}_{\mathrm{OBc15,100°C}} = I^{P}_{\mathrm{lecithin}} \cdot \gamma_{\mathrm{lecithin}} \tag{5.8}$$

$$I^{N}_{\mathrm{OBc15,100°C}} = I^{N}_{\mathrm{oleosin}} \cdot \gamma_{\mathrm{oleosin}} \tag{5.9}$$

In this case, the matrix is overdetermined and was solved by the least square method.[56] This procedure was applied to all measured samples.

5.9. Methods for characterisation of reconstituted oleosomes

5.9.1. Particle size and ζ-potential measurements

Powder samples were redispersed in buffer solution of pH 7 and at an ionic strength of 10 mM (NaCl). Therefore, powder was weighted into a glass container and buffer was added while continuously stirring. The oleosome dispersions were stirred at 600 rpm for at least 1 h. Particle size measurements were performed using the laser diffractometer LS 13320 (Beckmann-Coulter, Krefeld, Germany). The obtained scattering data was calculated based on Mie-theory [131] using the real refractive index $n_{\mathrm{r}} = 1.6$ and $n_r = 1.47$ and an attenuation coefficient of 0.01, respectively. Measurements were conducted in triplicate using two different samples. ζ-potential measurements of reconstituted oleosomes were performed as explained in Subsec. 5.6.1.

5.9.2. Fourier-transform infrared spectroscopy

Sample technique and spectra recording The FTIR spectra were recorded on a Nicolet 730 equipped with a MCT (mercury-cadmium-telluride) detector in either the transmission mode or by attenuated total reflection (ATR). The spectral range has been in the near-infrared region, ranging from 4,000 to 800 cm^{-1}. For each spectrum, 100 scans were averaged at a resolution of 2 cm^{-1}. All spectra were recorded at 21 °C.

In transmission measurements, the incident infrared light passes a CaF_2 window and is absorbed according to the Beer-Lambert law [14] (Eq. 5.10)

$$A(\tilde{v}) = \log\frac{I_0}{I} = c\varepsilon(\tilde{v})d, \tag{5.10}$$

where A is the absorbance, $\tilde{v}$ is the wavenumber, I_0 the light intensity of the incident light beam, I the light intensity after transmission, c the concentration of the absorbing substance, ϵ the molar absorption index or extinction coefficient and d the path-length. In the transmission mode, highly concentrated emulsions (cream layer) of either native or spray dried and redispersed oleosomes were measured. After purification (native oleosomes) or redispersion (spray dried oleosomes) in buffer solution (pH 7, 10 mM), oleosome dispersions were centrifuged for 10 min at 14,500 rpm (MiniSpin plus Eppendorf, Hamburg, Germany) to again separated most of the aqueous phase from oleosomes. This was required in order to avoid any absorbance of water molecules, whose vibrational modes would otherwise overlap with the amide I band (1,655 cm^{-1}).[12] The obtained cream layer was then applied finely on a CaF_2 window. The bare CaF_2 was used as background measurement. Prior to measurement, the sample cell was purged for 30 min to replace the ambient humid air by dry nitrogen to avoid water absorbance.

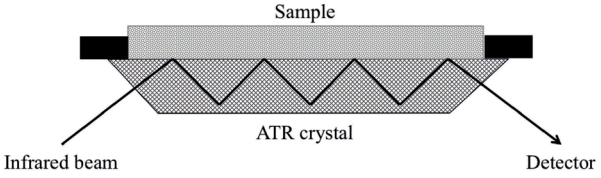

Figure 5.5.: Setup of a typical ATR crystal. Redrawn from [12].

The set-up of the attenuated total reflection is depicted in Fig. 5.5. In

contrast to transmission experiments, ATR allows to measure samples in their solid state. In principle, changes of infrared light directed into a dense crystal (here a diamond) and then, when coming into contact with the sample, totally reflected at the interface between sample and crystal, are measured. The refractive index of the crystal is ideally larger than that of the sample and typically larger than 2. Upon contact with the sample, the light is reflected several times before it leaves the crystal and is directed to the detector. This internal reflectance causes penetration of light into the sample and creates a so-called evanescent wave [130]. The penetration depth of the evanescent wave is only a few microns (0.5 to 5.0 µm). The frequency of this wave is the same as for the incident light, but its amplitude decreases exponentially with the distance from the interface. Upon absorption by the sample, the evanescent wave is attenuated and thus the intensity of the light changes, which then transmits information of the sample to the detector.[12]

Powder samples of spray dried (encapsulated) oleosomes were placed on the crystal area just enough to fully cover it. By positioning the pressure arm onto the sample/crystal area, the powder was clamped to the surface area to provide a good optical contact. An empty crystal was used for background measurements. Additional to the spray dried oleosomes, ATR measurements of the oleosome constituents, lecithin/PL (Serva, Heidelberg, Germany), extracted soybean oleosin and soybean oil, as well as MD (Sigma-Aldrich, Saint Louis, USA) were performed. The spectra of these control samples were utilised for comparison with native oleosomes.

Spectra interpretation Since the amide I band is instrumentally unresolvable, mathematical-supported resolution enhancement methods were applied to identify absorption maxima of underlying bands. Prior to spectra analysis, the amide I band in the range between 1580-1750 cm^{-1} was isolated from the complete spectra followed by baseline correction. The amide I band was then resolved by employing second derivatives and Fourier-self deconvolution (FSD). Both methods are essential for parameter estimation as starting position for the following curve fitting.[87] Second derivatives were calculated on basis of the Savitzky-Golay algorithm with a degree of 2 and a width of 9 points using Origin 9 (OriginLab Corporation, Northampton, MA/USA). By applying FSD, the amide I band was deconvoluted by a Lorentzian line shape function with a FWHM of 13 cm^{-1} and a resolution enhancement factor of 2.4 [173] using the Nicolet Software package.

Both the minima (2^{nd} derivative) and maxima (FSD) positions were considered for the identification of the individual peak positions of overlapping bands.[87] The identified peak positions were fixed and the unknown parameters, such as width (FWHM), height and area of the underlying profile were determined by Gaussian curve fitting. The curve fitting procedure was based on the Levenberg-Marquardt method [118].

6. Oleosome characterisation

Aqueous extraction of oleosomes from soybeans yields an oil-in-water emulsion. Any further processing of this oil-in-water emulsion, whether into an intermediate or final product, requires a profound knowledge about the micro- and macroscopic properties of the oleosomes, in particular with regard to factors influencing their stability. The micro- and macroscopic properties and the stability of oleosomes are mainly based on the molecular structure of the oleosin and the intra- and intermolecular interactions between the constituents. In order to investigate the role of oleosins for the stability and function of oleosomes, the oleosomes are enzymatically digested and compared to native oleosomes by performing spectroscopic and biophysical methods. The results thereof have been already published in: "The Role of Intact Oleosin for Stabilization and Function of Oleosomes", 2013, *J Phys Chem B*, 117, 13872-13883 by Maurer et al.. A brief overview of the characterisation of native and digested oleosomes in solution, with emphasis on the particle size and ζ-potential determination and their interfacial behaviour at the air-water interface is given in this chapter. The interfacial behaviour of oleosomes at the air-water interface is examined by axisymmetrical drop shape analysis (ADSA). By this technique, almost the same situation that occurs during atomisation, the most relevant process during spray drying, can be reproduced. Thereby, the accumulation of the oleosomes at the drop surface can be evaluated, which is supposed to directly correspond to the particle surface composition after drying [133].

During spray drying, oleosomes are subjected to different stress factors, such as temperature, shear stress and dehydration. To evaluate if the oleosomes remain intact under such conditions, their particle size distribution (PSD) and their ζ-potential are determined after being subjected to temperatures up to 100 °C and to shear stresses that occur during atomization.

6.1. Role of oleosin for oleosome stability

6.1.1. Influence of the pH

The net surface charge distribution of oleosomes is governed by the different amino acid sequence of the oleosin's hydrophilic parts exposed at the oleosome's surface and thus depends on the pH-value and the ionic strength of the solution. Since the stability of oleosomes is based on a combined effect of electrostatic repulsion and steric hindrance, variations of the pH-value can result in flocculation or coalescence.[162, 142, 151] The stability of oleosomes against aggregation can be determined by means of the average particle size, here the Sauter mean diameter, $D[3,2]$ (µm), cumulative volume distribution, Q_3 (vol%), and the ζ-potential, ζ (mV), (Fig. 6.1). Particle size measurements have been performed at different pH-values, ranging from 2 to 8 (Fig. 6.1a and Fig. 6.1b). To emphasise the effect of pH-values close to the isoelectric point of native oleosins on the particle size distribution of the oleosomes, the particle size distribution has also been determined at intermediate pH values between 4 and 6 (Fig. 6.1c).

In the pH range of 2 - 4.2 and 5.7 - 8, 60 vol% of soybean oleosomes exhibit a particle size of $d < 0.2$ µm (Fig. 6.1b and Fig. 6.1c). For pH-values close to the isoelectric point (pI ≈ 5.3) of the oleosins, the cumulative volume distribution reveals an increasing volume of oleosomes larger than 0.2 µm and thus a higher tendency to the formation of aggregates. While about 50 vol% of oleosomes are at pH-values 4.5 and 5.7 still smaller than 0.3 µm, a distinct increase in the particle size occurs for pH-values (4.7 - 5.5) very close to the pI. At these pH-values, 80 to 90 vol% are significantly larger than 2 µm. The largest aggregates are measured at the pI. In accordance to the particle size measurements, light microscopy images show at pH 2 and pH 8 well dispersed small entities of similar size and at pH 5 large structures of aggregated oleosomes (Fig. 6.2).

It can be concluded that the larger the differences between the pH and the pI become, the stronger is the repulsion between adjacent oleosomes. Close to the pI, the remaining Coulombic (electrostatic) repulsion forces diminish and are not sufficiently strong to overcome at the thermal energy kT attraction, such as van der Waals or hydrophobic interactions, and thus aggregation occurs. These findings are contradictory to similar studies [85], which showed the formation of larger aggregates in a broad pH range from 3 to 6. Here, the pH range, in which the oleosomes are unstable, is re-

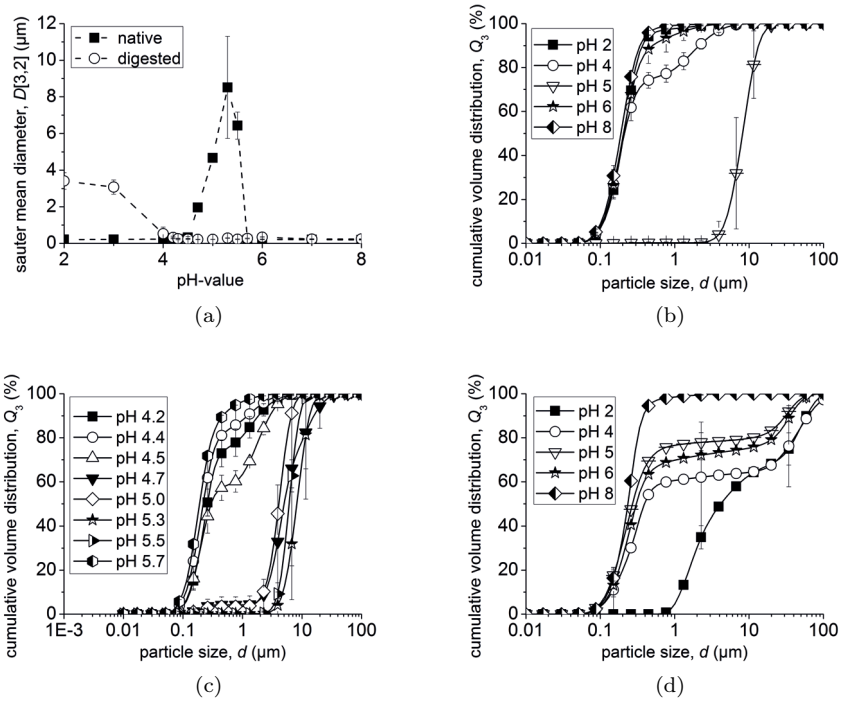

Figure 6.1.: Sauter mean diameter, $D[3,2]$ (µm), and cumulative volume distribution, Q_3 (vol%), of native and trypsin-digested oleosomes plotted against the particle size, d (µm) with representative error bars. (a) $D[3,2]$ (µm) of native and digested oleosomes. (b) Q_3 (vol%) of native oleosomes measured at pH 2-8. (c) Q_3 (vol%) of native oleosomes measured at intermediate pH-values between 4 and 6. (d) Q_3 (vol%) of digested oleosomes measured at pH 2-8. All figures has already been published in [122].

latively narrow, only ranging from pH 4.7 ($D[3,2] = 2.0$ µm) to pH 5.7 ($D[3,2] = 6.5$ µm). This discrepancy might result from different purification procedures during the aqueous extraction process. The centrifugation and purification of oleosomes at pH = 11 used here proved to provide a better separation from residual storage proteins.

Tryptic digestion of oleosomes causes a loss of structural integrity as the hydrophilic domains of the oleosins have been cleaved away. As a result of this, the particle size distribution measured in terms of pH is different than that for native oleosomes (Fig. 6.1a). In the pH range of 4 - 8, the average mean particle size of < 0.3 µm is comparable to the average particle

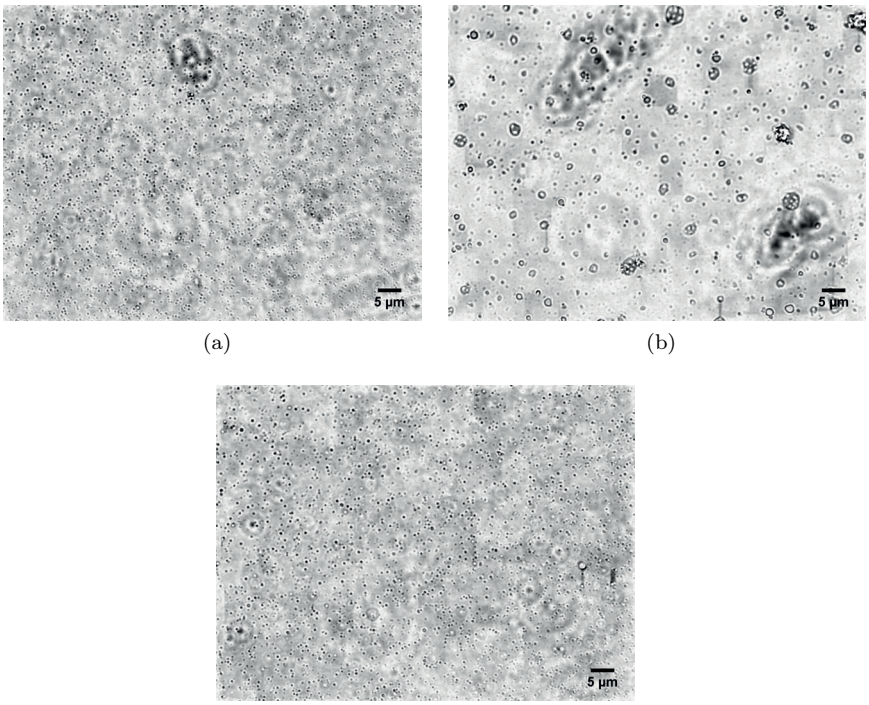

(a) (b)

(c)

Figure 6.2.: LM images of oleosomes dispersed in buffer solutions of different pH-value. (a) pH 2. (b) pH 5. (c) pH 8.

size of native oleosomes in the high acidic (pH 2 - 4) and weak acidic to alkaline (pH 5.7 - 8) region. However, in the very acidic region (pH 2 and 3), the particle size of digested oleosomes has significantly enlarged to 3.0 µm, revealing coalescence or aggregation of the particles. With regard to the cumulative volume distribution, first destabilisation effects, though to a lower extent, occur at higher pH-values (pH 4 - 5), where 50 vol% of the droplets are larger than 0.3 µm (Fig. 6.1d). The oleosomes remained stable only at pH 8.

Since the emulsion of digested oleosomes is a multicomponent mixture of protein fragments and lipids (TAG, PL, FFA, mono- and diglycerides), it is difficult to evaluate the destabilising effects that might have contributed to the distinct increase in particle size in the highly acidic region and the broadening of the particle size distribution. The formation of digested oleosomes to larger particles, in particular at very low pH-values, can be most probably

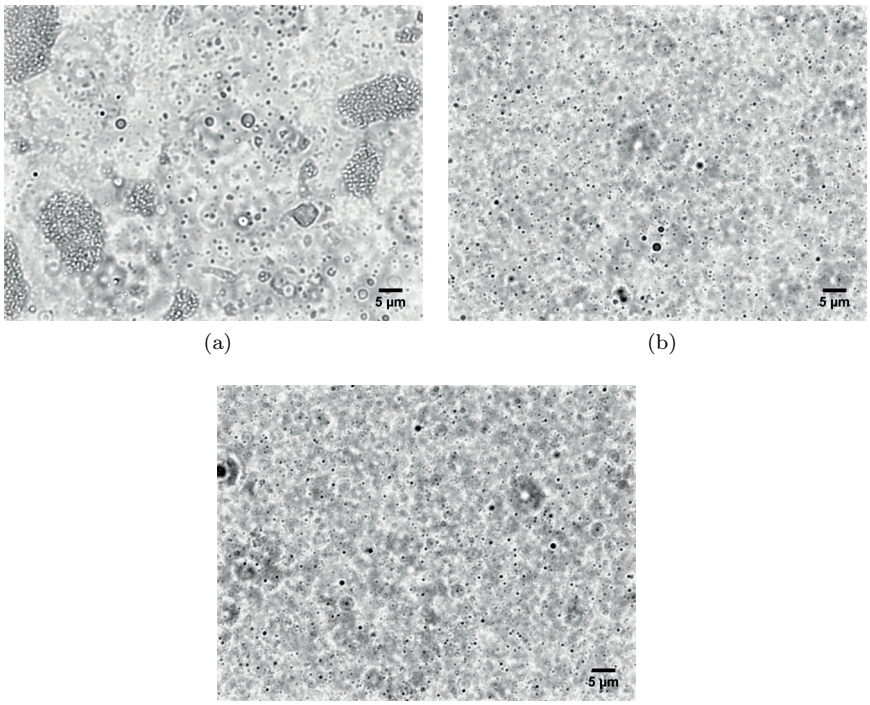

(a) (b)

(c)

Figure 6.3.: LM images of digested oleosomes dispersed in buffer solutions of different pH-value. (a) pH 2. (b) pH 5. (c) pH 8.

attributed to the cleavage of the hydrophilic and charged oleosin domains from the oleosome surface. Thereby, the electrical charge distribution of the oleosome surface is altered, resulting in a surface charge that predominantly originates from the zwitterionic character of the polar head groups of PL and FFA and no longer from the charge of the oleosin. Creaming stability tests and ζ-potential measurements indicate that, at critical pH-values, oleosomes with a PL monolayer tend to coalesce, while oleosomes covered with proteins aggregate to flocculate. This assumption is supported by the different structures observed by light microscopy at the critical pH-values (Fig. 6.2 and Fig. 6.3), here pH 5 in case of native oleosomes and pH 2 for digested oleosomes. Accordingly, it is concluded that along with the removal of the hydrophilic termini of the oleosins not only the surface charge is altered, but also the steric barrier against coalescence is removed.

In order to better understand destabilising phenomena, the ζ-potential

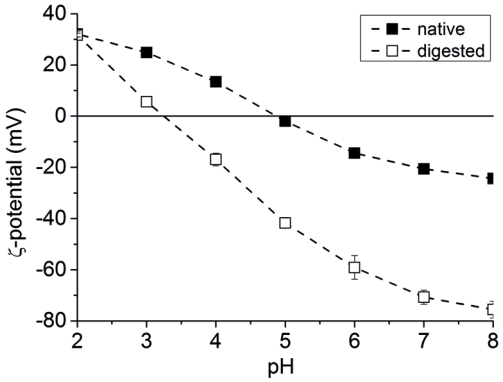

Figure 6.4.: ζ-potential (mV) of native and trypsin-digested oleosomes measured in terms of pH. This figure has already been published in [122].

was measured to quantify the electric double layer of native and digested oleosomes. This was supposed to be relevant for evaluation of the colloidal interaction and colloidal stabilisation (Fig. 6.4). The ζ-potential for native oleosomes changes from +32 ± 1.2 mV at pH 2 to -24 ± 1.6 mV at pH 8 reaching zero at pH 5, which is consistent with the pI of the oleosin. This behaviour, which is typical for protein-covered oil droplets [72], indicates that oleosins remained at the oleosome surface despite the harsh conditions during the extraction process. However, the pH dependency of the ζ-potential changes significantly for digested oleosomes. While in the highly acidic region the ζ-potential is similar to that of intact oleosomes (+30 mV), it becomes 0 mV at pH 3.2 and shifts to more negative values (-75 ± 3.3 mV at pH 8) in the alkaline region. Similar behaviour has been observed for so-called parenteral emulsions stabilised with PL and FFA [187]. Here, it is in particular governed by phosphatidylcholine, one of the most frequent PL in oleosomes.[64] It is likely, here, that the more negative values in the alkaline region result from the higher number of negatively charged phosphate head groups of PL, that are namely, phosphatidylethanolamine [146] and phosphatidylserine. However, despite the higher negative charges, these charges seem not to be sufficient to overcome attraction forces as shown in the particle size distribution, indicating that coalescence might have occurred. Although no destabilisation has been observed for native oleosomes from a ζ-potential of approximately 15 mV on, it has to be taken into account that

they are additionally sterically stabilised by intact oleosins at their interface. On the other hand, it is assumed that, at intermediated ζ-potentials, droplets of digested oleosomes might coalesce due to the lower stability of their interface, even at a lower probability to approach each others at such negative ζ-potential. Thus, digested oleosome droplets are only stable at a high ζ-potential (-75 mV at pH 8), when the probability of approaching each other is sufficiently reduced.

Figure 6.5 summarises the crucial role oleosins play in determining the stability and physicochemical properties of soybean oleosomes.

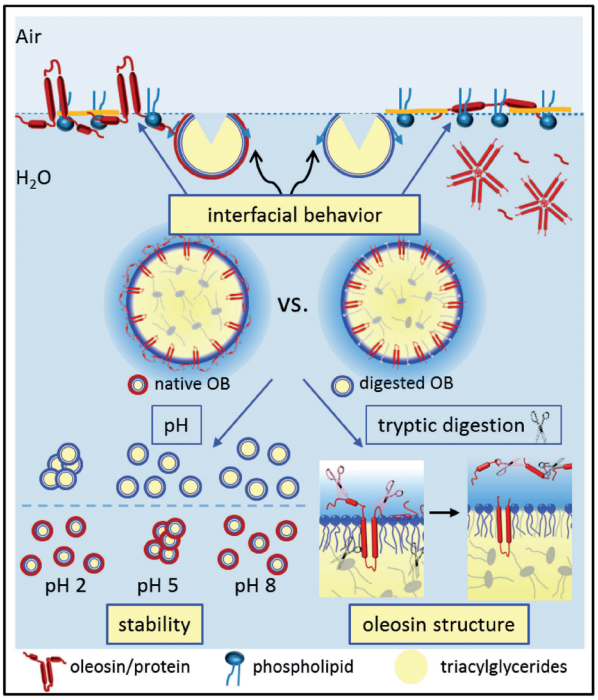

Figure 6.5.: Schematic overview of the effects of oleosin digestion on structure and function of oleosomes. Bursting and the subsequent spreading of the components of digested oleosomes might result in two different scenarios.[86] This figure has already been published in [122].

6.1.2. Interfacial behaviour

The interfacial behaviour of intact and trypsin-digested oleosomes at the air-water interface was investigated by ADSA. In contrast to measurements

by using a film balance [193], the analysis by ADSA additionally allows for the detection of very fast diffusion processes at the beginning of the kinetics under relatively stable conditions. Moreover, the interfacial behaviour can be investigated at a curved interface, which is more consistent with the situation during spray drying. In principle, diffusion of oleosomes to the air-water interface is driven by Brownian motion and not by buoyancy forces as it is the case for film balance measurements. In Fig. 6.6, representative kinetics of intact and digested oleosomes (78 mg/L, pH 2) recorded with ADSA are shown. Kinetics obtained for the other measured oleosome concentrations (15.6-1560 mg/L at varying pH) are not included in this discussion but shown in the appendix (Fig. A.1). Data evaluation is based on information from molecular spectroscopy at the air-water interface obtained by sum frequency generation (SFG) experiments. The results are published in detail in [122].

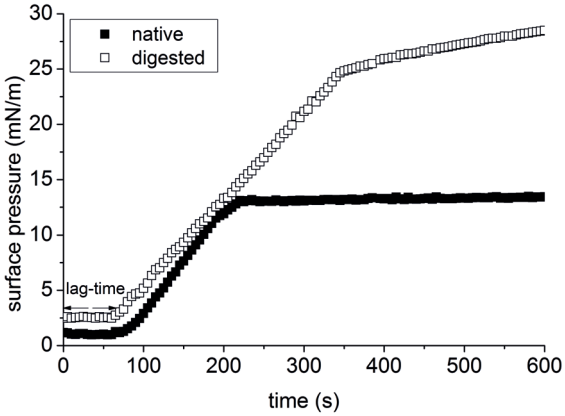

Figure 6.6.: Surface pressure (mN/m) of 78 mg/L of intact and digested oleosomes diluted in a buffer solution of pH 2. This figure has already been published in [122].

Oleosomes rupture and release their constituents at the air-water interface as soon as a sufficient amount of them has diffused from the bulk phase to the lower interphase. As a result of this, the surface pressure steeply increases. The lag-time, the sharp increase and then the kink in the surface pressure development can be explained by typical PL monolayer behaviour [95] and are comparable to a Langmuir (trough) isotherm. Initially, during the lag-time, oleosomes burst at the air-water interface and release parts of their PL (native oleosomes) or PL and FFA (digested oleosomes). Sub-

sequently, the components of the oleosomes spread at the air-droplet interface. In this stage, the distribution of oleosome components is comparable with a gaseous phase, which changes stepwise over in a coexistence with the liquid expanded phase. The more oleosomes diffuse to the interface and/or are disrupted, the more is the initial free surface reduced by decreasing the area per molecule. Consequently, the monolayer of PL and FFA reaches the liquid expanded phases, here indicated by the sharp kink. As soon as all oleosomes have diffused to the interface, directly after the kink, the surface pressure levels off due to depletion of oleosomes in the bulk phase. In case of intact oleosomes, the free PL can be considered to be in the condensed + liquid expanded coexistence phase [95], while the surface is filled with a large amount of oleosin-lipid conjugates [193]. For digested oleosomes, the final surface pressure (28.5 mN/m) is considerably higher than that for native oleosomes (13.3 mN/m). This discrepancy can be attributed to the dominating influence of PL that are, together with FFA, released to a greater extent after oleosome rupture due to the enzymatic cleavage of oleosin-PL binding sites.[111] However, SFG measurements revealed the presence of FFA at the air-water interface 20 minutes after the injection of oleosomes. Moreover, Dahmen-Levison et al. (1998) indicated that the PL head and tail interactions can be changed by adsorbing proteins that exhibit a special affinity for PL monolayers. As a result of this, the aliphatic chains in the condensed phase are less tilted, thus increasing the packing efficiency.

6.2. Impact of stress factors on oleosome stability

6.2.1. Influence of shear stress

During spray drying, soybean oleosomes are subjected to shear stresses caused by pumping and atomization. Such shear stresses may promote coalescence of oleosomes that can have negative consequences on the spray drying, *i.e.* oil encapsulation efficiency.[89, 125] Since shear stress provoked by atomization depends on numerous parameters such as orifice geometries, fluid dynamics and feed solution properties, precise shear rates are hardly quantifiable. Nevertheless, shear rates higher than 1,000 s^{-1} are assumed during atomization.[160]

In order to measure approximately the impact of shear stress on the integ-

rity of oleosomes, emulsions of different oleosome concentration ($c = 3.5$ wt% and $c = 15$ wt%) were subjected to shear stresses induced by either using an Ultra-Turrax or by atomizing the oleosomes. The use of the Ultra-Turrax allows a better repeatability and control of the stepwise regulation of shear stresses and thus facilitates an easier detection of possible thresholds. For atomizing oleosomes, a set of varying spray air and liquid flow rates was used to simulate shear stresses comparable to the real situation during atomization but without the drying step being involved.

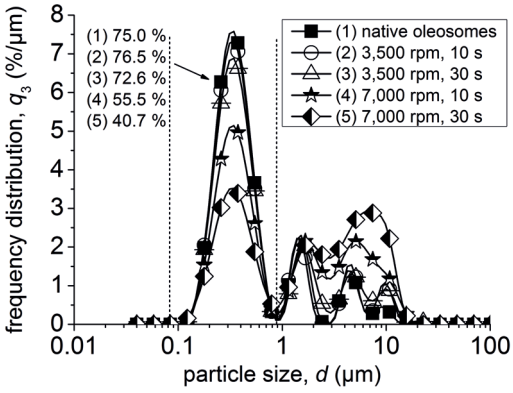

Figure 6.7.: Volume frequency distribution, q_3 (%/µm), of oleosomes after exposure to shear stresses of different magnitude and duration. Shear stress tests were induced by using an Ultra-Turrax and operated at 3,500 or 7,000 rpm for 10 and 30 s, respectively. Oleosome concentration was 15 wt%. Data was generated using $n_\mathrm{r} = 1.6$ and $n_\mathrm{i} = 0.01$.

In Fig. 6.7 and Fig. 6.8, the volume frequency distribution, q_3 (%/µm), of oleosomes before and after the application of shear stress, either by using the Ultra-Turrax (Fig. 6.7) or by atomization (Fig. 6.8a and Fig. 6.8b), respectively. Only in the former case, a direct time-dependent measurement was possible, since the duration of shear stress during atomization was indirectly given by the fluid flow rates and thus not manually adjustable. The differences in the particle size distribution of native oleosomes derive from the, in partial, poor dispersibility of the oleosome cream layer, evolving from the flotation-centrifugation extraction process. In principle, the volume of intact oleosomes (confined by dashed lines) decreases with increasing shear stress, with the effect being the greatest for shear stresses (7,000 rpm)

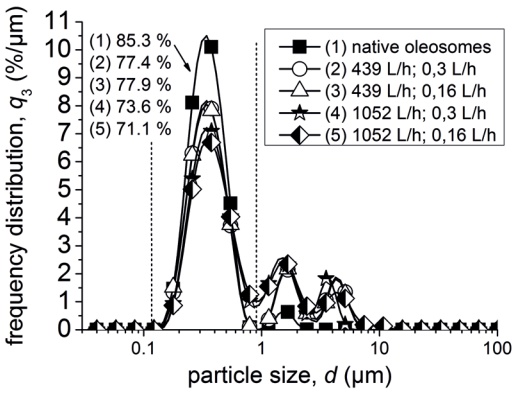

(a)

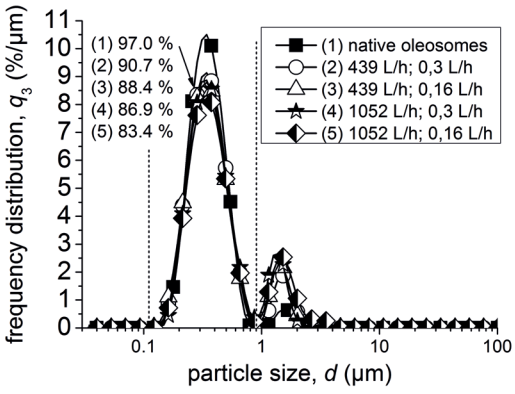

(b)

Figure 6.8.: Volume frequency distribution, q_3 (%/µm), of oleosomes after exposure to shear stresses of different magnitude and duration. (a) 3.5 wt% and (b) 15 wt% oleosome emulsion subjected to shear stress that is induced by different sets of air and liquid flow rates upon spray drying. The dashed vertical lines confine the particle size range from 0.1 to 0.9 µm in order to allow a better comparability between native oleosomes before and after subjection to shear stress. Data was generated using $n_{\mathrm{r}} = 1.6$ and $n_{\mathrm{i}} = 0.01$.

generated by using the Ultra-Turrax (Fig. 6.7). Only 40.7 % of oleosomes remain intact when exposed to 7,000 rpm for 30 s. Shear stresses generated by 3,500 rpm have a lower impact on the integrity of oleosomes, here 72 to 76 % remain intact, irrespective of the duration of the applied shear stress. At shear stresses that occur during atomization (Fig. 6.8a and Fig. 6.8b), the destructive effect is less detrimental than for shear stresses generated by 7, 000 rpm. While for the later up to 34 % of oleosomes are disrupted, it is maximal 14 % for the former, irrespective of the oleosome concentration (3.5 or 15 wt%). Resulting from this, it can be assumed that shear stresses generated at 7,000 rpm are higher than those occurring during atomization. In general, it is stated that the higher the volume flow rate of the spray air in relation to the liquid flow rate is, the higher is the shear stress acting on the liquid flow of oleosomes.[75, 160] In accordance to this, the volume of intact oleosomes diminishes with increasing ratio between the spray air and the liquid flow rate.

Shear stress tests reveal that oleosomes are only stable to shear stress to a limited extent, otherwise they are disrupted and coalesced. With regard to spray drying, more than 90 % of the oleosomes remain intact when the liquid feed emulsion was atomized at a spray air flow rate of 439 L/h and at a liquid feed flow rate of 0.16 or 0.3 L/h. However, the fraction of poorly dispersed oleosomes might have contributed to the increase in particle size. This might, in particular, accounts for the significant increase in the volume fraction of larger particles for 15 wt% oleosome emulsions subjected to shear stresses induced by the Ultra-Turrax (Fig. 6.7), as well as for 3.5 wt% oleosome emulsions (Fig. 6.8a) atomized at different spray air and liquid flow rates, although to a lower extent.

In general, the cream layer of oleosomes is comparable with a highly concentrated emulsion, also referred to as “high internal phase ratio emulsion” or “biliquid foam”.[183] In such an emulsion, the concentration of dispersed oil droplets is so high that the oil droplets are in direct permanent contact with each other and thus immobilised. These droplets are linked with thin films formed by the stabilising surfactant, here the oleosin. The interspaces between the droplets are filled with varying amounts of water. Due to the compact arrangement of droplets, deformation of droplet from spherical to more or less polyhedral entities occurs, governed by the so-called “osmotic stress”.[183, 149] Thus, it is assumed that the concentration of oleosomes in the cream layer results in the formation of strong bonds

between the oleosomes that partially remained aggregated upon redispersion, respectively dilution. Such aggregates of oleosomes can be regarded as small volumes with locally much higher volume fractions of dispersed oil phase. If the aggregates are deformed by shear forces, the bonds between the aggregated oleosomes are presumably strong enough to rupture the thin surface layer of oleosins, and thus to induce separation of oil from the aggregates followed by coalescence of oil droplets.

6.2.2. Influence of temperature

The purpose of these experiments was to examine the influence of heat treatment on the stability of oleosomes extracted from soybeans. Particle size and ζ-potential measurements of oleosomes in dependence of temperature may facilitate an estimation of the impact of spray drying process parameters on their integrity and thus their drying efficiency. Oleosome emulsions of 15 wt% (pH 3 and 7) were heat-treated at temperatures of 40, 60, 80 and 99 °C for 1 h. After cooling them to room temperature, the mean particle size, D(v, 0.5), (see Fig. 6.9a) and ζ-potential (mV) (see Fig. 6.9b) were determined for each pH-value and temperature.

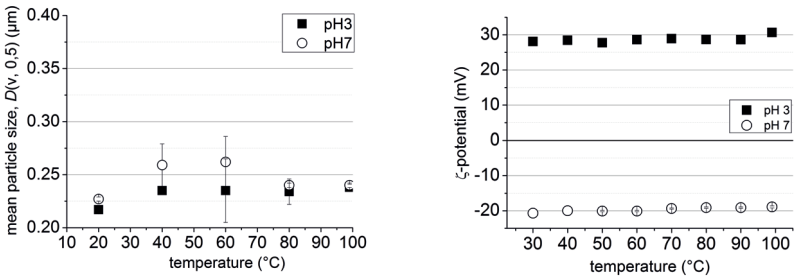

(a) (b)

Figure 6.9.: (a) Mean particle diameter, D(v, 0.5) (µm), (b) and ζ-potential (mV) of oleosome emulsions (15 wt%) of different pH-value measured after thermal heat treatment applied for 1 h.

At room temperature (21 °C), oleosomes have a mean particle diameter, D(v, 0.5), of 0.22 µm (pH 3) and 0.25 µm (pH 7) and exhibit a ζ-potential of $+28 \pm 0.1$ mV and - 21 ± 0 mV, respectively. Upon heat treatment, no significant change in neither the mean particle diameter (Fig. 6.9a) nor in the ζ-potential (Fig. 6.9b) is observable for any temperature. Only for samples

heat-treated at 99 °C, a slight increase of the ζ-potential from +28 mV to +30 mV at pH 3 and from -21 mV to -19 mV at pH 7 is observable. Additionally, there was no evidence of flocculation, coalescence or phase separation in any of the heat-treated oleosome samples. Consequently, it is assumed that the applied heat induces negligible changes in both the surface chemistry and the interfacial composition of the oleosomes.

The stability of oleosin-covered oleosomes is remarkable, since in general emulsions stabilised by globular proteins are susceptible to destabilising effects upon heat treatment. A considerable amount of such proteins is sensitive to heat-induced denaturation.[125] In principle, when the denaturation energy is sufficiently high, hydrogen bonds between the secondary and tertiary structure of proteins become disrupted. Consequently, the proteins unfold, lose their original structure and function. Furthermore, amino acid sequences originally located in the interior are exposed to the outer phase of the emulsion droplets. Attraction forces, *e.g.* van der Waals or hydrophobic interaction, between such newly arranged functional groups at the droplet surface can cause coagulation or precipitation. Denaturation temperatures of the most proteins range from 50 to 75 °C. The occurrence of heat-induced protein denaturation and its consequences on the protein's structural integrity and function depend on several factors, such as duration and intensity of heat exposure, protein concentration, pH-value and ionic strength of the continuous phase.[44, 124] Differential scanning calorimetry assays of recombinant oleosin isoforms revealed thermal midpoint denaturation temperatures between 50 and 59 °C.[23] Temperatures during spray drying are commonly two to four times higher (100 - 200 °C) though the exposure to such extreme temperature persists merely milliseconds or less. However, the actual thermal load is defined by the outlet temperature, which is, due to the evaporation of heat and thus the release of latent heat, significantly lower (50 - 90 °C).

Nevertheless, particle size and ζ-potential measurements reveal that oleosomes extracted from soybeans exhibit a very good thermal stability, which is in line with studies by [85, 138]. However, these studies revealed that their stability against heat treatment is limited to temperatures lower than 70 °C when salt (NaCl, 0.2 - 0.6 M) and/or a critical amount of non-oleosome associated proteins are present. From this it follows that also the proximity of oleosomes within the continuous phase is crucial for their stability to heat stress. In the absence of salt, electrostatic repulsion forces

between oleosomes are sufficiently strong to keep them separated. At higher ionic concentrations, electrical charges at the oleosome surfaces become screened, thus weakening the electrostatic repulsion and strengthening attractive interactions that cause aggregation. Extraneous proteins may denature at lower temperatures, unfold and act as flocculation bridges between oleosomes contributing to their aggregation.[138]

Thus, the resistance of properly purified oleosome emulsions to heat-induced denaturation can be presumably attributed to the umbrella-like structure of oleosins, which almost completely cover the surface of the oleosomes. The hydrophilic N- and C-terminal domains of the oleosin are peripherally arranged and flank the long hydrophobic domain, which penetrates through the PL monolayer into the lipid core.[81, 182] Interactions between AA residues of the hydrophilic domains and PL head groups at the oleosomes surface [151] are presumed to be sufficiently strong to resist unfolding and the interfacial composition remains more or less intact upon heating. In addition, it is likely that the hydrophobic domain is protected against heat by surrounding TAG.

7. Spray drying and encapsulation of oleosomes

Spray drying is widely employed to transform liquids into the solid form, thereby reducing the risk of microbial spoilage during storage. Commonly, it is also used to encapsulate nutritionally valuable compounds, such as oil high in unsaturated fatty acids and vitamins, to prevent them from any degradation. Soybean oleosomes proved to provide excellent pre-requisites for being spray dried: They exhibit a narrow particle size distribution (PSD), ranging from 0.2 to 0.8 µm and are stable to temperatures up to 100 °C, as well as shear stresses induced by an air flow rate of 439 L/h and a liquid flow rate of either 0.16 or 0.3 L/h. However, in contrast to the most commonly spray dried food, the milk, oleosomes contain relatively low amounts of encapsulating agents, such as proteins and phospholipids (PL), relevant for the oil encapsulation. Therefore, maltodextrin (MD) with a dextrose equivalent (DE) of 16.5-19.5 is added.

Process parameters, such as the drying temperature (T_{in}), the ratio between the spray air and liquid feed flow rate and the aspirator rate, can have a different impact on the resulting powder properties and thus on the spray drying efficiency. Here, spray drying efficiency is understood in terms of level of non-encapsulated soybean oil and loss of oleosome integrity, as well as of powder collection efficiency, which directly correlates with the former. In order to identify the optimal spray drying conditions, 3.5 wt% oleosome emulsions were spray dried with 5 or 10 wt% MD at a T_{in} of 100, 130 or 180 °C and at varying sets of spray air flow rate (439 and 1,052 L/h) and liquid feed flow rate (0.16 and 0.3 L/h), respectively, if not stated otherwise. As reference, pure oleosome emulsions of 15 wt% and 30 wt% have also been spray dried. After spray drying of each sample, the macroscopic properties of the resulting powder were documented by photographs and qualitatively described. According to this, powders with distinct differences were chosen for further analysis. This chapter is divided into three parts. First, the

most appropriate process parameters are determined. Second, the powder characteristics, such as surface morphology, powder composition and surface composition, in dependence of the applied process parameters are evaluated by means of SEM, CLSM and ESCA. Powders were redispersed in buffer solutions and the resulting oil droplet dispersions characterized with respect to their PSD and ζ-potential. These were then compared to the corresponding values for crude oleosome emulsions. Furthermore, the impact of spray drying on the oleosin secondary structure is analysed by FTIR.

7.1. Influence of process parameters

By spray drying oleosomes with or without MD in a lab-scale spray dryer, yields ranging from 0 to 51 % are obtained. Here, yields are defined in terms of powder collection efficiency. The main product loss occurs due to particle deposition to the dryer walls. The moisture content of all powder samples was 0.05 %. For almost all spray dried sample compositions, the highest yield is achieved at a relatively low spray air (439 L/h) and liquid feed (0.16 L/h) flow rate, as well as at a T_{in} of 180 °C (Fig. 7.1). While changes in the T_{in}, as well as in the ratio between the spray air and the liquid feed flow rate of spray drying 15 wt% oleosome emulsions have merely little impact on the yield (Fig. 7.1a), the influence of these parameters is more distinct for oleosomes encapsulated with MD (Fig. 7.1c and Fig. 7.1d).

Here, drying temperatures of 100 and 130 °C and an increasing impact of the spray air flow result in a significant decrease of the yield. This effect is comparatively less pronounced for 3.5 wt% oleosome emulsions encapsulated with 10 wt% MD but has severe consequences on the overall spray drying efficiency for 3.5 wt% oleosome emulsions spray dried with 5 wt% MD. Only at very high T_{in} of 180 °C and at a low spray air flow rate (439 L/h), a reasonable yield ranging from 23 to 44 % of powder is obtained for the latter. In order to determine the influence of the solid content on the spray drying efficiency and the powder properties, emulsions with 30 wt% of oleosomes were also spray dried.

However, the amount of such relatively high concentrated samples required to perform a reasonable number of spray drying runs could not be sufficiently provided by the used lab-scale extraction process. Therefore, only a few samples could be spray dried at 100 °C and at all sets of employed spray air and liquid feed flow rates. As shown in Fig. 7.1b, the yield

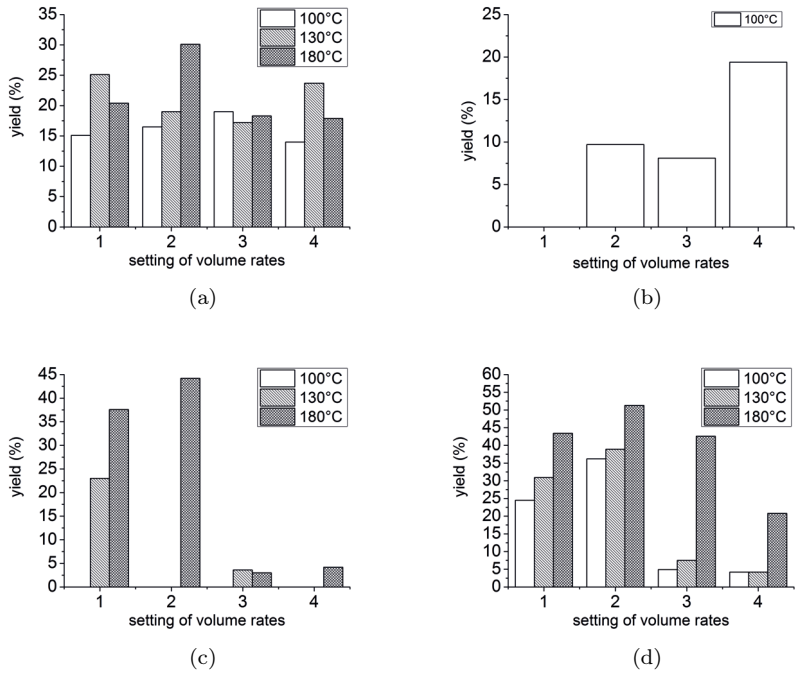

Figure 7.1.: Yield of oleosome emulsions with or without MD spray dried at different T_{in} and different settings of spray air and liquid feed flow rates employed: **1:** Air: 439 L/h, liquid: 0.3 L/h, **2**: Air: 439 L/h, liquid: 0.16 L/h, **3:** Air: 1,052 L/h, liquid: 0.3 L/h, **4:** Air: 1,052 L/h, liquid: 0.16 L/h. Figure (a) 15 wt% oleosome emulsion, (b) 30 wt% oleosome emulsion, (c) 3.5 wt% oleosome emulsion with 5 wt% MD and (d) 3.5 wt% oleosome emulsion with 10 wt% MD.

increases up to 19 % with increasing impact of the spray air flow (1,052 L/h) on the liquid feed stream. However, when a spray air flow rate of 430 L/h and a liquid feed flow rate of 0.3 L/h are used, no powder is collected at all.

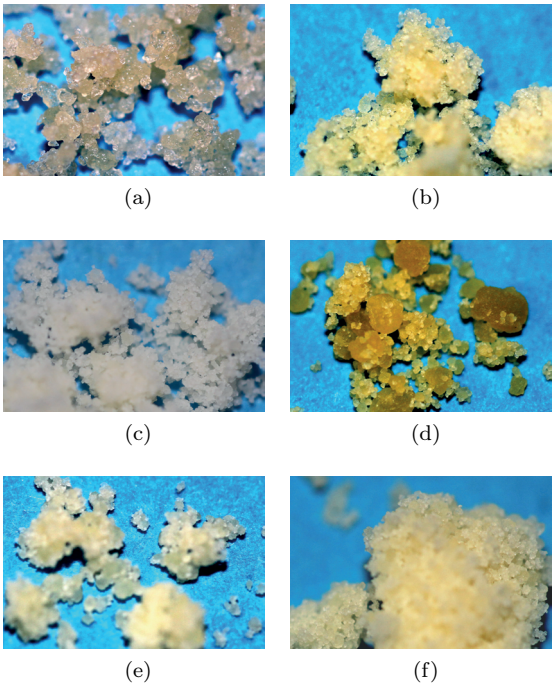

Figure 7.2.: Powders of oleosome emulsions spray dried at different T_{in} and at varying sets of spray air and liquid feed flow rates. **First row:** 15 wt% oleosome emulsion, **(a)** T_{in} = 100 °C, air: 439 L/h, liquid: 0.16 L/h and **(b)** T_{in} = 130 °C, air: 1,052 L/h, liquid: 0.3 L/h. **Second row: (c)** T_{in} = 130 °C, air: 1,052 L/h, liquid: 0.16 L/h and **(d)** T_{in} = 180 °C, air: 439 L/h, liquid: 0.16 L/h. **Third row:** 30 wt% oleosome emulsion, T_{in} = 100 °C **(e)** air: 439 L/h, liquid: 0.16 L/h, **(f)** air: 1,052 L/h, liquid: 0.16 L/h.

Macroscopic observations of the collected powder samples facilitated a first rough evaluation of the impact of process parameters on the powder properties, like particle size and surface composition, and encapsulation efficiency of soybean oleosomes (Fig. 7.2 and Fig. 7.3, as well as Fig. B.2). Spray drying of pure oleosome emulsions results in oily, highly agglomerated particles, having less in common with a typical powder, here understood as a substance of finely dispersed particles. Despite the small emulsion particle

size of the oleosome emulsion favourable for oil encapsulation [155, 170] and the good stability of oleosomes against high temperatures and shear forces (see Ch. 6), extensive coalescence of oil has very likely occurred during spray drying. Based on the oily but recognisable particulate structure of the powder, the soybean oil, although it is liquid at room temperature (melting point -20 °C, [53]), seems to have hardened upon dehydration (Fig. 7.2a - Fig. 7.2d). This phenomenon can be presumably explained by the high content of unsaturated fatty acids with isolated double bonds in soybean oil, which contains, amongst others, approximately 50 % of linoleic acid. Upon contact with the oxygen of the drying air, the unsaturated fatty acid chains undergo complex, yet not fully understood, chemical reactions, like auto-oxidation, dehydrogenation and isomerization, resulting in film formation. Thus, soybean oil is also classified as a semi-drying oil.[147] Moreover, the images of spray dried soybean oleosomes point out that increasing yellowing of the soybean oil has occurred with increasing T_{in}. This can also be ascribed to the high content of unsaturated fatty acids in the soybean oil and their film forming properties. Yellowing is supposed to be a result of the formation of coloured polyenes or quinone structures evolving from conjugated unsaturated hydroperoxides by means of intermediate ketones.[147]

By the addition of 5 wt% MD, the encapsulation of soybean oil is improved, provided that a favourable set of process parameters is employed, as already discussed above. However, a reasonable yield does not necessarily imply an acceptable encapsulation efficiency as shown by Fig. 7.3a. Here, the concentration of 5 wt% MD is insufficient and the process conditions of $T_{\mathrm{in}} = 180$ °C, as well as a spray air flow of 439 L/h and a liquid feed flow rate of 0.3 L/h are inappropriate for protecting oleosomes against coalescence. As a result of this, lumps have been formed due to free oil. When spray drying occurred at similar conditions but a slightly low liquid feed flow rate of 0.16 L/h, a qualitatively better result is obtain. Here, a white-yellowish powder of relatively well dispersed, though partially agglomerated particles, is produced (Fig. 7.3b). Powders produced from 3.5 wt% oleosome emulsions with 10 wt% MD (Fig. 7.3c and Fig. 7.3d) exhibit a similar macroscopic appearance. However here, the particulate features are for all powders produced from this composition the same, irrespective of which process parameters have been employed. Nevertheless, distinct differences in the yield (Fig. 7.1d) reveal that T_{in}, as well as the spray air flow and liquid feed flow rate have a significant impact on

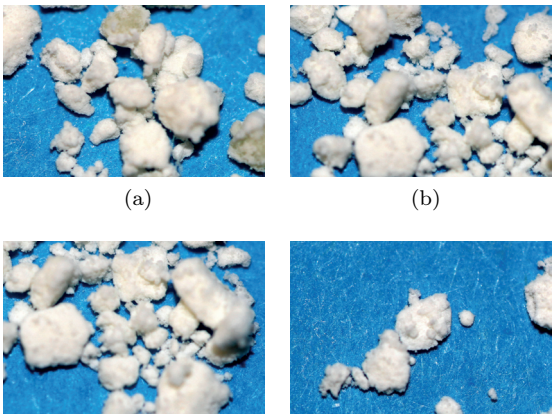

(a) (b)

(c) (d)

Figure 7.3.: Powders of oleosome emulsions with MD spray dried at different T_{in} and at varying sets of spray air and liquid feed flow rates. **First row:** 3.5 wt % oleosome emulsion with 5 wt% MD, T_{in} = 180 °C, **(a)** air: 439 L/h, liquid: 0.3 L/h. **(b)** air: 439 L/h, liquid: 0.16 L/h**. Second row:** 3.5 wt% oleosome emulsion with 10 wt% MD, air: 439 L/h, liquid: 0.16 L/h **(c)** T_{in} = 100 °C and **(d)** T_{in} = 180 °C.

the drying efficiency.

Although these results are achieved macroscopically and qualitatively, some correlations between the spray drying efficiency and process parameters derived from the general appearance and the corresponding yields of spray dried oleosomes can be identified here:

Pure oleosome emulsions In the case of pure oleosome emulsions, the influence of the volume fraction of the dispersed phase becomes apparent. As shown in Fig. 7.4, the shear rate dependent viscosity of oleosome emulsions strongly depends on the dispersed phase content. Emulsions of 15 wt% soybean oleosomes (φ_{oil}[1] = 0.16) exhibit Newtonian flow behaviour and emulsions of 30 wt% oleosomes (φ_{oil} = 0.32) are increasingly shear thinning with increasing shear rate.

Based on the significant difference in the obtained yields in dependence on the applied spray air and liquid flow rate, it is assumed that the higher disperse phase content counteracts the droplet disintegration upon atomi-

[1] volume fraction is estimated using a density of 0.93 kg/L for soybean oil and assuming that the volume of an oleosome exclusively consists of oil

zation. Since the atomization efficiency increases with increasing spray air flow rate in relation to the liquid feed flow rate [120], a lower spray air flow rate (439 L/h) presumably results in a larger droplet formation that in turn impedes heat and mass transfer to and from the oleosomes. The relatively low inlet temperature of 100 °C further contributes to the low drying efficiency in case of 30 wt% oleosome emulsions.

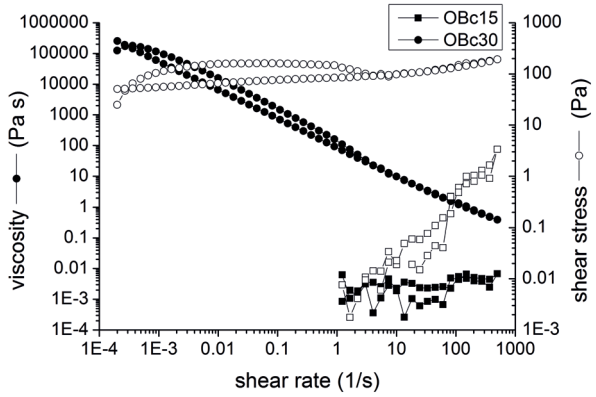

Figure 7.4.: Viscosity (full symbols) and shear stress (empty symbols) as a function of shear rate for differently concentrated emulsions of oleosomes.

Here, a reduced film formation due to less exposure to the oxygen of the ambient air and a slow migration of surface stabilising agents (oleosins and PL) might have contributed to the high amounts of free oil, resulting in a poor yield. Consequently, no spray dried oleosomes are collected as all particles deposit to the dryer walls due to a significant amount of free oil, which acts as liquid bridges, causing inter-particle stickiness (cohesion) and particle-wall sticking (adhesion) [30]. However, with dominating influence of the spray air flow rate, the yield increases. Moreover, at the highest spray air flow rate (1,052 L/h) employed, a powder which is macroscopically finer and of whiter colour than the ones spray dried at lower spray air flow rate (439 L/h) is obtained. Similar macroscopic features can be observed for powders produced from 15 wt% oleosome emulsions at 130 °C, as well as at a spray air flow rate of 1,052 L/h and a liquid feed flow rate of 0.3 L/h (Fig. 7.2b) and 0.16 L/h (Fig. 7.2c), respectively, whereby for latter a even whiter powder is obtained. In conclusion, despite the general poor encapsulation efficiency, it seems to be that the a spray air flow rate

of 1,052 L/h and a liquid feed flow rate of 0.16 L/h are optimal for both, 15 wt% oleosome emulsions spray dried at 130 °C and 30 wt% oleosome emulsions spray dried at 100 °C. However, the impact of T_{in} on the spray drying efficiency of 30 wt% oleosomes needs to be further investigated.

Oleosome emulsions with MD In contrast to the pure oleosome emulsions, a spray air flow rate of 1,052 L/h has adverse effects on the spray drying and powder collection efficiency of oleosome emulsions containing 5 wt% or 10 wt% MD. Additionally, T_{in} seems to be crucial in order to achieve a sufficient oil encapsulation, which is particularly noticeable in the obtained yields (Fig. 7.1c and Fig. 7.1d). In general, with the addition of MD, the mechanisms involved in heat and mass transfer during droplet drying become more complex. The failure of spray drying 3.5 wt% oleosome emulsions with 5 wt% MD at T_{in} of 100 and 130 °C indicates that extensive component segregation must have occurred, irrespective of the intensity of the chosen spray air and liquid feed flow rate. For samples dried at spray air flow rates of 1,052 L/h, the low amount of powder that could be collected appears finer, more dispersed and whiter than the other ones, which leads to the assumption that only MD is obtained. The same applies for oleosome emulsions with 10 wt% MD spray dried at T_{in} of 100 and 130 °C, as well as at a spray air flow rate of 1,052 L/h and a liquid feed flow rate of 0.16 and 0.3 L/h, respectively. According to the observations made here, a relatively low spray air flow rate of 439 L/h, an inlet drying temperature of 180 °C and a MD concentration of 10 wt% seem to be favourable for an adequate soybean oil encapsulation.

Based on the findings discussed above, it is regarded as likely that segregation of the oleosome components has occurred during spray drying. Segregation of components is a widely observed phenomenon during spray drying of multi-componential solutions.[16, 54, 104] It is assumed that segregation of materials inside the drying particle takes place due to different diffusivities and variations in the local concentrations of the present components during moisture evaporation. Simultaneously with the moisture evaporation, a layer of precipitated solids is formed at the droplet surface, initialising the crust formation. In general, the crust formation depends on several factors differently related to each other. At higher operating temperatures, moisture evaporates quicker and the composition of the resulting crust depends on the physicochemical properties of the solution components.[104, 39]

However, at this point, the available data is not yet sufficient to derive any conclusive assumptions of how process parameters correlate with mass transfer mechanisms of the emulsion components during drying, contributing to the encapsulation efficiency. Surface compositions analysis by means of ESCA along with microscopic evaluation of the powder morphology and composition by utilising SEM and CLSM, as well as the examination of the powder reconstitution properties presented in the following might help to better understand the impact of the process parameters on the segregation mechanisms.

7.2. Characterisation of oleosome powders

In general, multi-componential materials, containing skin-forming components, have shown to result in a great diversity morphology due to their structural plasticity during drying.[188] The formation of a shell or a crust and thus the evolving morphological features are governed by complex mechanisms that depend on the physicochemical properties of the particle components and the operating parameters. By employing different techniques, such as SEM, CLSM and ESCA, to investigate the powder morphology, powder composition and powder surface composition, valuable information can be gathered to better understand the drying kinetics and transport mechanisms that have occurred during spray drying and to evaluate the encapsulation efficiency of oleosomes by introducing MD.

7.2.1. Powder morphology

Pure oleosomes Scanning electron micrographs of spray dried oleosome powders are presented in Fig. 7.5 to Fig. 7.8, revealing information about the surface topography, particle shape and size and the degree of agglomeration on the micron scale. Powders composed of pure oleosomes produced at different T_{in} show highly agglomerated particles that are partially merged to structures of undefined shape (Fig. 7.5). In the case of 15 wt% oleosome emulsions, drying temperatures of 100 °C (Fig. 7.5a) and 130 °C (Fig. 7.5b) result in spherical particles with crinkled surfaces that exhibit a broad size distribution, ranging from 1 to 14 µm. Particles produced at 100 °C have a comparatively smooth surface while drying temperatures of 130 °C caused the formation of small cavities, occasionally distributed at the surface of

the particles. Drying temperatures of 180 °C resulted in the formation of powder particles of rather undefined structures.

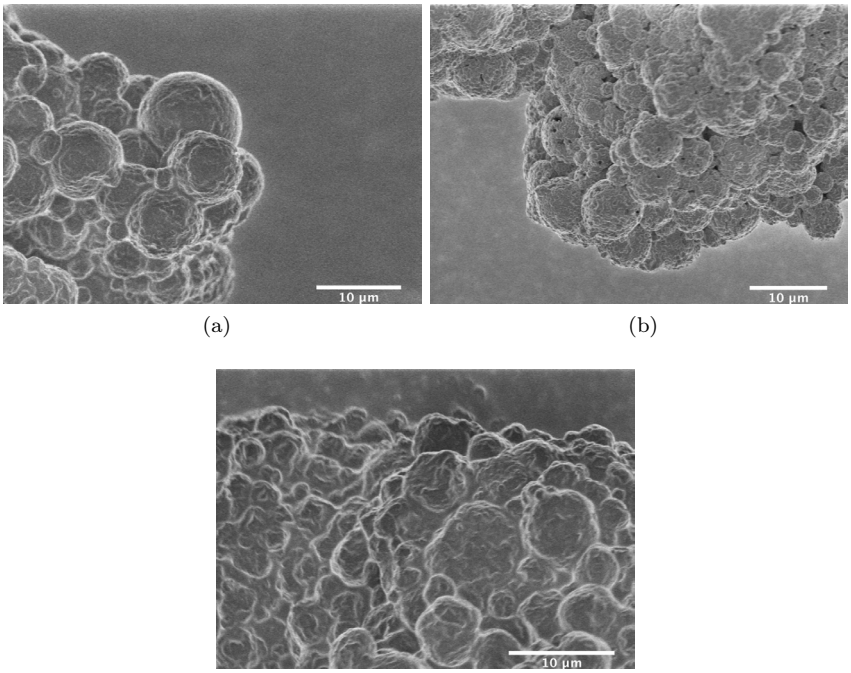

(a) (b)

(c)

Figure 7.5.: Scanning electron micrographs of surfaces of spray dried powder particles produced from emulsions composed of 15 wt% soybean oleosomes at different drying temperatures: (a) $T_{\mathrm{in}} = 100$ °C (b) $T_{\mathrm{in}} = 130$ °C, (c) $T_{\mathrm{in}} = 180$ °C. In all cases a spray air flow rate of 1,052 L/h and a liquid feed flow rate of 0.16 L/h were used.

According to the macroscopic observations as discussed in Sec. 7.1, it is regarded as most likely that oleosomes have ruptured during spray drying and thus released oil. In case of $T_{\mathrm{in}} = 100$ °C, it is assumed that drying of the droplet suspension of oleosomes took longer, so that the surface of the particles had more time to smooth out. Here, the free oil acts as an effective plasticiser.[94] With increasing drying temperature, the drying rate increases, thus affecting transport mechanisms of the segregated components of the oleosomes during the drying process. Accordingly, it is likely that the tiny cavities result from the inclusion of air bubbles originally entrained during atomization or of vapour bubbles evolved during

water evaporation. Changes in droplet/particle temperatures along with changes in the ambient and droplet vapour pressure might have contributed to gas expansion and quick release, causing cracks, particularly when the surrounding surface layer is thin. Powders produced from 30 wt% oleosome emulsions but at a T_{in} of 100 °C (Fig. 7.6) show a similar surface topology than those from 15 wt% oleosomes spray dried at 130 °C (Fig. 7.2b and Fig. 7.3b). Here, the structure formation is presumably also based on modified componential transport mechanisms but rather due to an increased solid content than to larger drying temperatures. Interestingly, the cross section of a powder particle represented in Fig. 7.6, gives evidence that some kind of shell or crust formation occurred during drying, encapsulating a dense, yet undefined mass. Drying temperatures of 180 °C in case of 15 wt% oleosome emulsions evolve highly deformed particle structures, in which the original spherical shape is covered with a layer of a greasy substance (Fig. 7.5c). Also here, the formation of this layer is attributed to the plasticising effect of the free oil. Particularly at these high drying temperatures, the free oil seems to have a detrimental effect on the particle structure formation, which might be explainable by its reduced viscosity and thus higher tendency to accumulate at the particle's surface.

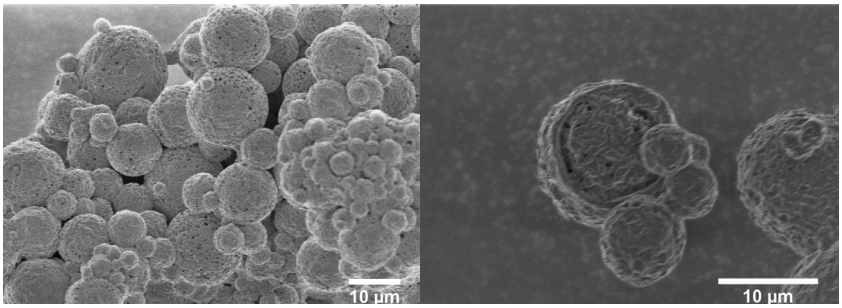

Figure 7.6.: Scanning electron micrographs of the surface of spray dried powder particles produced from an emulsion composed of 30 wt% soybean oleosomes. Processing parameters: T_{in} = 100 °C, air: 1,052 L/h, liquid: 0.16 L/h.

In general, the formation of liquid bridges between patches of free oil on the particle surfaces caused significant agglomeration, presumably provoked upon collision of approaching particles due to the turbulent motion of the gas flow. As a result of this, the formation of fine dispersed, free flowing particles is hindered. The height of drying temperature influences

significantly the degree of agglomeration, as well as the structure and surface topology formation. Furthermore, no evidences of hollow particles, like fractures of shells or convexities is visible, thus it is rather likely that dense structures are formed upon spray drying.

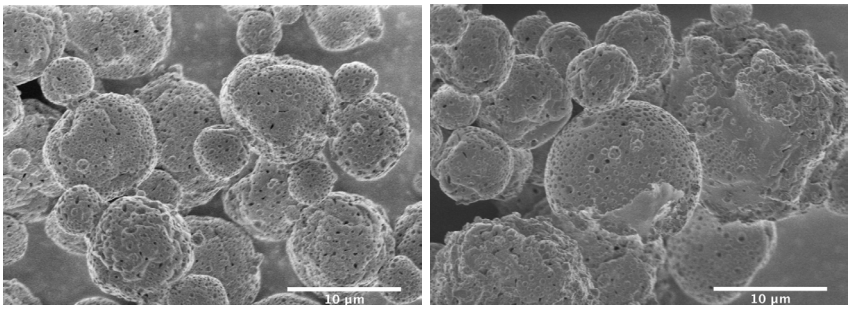

(a) (b)

Figure 7.7.: Scanning electron micrographs of surfaces of spray dried powder particles produced from emulsions composed of 3.5 wt% soybean oleosomes and 5 wt% MD at different drying temperatures: (a) $T_{\text{in}} = 130$ °C, (b) $T_{\text{in}} = 180$ °C. In both cases a spray air flow rate of 439 L/h and a liquid feed flow rate of 0.3 L/h were used.

Oleosomes with MD Fig. 7.7 shows micrographs of powder samples obtained by spray drying emulsions composed of 3.5 wt% oleosomes and 5 wt% MD. Drying occurred at 130 and 180 °C, as well as at a spray air flow rate of 439 L/h and a liquid flow rate of 0.3 L/h, respectively. As shown in Fig. 7.1c, drying of this sample composition at 100 °C did not result in collectable amounts of powder. Contrary to powders made from pure oleosome emulsions, which are nearly perfectly spherical, the shape of the powder particles changes with the addition of MD to particles with distinct shallow dents and wrinkles, irrespective of the applied temperature. Similar to powders without MD, the surface topology of powders spray dried at 130 °C exhibits tiny cavities, though to a higher degree (Fig. 7.7a). Furthermore, the surface of the particles is uniformly covered with many shallow indentations. At drying temperatures of 180 °C, a larger diversity of particle shapes is observable. In the lower left and the upper right of Fig. 7.7b, large structures of merged bulk and of comparatively irregular shape are visible. It is very likely that such structures result from segregation processes that might

have occurred during the drying process. Moreover, spherical particles are observable, showing evidence of void formation followed by particle fracture during or after drying. The inner surface structure of the particle shell is smooth. In contrast to the other particles, the particle size of this spherical particle seems to be larger than the average.

Thus, assuming that segregation has caused locally higher concentrations of MD, the formation of voids in the centre of particles might result from the formation of rigid shells at early stages of drying. This might then prevent the escape of water or water vapour from the droplet, respectively particle interior.[188] Particularly at higher drying temperatures, evaporation of water occurs faster than water diffusion from the particle interior to its exterior can take place. As a result of this, dissolved or dispersed solids deposit near the particle surface, thus locally increasing the viscosity of the dispersed phase. With continuing drying and water evaporation, the droplet or particle temperature exceeds the local ambient boiling point and the internal vapour pressure increases above the local ambient pressure.[169] Due to this, the particle, respectively the formed void within the particle inflates and the physical properties of the shell, such as thickness, porosity and rigidity, influence the subsequent structure formation of the dried particle. Dry and hard shells can prevent deflation of the hollow particle when the vapour condenses within the void as the particle temperature decreases upon progressing drying. However, a quick expansion of vapour pressure can also cause shell fracture. At lower drying temperatures, the shell might remain moist and more elastic for a longer drying period so that the hollow particle can deflate and shrivel upon cooling.[137, 169] The formation of hollow particles has been particularly observed for powders composed of high portions of proteins in relation to other components [7, 55, 94], though carbohydrates such as MD can also cause void formation.[94]

The ability of such components to create hollow particles upon spray drying is attributed to their film forming properties. While MD forms an amorphous and rigid solid upon spray drying, resulting in a sharp viscosity increase up to $10^{12\text{-}14}$ Pa·s, proteins tend to unfold at the air-water interface and form an elastic film.[90] However, the level of protein, here oleosin, present in the powder is, in particular in comparison to MD, very low (1.1-1.6 wt% on dry weight basis) and its impact on the powder morphology is presumably less pronounced.

Micrographs of powder particles composed of 3.5 wt% oleosomes and

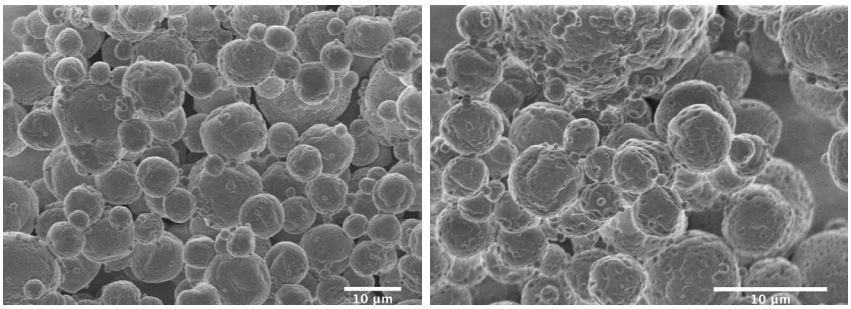

(a) (b)

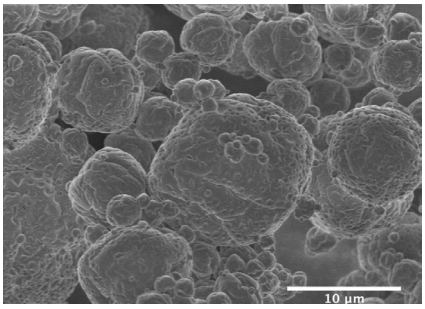

(c)

Figure 7.8.: Scanning electron micrographs of surfaces of spray dried powder particles produced from emulsions composed of 3.5 wt% soybean oleosomes and 10 wt% MD at different operating parameters: (a) T_{in} = 100 °C (b) T_{in} = 130 °C (c) T_{in} = 180 °C. In all cases a spray air flow rate of 1,052 L/h and a liquid feed flow rate of 0.16 L/h were used.

10 wt% MD reveal that higher concentrations of MD have smoothed out the surface topology of particles (Fig. 7.8). However, shallow dents and wrinkles are still visible though their amount is at its lowest for the sample dried at 100 °C (Fig. 7.8a). A distinct difference in surface topology of the samples dried at 130 °C (Fig. 7.8b) or 180 °C (Fig. 7.8c) is not observable in the micrographs. However, these findings are contrary to the results published in a patent by D. Gray in 2012 [70], where oleosomes from *Echium plantageneum* (*Echium*) were also spray dried with MD. SEM micrographs from these oleosomes encapsulated with MD reveal a relatively high amount of spherical, hollow particles with smooth surfaces. Additionally, the surface of a considerable amount of particles exhibits comparatively distinct dents, which are regarded as typical for particles with protein surface coverage.[55]

In general, the molecular weight of the MD used for encapsulations is crucial for the surface structure formation. Various studies [158, 163] proved that a lower molecular weight and thus a higher DE of MD yields particle surfaces free of cracks or wrinkles. Here, a DE of 15 for MD is regarded as sufficient. Since in this study a MD with a DE of 16.5 to 19.5 is used, the discrepancies in the particle morphology presumably result from the different oleosome extraction procedure. Depending on the purification method, the amount of non-oleosome associated soybean proteins can vary. It is therefore regarded as likely, that in case of the results obtained by D. Gray, a higher level of proteins is present in the powder. Apart from that, an acceptable oleosome encapsulation is reported, yielding intact oleosomes upon redispersion. In relation to the findings stated here, it is assumed that the higher level of proteins, which, besides, have different physicochemical properties than oleosins, contributed to a better encapsulation efficiency and the previously described particle morphology.

7.2.2. Powder composition

Since SEM is restricted to the powder surface, another technique is required in order to examine the microstructure of the bulk and to obtain information of the powder composition, particularly with regard to the location and amount of the encapsulated oil phase. Here, CLSM is utilised to analyse sections of the powder microstructure at any desired plane in a non-invasive and non-destructive manner. By staining the oleosome emulsions with Nile red and FITC prior to spray drying, the soybean oil can be distinguished from the oleosin, respectively the encapsulating matrix.

Figure 7.9 represents the CLSM micrographs of spray dried powders produced from 15 wt% oleosome emulsions (Fig. 7.9a) and from 3.5 wt% oleosome emulsions with either 5 wt% (Fig. 7.9b) or 10 wt% MD (Fig. 7.9c and Fig. 7.9d). Drying occurred for all sample compositions at 180 °C, for compositions with 10 wt% MD additionally at 100 °C. The spray air flow rate (1,052 L/h) and the liquid feed flow rate (0.16 L/h) were kept the same for all drying runs. The oil is coloured in red and the protein, respectively the oleosin is supposed to be green. However, despite extensive washing, it was not possible to entirely remove the non-covalently bound fluorescent dye, here FITC used for labelling the oleosin. As a result of this, disproportional amounts of the powder particles are stained, thus impeding the discrim-

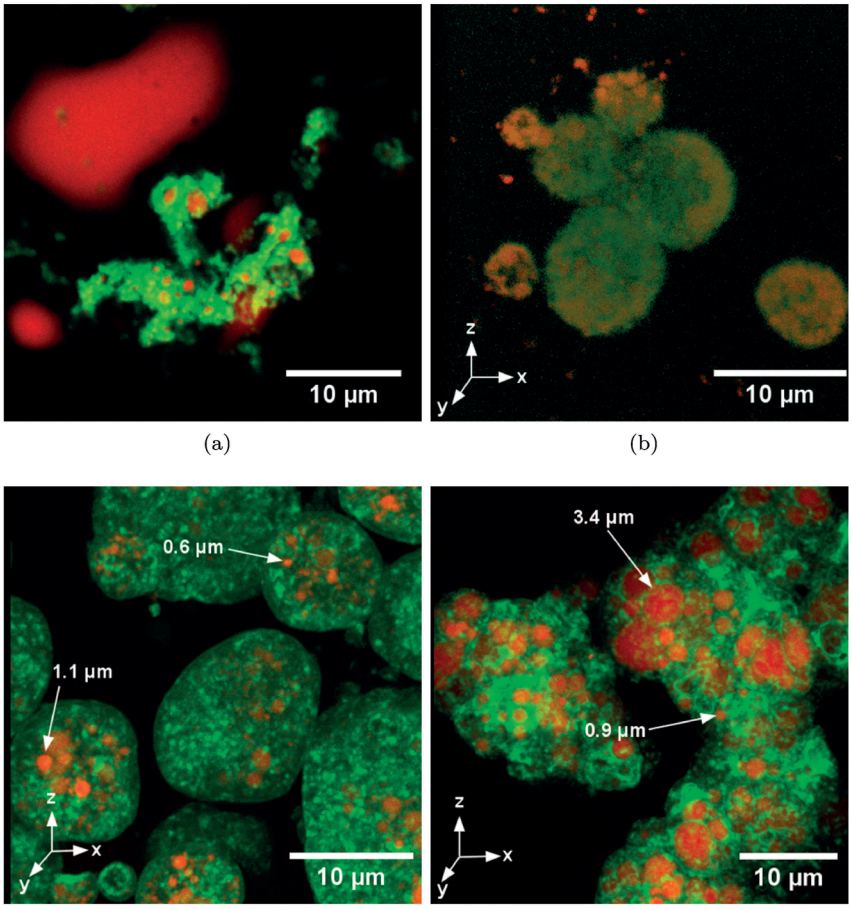

Figure 7.9.: CLSM micrographs of powders obtained by spray drying (a) 15 wt% oleosome emulsions or (b-d) 3.5 wt% oleosome emulsions with different concentrations of MD at different operating parameters; (b) oleosomes with 5 wt% MD, (c) oleosomes with 10 wt% MD dried at $T_{\mathrm{in}} = 100$ °C and (d) oleosomes with 10 wt% MD dried at $T_{\mathrm{in}} = 180$ °C. The oil is labelled with Nile Red (red) and the protein with FITC (green). Coordinates indicate that individual micrographs made in the xy-plane at different z-positions are stacked to achieve a three-dimensional illustration.

ination of encapsulating material and oleosin. Apart from the problems in sample preparation, it can be assumed that a proper evaluation of the oleosome interface would have been difficult in any case, as the layer thickness of the oleosin is of nanoscale, which is below the instrumental resolution threshold. Accordingly, the focus is rather put on the oil localisation and encapsulation efficiency. In order to visualise the entire three-dimensional microstructure of the powder particles, sections made in the xy-plane at different z-positions are stacked. The respective micrographs to which this function was applied here, are denoted by coordinates (Fig. 7.9d-Fig. 7.9d).

In general, imaging of spray dried samples of pure oleosomes emerged as problematic, since the immersion medium (distilled water, glycerol or immersion oil) used to obtain a reasonable imaging depth caused oil leakage due to the large amount of free surface oil on the powder particles and the water solubility of MD (Fig. 7.9a). Thus, discrimination between oil and oleosin, or at least the evaluation of any segregation effects is not possible here.

Powder particles produced from 3.5 wt% oleosome emulsions with 5 wt% MD show large portions of coalesced oil mainly accumulated in the close proximity of the surfaces (Fig. 7.9b). CLSM micrographs of oleosomes encapsulated with 10 wt% MD and spray dried at 100 °C (Fig. 7.9c) or 180 °C (Fig. 7.9d) reveal clear differences in the degree of coalescence and thus in the encapsulation efficiency of the soybean oil. At lower drying temperatures, the size and amount of coalesced oleosomes, respectively oil droplets is lower than in comparison to those dried at higher drying temperatures. Random measuring of droplet sizes yields oil droplets, whose size of approximately 0.6 µm is comparable to that of native oleosomes, assuming that the oleosomes remained intact upon spray drying. While a major part of coalesced oil droplets seems to be more located in the interior of the particles dried at 100 °C, oleosomes that have been subjected to temperatures of 180 °C exhibit droplets rather accumulated at closer proximity to the particle surface. Particularly in the latter case, the average size and amount of coalesced oleosomes vary among individual particles of one sample composition. Therefore, spray drying of oleosomes with MD at such high temperatures produces powder particles with different levels of encapsulated oil. Although neither macroscopic observations nor the determination of the yield nor SEM micrographs revealed any significant differences in the drying temperature applied to dry 3.5 wt% oleosome emulsions with

10 wt% MD, CLSM proves the contrary. Hollow particles or particles exhibiting large voids are not observable by CLSM, though only a fractional amount of the respective powder sample was analysed.

7.2.3. Powder surface composition

Surface composition of spray dried oleosomes, with and without MD, was examined by using ESCA. The ESCA-method allows to quantify the surface coverage of oleosome components and MD on the powder particles. Particularly the presence of fat/oil on particle surfaces is a valuable quality parameter to estimate the encapsulation efficiency of oleosomes by MD.

Since only a limited amount of powder samples could be analysed by ESCA, samples with the most distinct differences in particle structure and appearance, as observed by the macroscopic evaluation of process parameters in Sec. 7.1, were studied. For reasons of simplicity, the analysed samples produced at different operating parameters are denoted with capital letters. Thus, powders produced from 15 wt% oleosome emulsions spray dried at either 100 °C (Sample A) or 180 °C (Sample B) were examined. Further, ESCA-measurements of powders obtained by spray drying 3.5 wt% oleosome emulsions and 10 wt% MD at either 100 °C (Sample C) or 180 °C (Sample D) were conducted. In all cases, spray drying was performed at a spray air flow rate of 439 L/h and liquid feed flow rate of 0.16 L/h. Moreover, it is assumed that the sample composition has not changed during spray drying and that the elemental composition of the different molecular components in the powder samples can be linearly combined to obtain information about the elemental composition of the surface.

The elemental composition of the pure components used as reference samples for the calculation of the compositional surface analysis of the spray dried oleosome emulsions is represented in Table 7.1. To prove the reliability of the measurements by ESCA, the experimental values are compared to the theoretical calculated ones. It can be seen that the experimental values for soybean oil, soy lecithin and MD agree relatively well with the theoretical ones. However, significant errors are obtained for oleosin. The distinct differences between the experimental and theoretical values can be presumably attributed to the poor purification degree of oleosin isolated from soybean oleosomes. Despite extensive washing with different organic solvents, it was not possible to entirely remove residual oil fractions. In vari-

Table 7.1.: Relative atomic concentration (at%) of pure oleosome components and MD, used here as encapsulating material, as measured by ESCA

Reference sample	**Relative atomic concentration (at%)**				
		C	**O**	**P**	**N**
Soybean oil	Experimental value	87.0	13.0	0	0
	Theoretical value[a]	86.4	13.6	0	0
	Error[b]	0.7	4.6	0	0
Soy lecithin	Experimental value	82.4	16.4	1.2	0
	Theoretical value[c]	80.8	15.4	1.9	1.9
	Error[b]	1.9	6.1	58	-
Oleosin	Experimental value	76.7	18.0	0	5.3
	Theoretical value	62.8	19.4	0	17.8
	Error[b]	18	7	0	235
MD	Experimental value	56.0	44.0	0	0
	Theoretical value[d]	54.5	45.5	0	0
	Error[b]	2.7	3.4	0	0

[a] Assuming that the fatty acids are composed of $C_{18}(H_{36})O_2$, which is accordingly to the elemental composition of linoleic acid and oleic acid, the two most present fatty acids in soybean oil. [102]

[b] $Error\,(\%) = \left|\frac{measured\,value - theoretical\,calculated\,value}{measured\,value}\right| \times 100$

[c] Taking into account the elemental composition of phosphatidylcholine, which is the most present PL in soy lecithin. [64]

[d] Calculated on basis of the elemental composition of glucose ($C_6(H_{12})O_6$)

ous studies, it has been stated that oleosins purely dissolve in apolar and polar media due to their strong amphiphilic nature.[162, 156] Therefore, it is likely that oleosins have agglomerated during the extraction process, thereby enclosing residual fractions of oil, which are then inaccessible for the solvent. In order to consider this discrepancy in the compositional analysis of spray dried oleosome emulsions, both the experimental and theoretical values were used in the calculations (see Subsec. 5.8.3). The results are summarised in Table 7.2.

The values clearly show that the ratio of components on the surface significantly differs from the bulk composition of the powders. For almost all

Table 7.2.: Powder composition on dry matter basis and surface composition of spray dried oleosomes calculated by means of experimental and theoretical values (bold characters)

Sample	Bulk composition (% of dry weight)				Surface composition of spray dried emulsions (%)			
	Oil	Oleosin	PL	MD	Oil	Oleosin	PL	MD
A	13.8	0.6	0.6	-	87.4	-	11.3	-
					85.2		**14.4**	
B	13.8	0.6	0.6	-	42.4	-	57.3	-
					44.0	**-**	**57.0**	**-**
C	23.8	0.14	0.14	74.0	58.9	39.0	-	2.5
					84.1	**11.3**	**-**	**4.6**
D	23.8	0.14	0.14	74.0	58.6	47.4	-	-
					86.2	**13.7**	**-**	**-**

samples, oil is the component present in the highest concentration on the powder surface.

Pure oleosomes In case of samples A and B, values obtained by using the theoretical elemental composition of the reference sample are in acceptable agreement with the experimental ones. Interestingly, PL are found, partly in quite significant amounts on the surface of powders made from 15 wt% oleosome emulsions. The percentage of PL increases by a factor of four when oleosomes were spray dried at a drying temperature of 180 °C. In this case, about 57 % of the particle's surface is covered with PL. However, no protein is detected on the surface of the powder particles.

In general, drying kinetics and transport mechanisms within a drying droplet are complex, particularly when multiple components with different physicochemical properties are present. To demonstrate why PL are accumulated at the surface of pure oleosome powders, it is therefore helpful to consider the physicochemical properties of PL in general and in the context of oleosomes, as well as to correlate the ESCA data with findings from SEM and CLSM.

Phospholipids are low molecular weight surfactants characterised by a

hydrophilic head group and a hydrophobic fatty acid tail. Due to their amphiphilic nature, PL poorly dissolve in both water and oil. In water, PL can adopt various lamellar and hexagonal structures to build micelles and membranes.[38, 43, 76] In general, the stability of the oil-droplet interface depends on the nature of the protein-surfactant interaction and is determined by the competitive adsorption between proteins and surfactants at the interface. Upon adsorption, proteins form an immobile viscoelastic network whereas surfactants, respectively PL are highly mobile. The stabilisation of interfaces by surfactants is based on the Gibbs-Marangoni mechanism.[196] Both, the protein and the PL adsorption mechanisms are incompatible. As a result of this, competitive adsorption between the surfactant and the protein occurs, which can either lead to an enhancement or reduction of the interfacial, respectively emulsion stability.[90] Although surfactants like PL are more efficient in lowering the surface tension due to closer packing at the interface, only molar protein concentrations 10^3 - 10^4 times lower than for surfactants are required to reach effective surface saturation. With regard to the oleosomes, it is also assumed that PL, here present in form of a monolayer, exhibit better emulsifying properties than oleosins.[43] However, the stability of oleosomes is attributed to synergistic effects between PL and oleosins and mainly depends on the steric and electrostatic repulsion of the oleosin, completely covering the oleosome surface.[43, 156]

On the basis of the findings obtained here by ESCA and also by SEM and CLSM micrographs, it is very likely that the oleosomes ruptured and segregation effects have occurred during drying. Investigations of the interfacial behaviour of oleosomes at the air-water interface by utilising ADSA, as already discussed in detail in Subsec. 6.1.2, revealed that oleosomes burst and spread their components on the air-droplet interface. However, a dominating influence of PL on the droplet surface characteristics is only observed, when the oleosin structure is modified by enzymatic digestion. Thus, in time-scales relevant to spray drying, it is rather assumed that both the protein and the PL are present at the droplet interface, at least at the very early drying stage. Referring to [51], upon droplet drying, the adsorbed species remain at the interface and consequently, the surface is mainly covered by the surface-active material. Elversson and Millqvist-Fureby (2006) stated that the powder surface composition is determined by the adsorption kinetics of the adsorbing species with regard to the competitive adsorption between

the surface active components, proteins and surfactants. According to this, it has been reported in various studies [90, 51, 116, 137] that surfactants can prevent or reduce protein-surface interactions and, when the surfactants have a higher equilibrium surface tension than a protein, even replace proteins at the interface. With regard to the here obtained ESCA-data, it might be likely that the PL have displaced the oleosin from the droplet interface, since only PL and no protein are found within the surface layer of the powder. Contradictory to this, dynamic interfacial tension measurements presented in [43] revealed that PL are not capable of displacing oleosins from the oil-water interface but rather enhance the interfacial stability due to synergistic effects. Similar was observed for emulsions composed of casein and a mixture of lecithins.[76] However, here, the competitive behaviour of PL in accordance to proteins was different, depending on the structural composition of present PL. Thus, displacement of proteins occurs when PL are initially partly present as small aggregates or monomolecular species in the oil phase. By migration to the water phase, PL become hydrated and reorientate to mesophases or vesicular aggregates, incapable to displace proteins due to the interactions with the proteins. The latter is regarded as more likely to occur at large oil-water interfaces.[37, 76]

In contrast to the two previously stated scenarios of the competitive adsorption behaviour of PL and proteins, spray drying involves adsorption kinetics to the air-water interface. Thus, mechanisms of PL and oleosin competing interfacial adsorption behaviour might be different to the oil-water interface. Moreover, with progressing drying, the interface changes from an air-water to an oil-air interface, which might involve completely different structural orientations of components present at the surface than it is known from oil-water or air-water interfaces. With regard to air-water interfaces, Millqvist-Fureby et al. (2007) revealed by ESCA measurements that PL or lecithin can partially displace proteins due to complex-formation between PL and proteins. The degree of displacement depends on the different capabilities of proteins to form complexes with PL. Subsequently, protein-rich and PL-rich regions are formed at the powder surface.[134] Thus, the lack of protein coverage in pure, spray dried oleosomes can be presumably attributed to the unusual structure of the oleosin. To recall, in contrast to the most proteins present in food, the oleosin is not only peripherally located at the oil droplet interface but is also anchored with its long hydrophobic domain into the oil matrix.[81, 182] The exposure to large

air-water interfaces along with water evaporation and extensive oil droplet coalescence might have contributed to the formation of insoluble oleosin aggregates at early drying stages, which favoured the accumulation of PL on the interface. Studies performed by [192] regarded as likely that oleosins of low concentration might desorb from the, here planar, air-water interface a while after the rupture of oleosomes, resulting in a PL-dominated interface. Although this assumption is based on interfacial measurements performed at time scales significantly longer than the life time of a droplet, which is between 0.1 and 1 ms, [47], it can be assumed that the water reduction along with heat-induced oleosin degradation during drying has accelerated this effect.

Morphological properties of powder particles might also give some evidence about the surface composition. Particles that included surfactants exhibited a spherical shape with smooth surfaces. These features have been attributed to the formation of less visco-elastic films due to the higher mobility of the adsorbed surfactants.[116, 137] This corresponds in parts to the observations made in this study by SEM (see Subsec. 7.2.1). For powders produced from 15 wt% oleosome emulsions at 100 °C (Sample A), comparatively spherical particles with a relatively smooth surface are visible (Fig. 7.5a). However, as it was already discussed in Subsec. 7.2.1, it is also likely that the smooth surface is based on the plasticising effect of the free surface oil. Moreover, oleosomes spray dried at 180 °C disprove the assumption that the surface topology correlates with the level of PL coverage. As shown in the micrographs (Fig. 7.8c), the particles are neither spherical nor exhibit a smooth surface although a higher percentage of PL is measured by ESCA.

Oleosomes with MD Oleosomes encapsulated with MD exhibit a significant level of protein on the powder surface. The percentage of the protein content in the powder surface slightly increases from 39.0 to 47.4 %, respectively from 11.3 to 13.7 % in case of drying temperatures of 180 °C. Here, the experimental values differ significantly from the theoretical ones due to the large measurement error obtained in the reference measurement of the isolated oleosin. Thus, the actual surface composition is presumably best described by using the theoretical values. Respective SEM micrographs, see also Fig. 7.8, reveal powder surfaces with shallow dents. Such dents are assumed to be characteristic for protein accumulation in the surface

layer.[55, 94, 134] Thus, the dents shown in the SEM micrographs correlate well with the found protein coverage as measured by ESCA. In principle, dents appear to be more pronounced with increasing level of protein [55, 70, 94, 134], which is also in accordance with the observations made here.

Marginal amounts of about 4.6 % MD are detected in the surface layer of powders dried at 100 °C. At drying temperatures of 180 °C, no MD is found at all. These findings are quite surprising, since the dry weight of the spray dried emulsion is composed of three-quarter of MD. Comparable studies of dairy powder revealed that protein and fat accumulate at the surface, preferentially to lactose. Particularly at higher drying temperatures, film formation of protein near the surface is favoured and thus hinders the migration of lactose to the surface.[137] Thus, it is likely that this also applies to MD.

Powders dried at 180 °C exhibit with 86.2 % a higher oil content than powders dried at 100 °C (oil content 84.1 %). These differences seem to coincide well with the observations made by CLSM (see Subsec. 7.2.2). Micrographs of powders produced from 3.5 wt% oleosome emulsions with 10 wt% MD indicated that oil droplets of coalesced oleosomes are accumulated in closer proximity to the surface when drying occurred at 180 °C (Fig. 7.9d).

Besides all afore mentioned aspects, the location and thickness of layers or patches of components in the surface are crucial for the ESCA-data evaluation and the conclusions drawn consequently. In principle, it is assumed that all components are present in patches at the surface of the powders and that their layer is thicker than the analysing depth (here approximately 8 nm).[56] As indicated in the CLSM micrographs (Fig. 7.9), all oil droplets significantly exceed this size. According to the oleosome model, it is assumed that the monolayer of PL exhibits a thickness of about 2.5 nm, which is less than half the depth of analysis. The thickness of oleosins has not been specified so far but it is supposed to be thinner than the analytical depth. However, if aggregation of oleosins has occurred due to spray dried-induced denaturation, this thickness could be larger. Thus, it is likely that photoelectrons emitted from the molecular species located in different depths comparably contributed to the signal intensity. As a result of this, it is difficult to discriminate whether the component is situated within the outermost layer or some nanometres below the surface.

By considering all findings obtained by SEM, CLSM and ESCA measure-

ments, it is very likely that the oleosomes have coalesced and component segregation has occurred during spray drying. Both processes might involve one another. The mechanism and magnitude of component segregation are not yet fully understood and regarded as very complex due to multiple components, non-equilibrium processes and operating parameters involved.[191] Segregation of components can be described by two to three different processes that are not mutually exclusive: 1) Crust formation on the outermost layer of the droplet surface, 2) migration of water and dissolved solids within the droplet with progressing drying driven by differences in the diffusivity, here the effect of the components solubility is considered, and 3) migration and precipitation of the solids. The latter depends on the surface activity of the components, which is the driving force for the diffusion.[191]

Upon drying, the concentration of the solvent gradually decreases from the droplet surface to its centre. This gradient provokes the components to diffuse to the droplet centre. Depending on the physicochemical properties of the components, diffusion occurs at different velocities. Components with a larger molecular weight and thus lower solubility are supposed to precipitate first.[51, 104, 127, 191] This might provide a reasonable explanation why soybean oil, exhibiting highly insoluble molecules, is the dominating surface component at the powder particles. Surface active molecules like oleosins presumably rise more quickly to the droplet surface upon atomization and precipitate almost instantly at the air-liquid interface on initial heating.[52, 104, 127] The diffusion driven adsorption to the interface depends on the concentration, the surface hydrophobicity, the hydrodynamic radius and on the state of aggregation of the proteins.[47] Studies by Kim et al. (2003) showed that layers of protein bound to fat globules can be located underneath the free surface fat.

Particularly at low load (2-10 mg/L), proteins tend to denature when being exposed to the large air-water interface of atomized droplets.[51, 116] It is assumed that the addition of low molecular weight carbohydrates like lactose can keep the protein solubilised, thus providing a thermal stabilising effect and contributing to an enhanced oil, respectively fat encapsulation efficiency.[40, 51, 52] However, similar effects were not observed for MD.[94] Here, with the increasing amount of MD (DE 10) in the dry composition, increasing fractions of the powder surface are covered by the oil phase. The researchers regarded it as likely that the formation of a hard shell has caused rupture of oil globules when subjected to shear stresses during spray drying,

as its lower elasticity is unsuitable to withstand such destructive forces. These findings correlate quite well with the high oil coverage measured at the surface of oleosomes encapsulated with MD.

7.3. Characterisation of reconstituted oleosomes

By comparing particle sizes of soybean oleosomes before spray drying and after redispersion, valuable information can be obtained about the integrity of spray dried oleosome emulsions and about how well the original oleosome structure is maintained by the encapsulation with MD. In order to yield a stable emulsion after redispersion, a narrow distribution of small particles is a prerequisite, which consequently implies that the oleosomes remained intact and well dispersed in the powder matrix during spray drying. Since emulsions are thermodynamically unstable, coalescence that might have occurred during drying due to disrupted oleosomes would result in an increased particle size distribution of reconstituted oleosome emulsions upon redispersion.[55]

Along with surface charge distribution analysis by means of ζ-potential measurements and by utilising FTIR to evaluate the impact of spray drying on the secondary structure of oleosins, additional information about changes in the internal structure of the oleosomes can be gained.

7.3.1. Particle size and surface charge distribution

Spray dried powders composed of either pure oleosomes or oleosomes encapsulated with MD were redispersed in buffer solutions of pH 7. The volume frequency distribution (q_3) of all reconstituted oleosome emulsions is determined by laser diffractometry. Here, the impact of drying temperature (100, 130 and 180 °C) and the composition of the feed emulsion is evaluated.

As discussed in detail in Sec. 8.1, the real part of the refractive index (n_r) and attenuation coefficient (n_i), used as input parameters for the transformation of scattering intensities into volume-weighted PSD on basis of the Mie theory, can significantly influence the weighting of small and large particle fractions. Thus, the obtained PSD are computed twice by implementing the real part of refractive indices for either proteins ($n_r = 1.6$) or soy oil ($n_r = 1.47$) and an attenuation coefficient of 0.01, for both cases. In

Fig. 7.10, the PSD obtained by using $n_r = 1.6$ and $n_i = 0.01$ are shown on the left hand side and for $n_r = 1.47$ and $n_i = 0.01$ on the right hand side. To facilitate a comparison between the different PSD, the PSD of each analysed powder composition is confined to a particle size ranges of 0.08 to 0.8 µm, which is here indicated by two dashed vertical lines. From this limited size range, the volume percent of particles with a diameter comparable to that of crude oleosome emulsions is derived.

The particle size measurements reveal that the PSD of redispersed oleosome emulsions is significantly shifted to particles of larger volume, in contrast to native oleosome emulsions. The formation of larger particles can be either attributed to coalescence of oleosomes or to the poor dispersion of agglomerated powder particles. Aggregation effects are the greatest for oleosomes spray dried without MD (Fig. 7.10a), where only the use of $n_r = 1.47$ and $n_i = 0.01$ yields minor volume fractions (6.0 to 9.2 vol%) of particle sizes (Fig. 7.10b), which are comparable to those of native oleosomes. In general, the use of $n_r = 1.47$ leads to a larger volume fraction of particles with sizes comparable to those of native oleosomes than the use of $n_r = 1.6$.

The percentage of smaller particles, assuming that these are intact oleosomes, increases with increasing amount of MD added to the oleosome emulsion prior to spray drying. When 5 wt% of MD were added, 7.7 vol% (Fig. 7.10c), respectively 22.6 vol% (Fig. 7.10d) of oleosomes, depending on the input parameters used for the particle size computation, remained intact when drying at 130 °C. MD concentrations of 10 wt% and drying temperatures of either 100 or 130 °C yield the highest amount of intact oleosomes with 13 vol% (Fig. 7.10e) and 36 vol% (Fig. 7.10f). Thus, the integrity of oleosomes is best preserved when drying at lower inlet temperatures, whereas the differences between 100 and 130 °C are marginal. Despite the use of an encapsulating material, temperatures of 180 °C caused severe disruption of oleosomes and thus yield the lowest volume fraction of intact oleosomes. These results are in line with the observations made by CLSM (see Subsec. 7.2.2).

In principle, the reconstitution process of powders in water can be divided into four steps: Wetting, submerging, dispersing and dissolving.[61] In this context, the wetting of particles is often the rate-controlling step. Fast wetting is favoured with large particles exhibiting large pores and is best achieved when the contact angle between the powder surface and the penetrating water is small.[103, 105] Apart from the size and porosity of

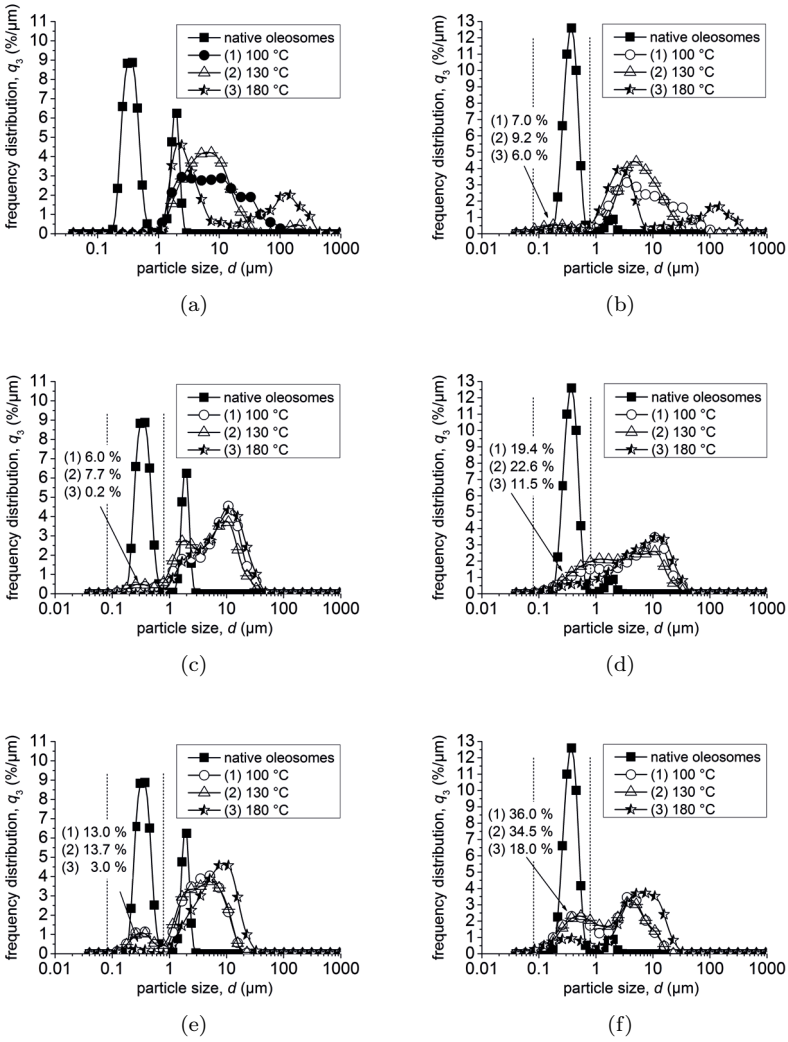

Figure 7.10.: Volume frequency distribution (q_3) of redispersed powders of different composition and spray dried at either 100, 130 or 180 °C in comparison to native oleosomes. On the left hand side, the PSD obtained by implementing the real part of refractive index for proteins ($n_r = 1.6$) and, on the right hand side, for soy oil ($n_r = 1.47$) in the particle size calculations based on Mie theory. The attenuation coefficient was 0.01 in all cases. The dashed vertical lines confine the particle size range from 0.08 to 0.8 µm in order to allow a better comparability between native and resuspended oleosomes. (a+b) pure oleosome emulsion. (c+d) oleosome emulsion with 5 wt% MD. (e+f) oleosome emulsion with 10 wt%.

the powder particles, the surface composition also plays a major role in the wetting process. Surface coverage by fat or oil deteriorates the wettability and dispersibility due to an increased contact angle between the powder surface and the penetrating water and a higher surface hydrophobicity.[56] As revealed by ESCA measurements (Subsec. 7.2.3), a significant part of the particle surface of all analysed powder samples is predominantly covered with oil. This impedes a proper wettability and dispersibility as the particles are adhered together by oil bridges, forming large insoluble aggregates.

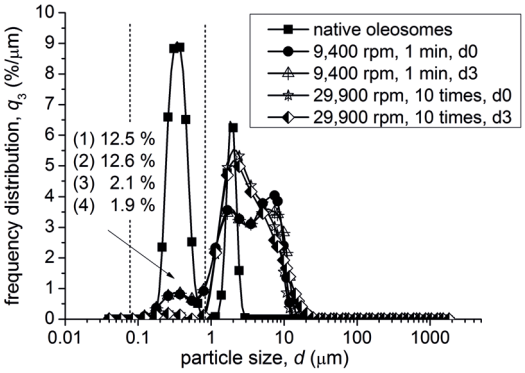

Figure 7.11.: Volume frequency distribution (q_3) of redispersed powders produced from emulsions of 3.5 wt% oleosomes with 10 wt% MD at 100 °C in comparison to the one of native oleosomes. Homogenisation of the redispersed powders was conducted at 9,400 rpm for one minute and at 29,900 rpm applied in ten quick successional intervals of 10 s each. For data generation, $n_r = 1.6$ and $n_i = 0.01$ were used.

Therefore, redispersed oleosome powders have been subjected to differently high shear stresses, generated by an Ultra-Turrax, to find out if a particle size distribution can be achieved, which is comparable to that of the crude oleosome emulsion. Here, only the emulsion of 3.5 wt% oleosomes and 10 wt% MD spray dried at 100 °C was examined, which proved to have the largest fraction of intact oleosomes (see also Fig. 7.10e). At revolutions of 9,400 rpm applied for 1 min, the level of intact oleosomes is maintained but the fraction of larger particles (around 4 µm) is slightly shifted to smaller sizes (around 1.8 µm) in comparison to the non-homogenised emulsion (Fig. 7.11). After three days of storage, no significant change in the PSD

is observed. By employing even higher shear stresses of 29,900 rpm applied in short (10 s) intervals for ten times, the amount of intact oleosomes is reduced from 12.5 % to merely 2 %. This indicates that a considerable amount of redispersed oleosomes could not withstand these high shear stresses. According to this, under these conditions, it is not possible to obtain an emulsion, of which PSD is comparable to that of the crude oleosome emulsions. An emulsion of similar PSD and stability is presumably only achieved when the oleosin, once removed from its natural environment, for example due to component segregation induced by spray drying, is capable to fold back into its original structure and to anchor into the oil droplet. Since the oleosome structure and in particular the targeting of the hydrophobic domain of the oleosin into the oil core is a result of complex mechanisms during the biogenesis of oleosomes [77], it is considered as unlikely that segregated oleosome components can arrange back into their original structure.

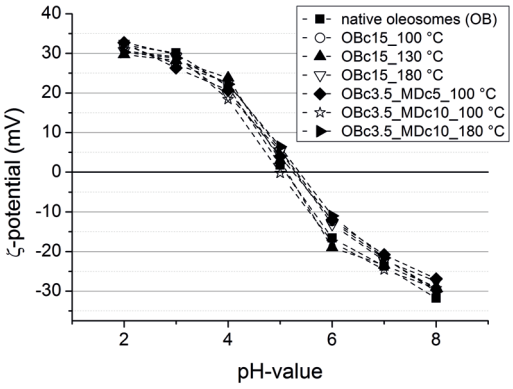

Figure 7.12.: ζ-potential (mV) of native oleosomes and redispersed powders spray dried at different drying temperatures in terms of pH.

The ζ-potential was determined in terms of pH to quantify the electric double layer of native and spray dried, redispersed oleosomes relevant for evaluation of colloidal interaction and colloidal stabilisation, particularly with regard to destabilisation phenomena that might have occurred during spray drying. The ζ-potential for native oleosomes changes from $+32 \pm 1.2$ mV at pH 2 to -24 ± 1.6 mV at pH 8 reaching zero at pH 5, which is consistent with the pI of the oleosin (Fig. 7.12). Interestingly, no change in the ζ-potential is observed in any of the redispersed powder com-

positions, irrespective of the applied drying temperature. This indicates that the measured samples exhibit the same surface charge distribution as crude oleosome emulsions. Such emulsions have shown to be highly stable to aggregation at pH-values that are far apart from the isoelectric point (pI $\approx$ 5.3) of the oleosin (see also Sec. 6.1.1). However, this is evidently not the case for reconstituted oleosome emulsions as shown in the particle size measurements, here performed at pH 7. Here, it is likely that exclusively the intact oleosomes have been measured as those are the only particles with a surface charge while highly agglomerated particles predominantly covered with oil or free oil, which originates from coalesced oleosomes, do not carry a surface charge.

7.3.2. Secondary structure analysis

FTIR spectroscopy was applied to estimate the conformational changes in the secondary structure of oleosins enclosed in spray dried oleosomes. In Fig. 7.13 the FTIR-spectra of isolated oleosins and of native oleosomes are shown. Both spectra have common characteristic bands at 1650 and 1548 cm^{-1}, which are attributed to amide I and amide II vibrational modes, respectively. The spectrum of the isolated oleosins further shows a prominent band at 3285 cm^{-1}, which is assigned to the amide stretch mode of the amide A band. In the spectrum of native oleosomes, the vibrational mode of the amide A band is overlapped by the modes of H-bonded C-H stretch groups, which originate from PL of the oleosomes (Fig. A.2). Moreover, distinct bands of TAG at 2800-3050, 1746, 1456 and 1200-1100 cm^{-1} are visible, which have been attributed to C-H stretch, carbonyl stretch, C-H bending and C-O stretch, respectively. Minor signals of these vibrational modes are present in the spectrum of the isolated oleosin, indicating residual amounts of non-extractable TAG. This observation corresponds to the surface compositional analysis of isolated oleosins by ESCA, as discussed already in detail in Subsec. 7.2.3.

Fig. 7.14 shows the deconvoluted amide I band, the Gaussian curve fit thereof, including the resolved individual bands, and the second derivative spectra of a soybean oleosin. Fourier self-deconvolution (FSD) and second derivative have been employed to identify quantitatively the different secondary structures present in the oleosin. Band positions indicated by these methods of mathematical resolution enhancement were used as basis for

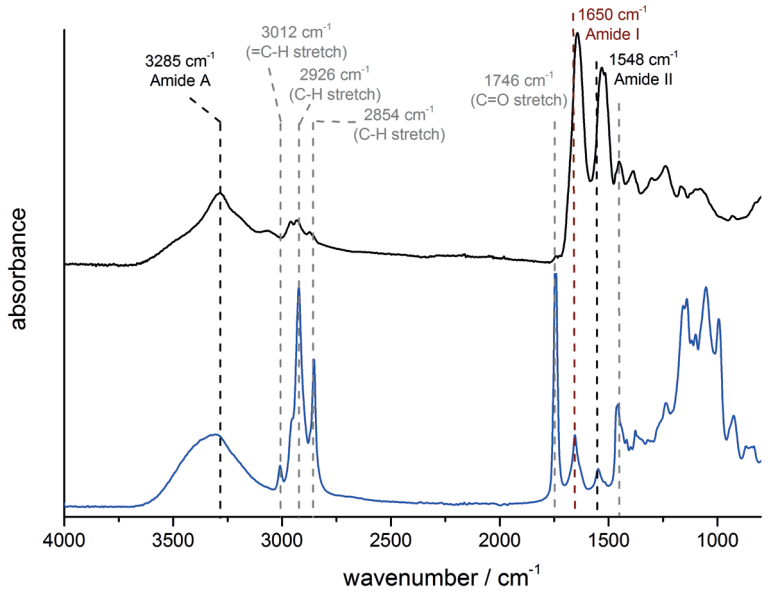

Figure 7.13.: Mid-infrared spectra of isolated oleosins (black) analysed in their solid state by using the ATR technique and of native oleosomes (blue), here in form of a dried cream layer, determined by transmission measurements.

the curve fitting procedure to calculate the area of each secondary element. Both, powder samples (here ATR was used as sampling technique) and redispersed powders centrifuged to a cream layer and dried on a CaF_2 window to avoid interference with water vibrational modes, were analysed. Thereby, conformational changes in the secondary structure of oleosins, and thus in oleosomes integrity, that might have occurred during spray drying, can be evaluated. Except for the isolated oleosins, all secondary structure assignments refer to oleosins that are embedded in their natural environment the oleosome or are at least somehow bound to its constituents. Some spectra of the amide I band of the redispersed samples, the resolved curve bands thereof and the curve fits to them are exemplarily shown in the appendix (Fig. A.3 and Fig. A.4). The percentages of secondary elements, contributing to the amide I signal, obtained by band assignment are listed in the following Tables 7.3-7.6.

Quantitative analysis of the spectra of both the native oleosome and the oleosin reveals a relatively strong signal at around 1655 cm^{-1} (Table 7.3).

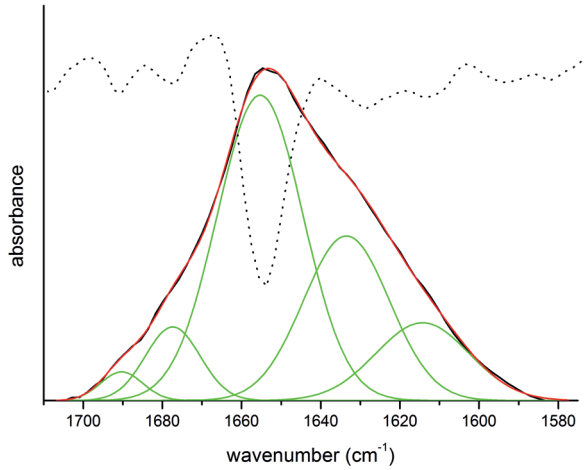

Figure 7.14.: Resolution enhancement of a complex band of overlapping FTIR bands. Here the amide I band of the isolated oleosin is used representatively. Deconvoluted amide I band (black), Gaussian curve fit thereof (red) including the resolved individual bands (green) and second derivative spectra (dotted).

This band can be assigned to α-helical structures, accounting for 57 % of the total amide I intensity in case of the native oleosomes and 48 % for the oleosins. In the spectra of the native oleosomes, shoulders on both sides of the main absorbance are determined at 1630 cm^{-1} (9 %), 1641 cm^{-1} (13 %), 1670 cm^{-1} (11 %) and 1681 cm^{-1} (5 %), which can be attributed to β-sheets or β-turns, respectively. An additional band at 1618 cm^{-1} (2 %) presumably results from strong intermolecular H-bonds, which occur in extended, denatured polypeptide chains.[87] In general, these findings are in line with the analysis of protein secondary structure for safflower and sunflower oleosins.[108, 122]

In comparison to native oleosomes, the secondary elemental composition of the amide I of the oleosin reveals distinct differences. The adjacent β-sheet at 1641 cm^{-1} found for native oleosomes, is not seen anymore and seems to have reorientated to anti-parallel β-sheet structures. Moreover, contributions attributed to α-helical structures are with 48 % of relative intensity less pronounced. It is assumed that the reorientation is induced by the removal of water molecules from molecules in close proximity of the oleosin's sur-

face and the spatial approach of peptide chains, when being solidified. The loss of water molecules can be presumably attributed to diminishing intermolecular H-bonds between amide groups of the peptide chain or carboxyl groups of the side chains and the water dipole.[11, 121] Since β-sheet structures can maintain a lower degree of solvation in comparison to α-helical, turn or random coil structures, the reorientation to intermolecular β-sheet elements is supposed to be more favourable.[148] Moreover, the additional band at 1618 cm^{-1} is slightly shifted to 1614 cm^{-1} and accounts for a higher relative intensity (14 %) of the total amide I signal (Table 7.3). Within such extended chains, typically found in denatured proteins, intramolecular hydrogen bonding is not feasible. However, due to the extended nature of these chains, adjacent chains can align with each other, thus favouring the formation of very strong intermolecular hydrogen bonds.[87] Therefore, a shift to these β-sheets is regarded as a logical consequence as, in order to isolate the oleosin, it was exposed to organic solvents and freeze dried. These factors plus the solid state might have contributed to these conformational changes.

Table 7.3.: Parameters resulting from the band fitting procedure of FTIR spectra in the amide I region for native, untreated soybean oleosomes (CaF_2 window) and isolated oleosins (ATR)

Sample	**Band (cm^{-1})**	**Area (%)**	**Assignment**
Native OB	1618	2	aggregated strands
	1630	9	anti-parallel β-sheet
	1641	13	β-sheet
	1655	57	α-helical
	1670	11	β-turn
	1681	5	β-sheet
Isolated oleosin	1614	14	aggregated strands
	1634	26	anti-parallel β-sheet
	-	-	β-sheet
	1654	48	α-helical
	1678	7	β-turn
	1691	2	β-sheet and turn

In Table 7.4, the parameters obtained from the quantitative analysis of

the protein secondary structure of 15 wt% oleosome emulsions spray dried at 100 or 180 °C are shown. Here, the band assignments of both powders and redispersed oleosomes are depicted. As well as for native oleosomes and the isolated oleosins, a predominant contribution to the total amide I intensity results from α-helical structures, irrespective of the sample physical state being analysed or drying temperature applied. In the solid state, the Gaussian curve fitting resolved five bands at wavenumbers similar to that of the isolated oleosin. Thus, no shoulder around 1640 cm^{-1} was evident in the deconvoluted spectra of the powder samples, resulting in a higher relative intensity for bands assigned to anti-parallel β-sheets and aggregated strands. Except for slight variations in the band position and the calculated areas, the structures attributed to β-strands (β-sheets and β-turns) are not very different from each other when the oleosomes were spray dried at either 100 or 180 °C. However, the quantitative determination of α-helical structures contributing to the total amide I intensity yields only 37 % for oleosomes dried at 180 °C. This is significantly lower than the 48 % determined for 100 °C. The relative intensity of the aggregated β-strands is in both cases slightly lower than for the isolated oleosin. Therefore, while only 35 % of β-strands accounts for the amid signal of the latter, it is 45 % for oleosomes dried at 100 °C and 57 % for those dried at 180 °C (Table 7.6). This difference can be presumably ascribed to the presence of higher amounts of oil in the spray dried powder with which the oleosins might still interact. Hydrophobic regions of the polypeptide chains were found to be better solvated by oil than by air and as a consequence, unfolding of the protein occurred at the interface to a greater extent.[135]

Upon redispersion of the spray dried oleosomes, the content of anti-parallel β-sheets diminishes and the band around 1640 cm^{-1} assigned to β-sheets becomes evident again (Table 7.4). No change in the total β-strand content is observed for oleosomes spray dried at 100 or 180 °C, being with a relative intensity of 46 %, respectively 58 % almost equal to the content measured for the powder samples (Table 7.6). The same applies for the α-helical content. In comparison to the native oleosomes, a conversion of a predominant α-helical structure to predominant β-strands has occurred upon spray drying, whereas the effect is larger for higher drying temperatures. As a result of this, it can be assumed that some major conformational changes in the secondary structure of the oleosin occurred during spray drying, that are irreversible. In this context, it has to be mentioned that due to the

Table 7.4.: Parameters resulting from the band fitting procedure of FTIR spectra in the amide I region for 15 wt% oleosome emulsions spray dried at either 100 or 180 °C and analysed in the solid and redispersed form (values in brackets)

Sample	Band (cm^{-1})	Area (%)	Assignment
OBc15_100 °C	1618 (1618)	8 (8)	aggregated strands
	1635 (1630)	27 (11)	anti-parallel β-sheet
	- (1641)	- (21)	β-sheet
	1653 (1655)	48 (46)	α-helical
	1672 (1669)	12 (8)	β-turn
	1685 (1678)	6 (6)	β-sheet
OBc15_180 °C	1617 (1616)	6 (6)	aggregated strands
	1638 (1628)	33 (11)	anti-parallel β-sheet
	- (1642)	- (27)	β-sheet
	1655 (1655)	37 (35)	α-helical
	1672 (1669)	16 (13)	β-turn
	1687 (1680)	8 (7)	β-sheet

high level of free surface oil of these powder samples, as verified by ESCA measurements (Subsec. 7.2.3), the accessibility of the aqueous solvent, and thus the protein solvation, is impeded.

For powder samples containing also MD, the quantitative secondary structure analysis revealed similar contents of secondary elements as for the pure oleosome powders (Table 7.5). However, the relative intensity for extended, aggregated chains, contributing to the amide I signal, is, in case of samples dried at 100 or 180 °C, with 16 % and 13 %, respectively, considerably higher. Segregation effects, causing a different disposition of proteins, PL, TAG and MD within the powder particles might explain why the content of aggregated chains is rather comparable to that of isolated oleosin, than to that of native oleosomes. According to the segregation effects and the subsequent distribution of components, proteins might interact with oil patches or have formed non-interacting aggregates.

On redispersion of the solids in buffer solutions, the respective contribution of the assigned elements to the amide I signal is significantly different to the previously described samples. While the β-strand content has not

Table 7.5.: Parameters resulting from the band fitting procedure of FTIR spectra in the amide I region for 3.5 wt% oleosome emulsions with 10 wt% MD spray dried at either 100 or 180 °C and analysed in the solid and redispersed form (values in brackets)

Sample	**Band (cm^{-1})**	**Area (%)**	**Assignment**
OBc3.5_MDc10	1618 (1619)	16 (4)	aggregated strands
100 °C	1636 (1631)	27 (9)	anti-parallel β-sheet
	- (1641)	- (11)	β-sheet
	1656 (1655)	42 (52)	α-helical
	1675 (1670)	8 (10)	β-turn
	1688 (1680)	7 (11)	β-sheet
OBc3.5_MDc10	1613 (1619)	13 (4)	aggregated strands
180 °C	1634 (1631)	27 (9)	anti-parallel β-sheet
	- (1641)	- (12)	β-sheet
	1656 (1655)	44 (49)	α-helical
	1676 (1669)	8 (14)	β-turn
	1692 (1681)	9 (7)	β-sheet

changed fundamentally, transformation of aggregated chains back into the α-helical conformation occurred. No significant differences in the structural conversion in terms of drying temperature are evident. With slight differences in the relative intensities of the respective β-strands, the secondary composition of the spray dried and redispersed oleosomes is almost identical to that found in the native oleosomes. The result of the band fitting is a structural composition of 41 % β-strands and 52 % α-helices for oleosomes encapsulated with MD and spray dried at 100 °C and 42 % β-sheet and 49 % α-helices for those dried at 180 °C. According to this, it is very likely that structural transformations in the secondary conformation induced by spray drying are fully reversible upon redispersion when MD was added prior to drying. Similar observations have been also made, amongst others, for example: Poly-L-lysine spray dried in presence of trehalose [121], bovine serum albumin and trehalose [51], whey protein and lactose [53] and immunoglobulin G spray dried with sorbitol or trehalose [123]. The stabilising effect by low molecular weight carbohydrates, like by the low molecular weight fractions of MD with a high DE, can be explained by their capabil-

Table 7.6.: Total amounts of α-helical, β-strands and aggregated structures contributing to the amide I signal of spray dried oleosomes, here in comparison with native oleosomes and isolated oleosins

Sample	$\boldsymbol{\alpha}$ **(%)**	$\boldsymbol{\beta}$ **(%)**	**aggregated (%)**
native oleosomes	57	38	2
oleosin	48	35	14
OBc15_100 °C powder	48	45	8
OBc15_100 °C cream	46	46	8
OBc15_180 °C powder	37	57	6
OBc15_180 °C cream	35	58	6
OBc3.5_MDc10_100 °C powder	42	42	16
OBc3.5_MDc10_100 °C cream	52	41	4
OBc3.5_MDc10_180 °C powder	44	44	13
OBc3.5_MDc10_180 °C cream	49	42	4

ity to act, to some extent, as "water-replacer" and thus to keep the protein solubilised after drying.[90]

The phenomenon of protein stabilisation by carbohydrates, particularly when subjected to the large air-water interfaces upon atomization, has already been discussed in context of the powder surface composition analysis (see also Subsec. 7.2.3). Here, comparable studies by Jones et al. (2013) regarded it as unlikely that MD is capable of keeping the protein solubilised. According to the results obtained from secondary structure analysis by means of FTIR spectroscopy, the contrary could be shown, assuming that MD has indeed stabilising effects on the oleosins conformational structure during spray drying and could reduce protein-surface interactions. According to this, it is even more likely that the large amounts of free surface oil on the powder particles might result from the formation of hard, inelastic shells by MD upon spray drying that have caused disruption of oil droplets.

8. Evaluation of particle size

Isolated oleosomes form an oil-in-water emulsion. The size of oil droplets determines the stability, appearance, mouth-feeling and rheological properties of the emulsion. Therefore, an accurate characterisation of the oleosome size and droplet size distribution is a pre-requisite for their processing and implementation in intermediate or final food products.

8.1. Determination by light scattering

As a first approach, particle size measurements of oleosomes were performed by applying dynamic light scattering (DLS), revealing an average (hydrodynamic) diameter of 0.25 µm. However, when it has come to particle size measurements of oleosomes in terms of pH-value, DLS proved to be an inappropriate method as creaming of oleosomes resulted in significant measurement error. In order to cover a broad range of particle length scales, particle sizing was carried out by using laser diffractometers.

Concerning the evaluation of the appropriate complex refractive indices, test trials, where the measured scattering intensities were compared with the calculated ones (variance $\chi^2 = 0.45$), verified appropriate indices of 1.6 (n_r) and 0.01 (n_i). Since these results are based on computational-intensive calculations, they can only be regarded as rough estimation and do not necessarily reveal the true refractive index of oleosomes. Ray et al. (1983) stated that the contribution of the interfacial layer of the emulsion droplets to their optical properties is negligible, when the thickness of the layer is small enough in relation to the wavelength of the incident light. Thus, both the real parts of the refractive index for proteins ($n_\mathrm{r} = 1.6$) and soy oil ($n_\mathrm{r} = 1.47$) are used for the droplet size measurements by laser diffractometry (LD). In the following, the influence of the different real parts of the refractive index and attenuation coefficients on the obtained droplet size distribution is discussed.

Fig. 8.1 and Table 8.1 show the volume frequency distribution, q_3 (%/µm),

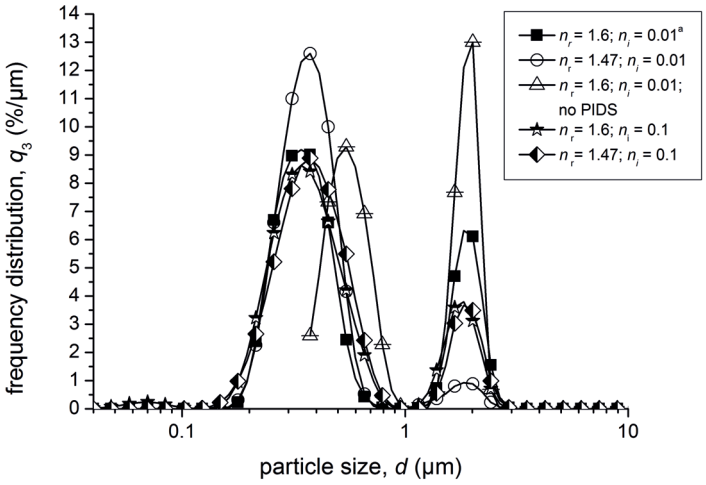

Figure 8.1.: Volume frequency distribution, q_3 (%/µm), of oleosomes measured as received after extraction and purification, having a solution pH-value of 7. Calculation of particle size distribution is based on Mie theory by using different real refractive indices (n_r) and attenuation coefficients (n_i). Except the green curve, PIDS data (see Subsec. 4.1.2) is included in the data processing of all other curves.

of oleosomes and the respective descriptive statistic parameters obtained by implementing different complex refractive indices in the calculations of intensity scattering pattern according to Mie theory. In principle, the particle size distribution of oleosomes is bimodal, whereby a significant amount of oleosomes (at least 70 %) is within a size range of 0.16 to 0.95 µm and a minor volume fraction exhibits a particle diameter between 1 to 3.2 µm. Particle size measurements by using the real part of the refractive index for protein (n_r = 1.6) and soy oil (n_r = 1.47), and an attenuation coefficient of 0.01, respectively, reveal the most pronounced differences in the volume frequency distribution. In the former case, approximately 30 % of the oleosomes are larger than 1 µm, while these are only 4 % in the latter. Measurements with an attenuation coefficient of 0.1 yield a comparable distribution as for n_r = 1.6 and n_i = 0.01 but the size range of the first mode is slightly broader and the volume fraction of larger droplets is reduced by half. Moreover, volume fractions of particle sizes <0.1 µm are

measured, indicating that an attenuation coefficient of 0.1 is inappropriate for the particle size measurements, since oleosomes are supposed to be significantly larger. The green curve in Fig. 8.1 depicts the distortion of results when the PIDS data (see Subsec. 4.1.2) is not included in the determination of the droplets size distribution.

Table 8.1.: Characteristic average oleosome diameters and the standard deviation (S.D.), here as a measure of the distribution width, derived from particle size measurements with different n_r and n_i

n_r and n_i implemented in data processing	D[4,3] (µm)	D[3,2] (µm)	D(v, 0.1) (µm)	D(v, 0.5) (µm)	D(v, 0.9) (µm)	S.D. (µm)
1.6; 0.01	0.83	0.46	0.27	0.42	2.1	0.75
1.47; 0.01	0.46	0.38	0.27	0.38	0.56	0.34
1.6; 0.01; no PIDS	1.24	0.83	0.49	0.76	2.2	0.74
1.6; 0.1	0.66	0.39	0.25	0.41	1.83	0.61
1.47; 0.1	0.67	0.42	0.26	0.43	1.88	0.61

Characteristic mean diameters of oleosomes and other descriptive statistical parameters selected from the acquired data are shown in Table 8.1. For example, the volume weighted average diameter D[4,3], which is an adequate parameter for the evaluation of emulsion stability [65], is 0.84 µm for $n_r = 1.6$ and $n_i = 0.01$ and 0.46 µm for $n_r = 1.47$ and $n_i = 0.01$. Distinct differences are also observed in case of D(v, 0.9). Here, for $n_r = 1.6$, 90 % of the volume fraction of particles are smaller than 2.1 µm, whereas for $n_r = 1.47$, 90 % are not larger than 0.56 µm. Thus, when using $n_r = 1.6$, volume fractions of larger particles are preferentially measured or, the other way round, large particles are not measured, when using $n_r = 1.47$. This pronounced difference in the characteristic average diameter of oleosomes emphasises explicitly that great care is required, when applying optical properties in order to achieve an accurate particle size determination. Consequently, these characteristic sizes can only be related to the corresponding information required for a subsequent production process after ensuring validity of the applied parameters.

Particle sizing methods by such standardised laser diffraction methods

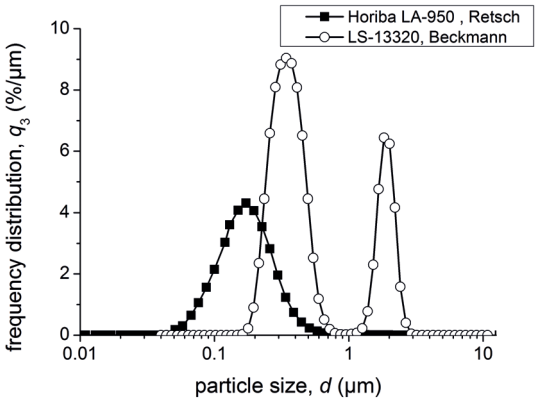

Figure 8.2.: Particle size measurements of native oleosomes (pH 7) performed by using two different laser diffractometers, one from Retsch Technology (Horiba LA-950) and one from Beckmann-Coulter (LS 13320). A real refractive index of $n_r = 1.6$ and an attenuation coefficient of $n_i = 0.01$ were used.

are regarded as questionable, in particular with respect to the use of refractive indices and the measurement of non-spherical particles, such as agglomerates.[100] Moreover, dilution of emulsions might result in a significant measurement error.[46] However, it is beyond the scope of this thesis to evaluate the general validity of laser diffraction. Nevertheless, the particle size distribution of oleosomes was measured by using two different laser diffractometers, one from Retsch Technology (Horiba LA-950) and one from Beckmann-Coulter (LS 13320). Indeed, both instruments yield completely different particle size distributions of native oleosomes, as shown in Fig. 8.2. Although the sample preparation, as well as the used optical parameters ($n_r = 1.6$ and $n_i = 0.01$) have been the same, the volume frequency distribution, Q_3 (%/µm), measured by Horiba LA-950 is monomodal, while that of the LS 13320 is bimodal. Moreover, in the former case, the average mean diameter, $D(v, 0.5)$, is 0.17 µm, while it is 0.42 µm for the latter.

8.2. Alternative particle sizing methods

Taking into account the probable measurement error due to dilution prior to particle analysis and the insecurity concerning the validity of refractive indices, it can be supposed that the results obtained by LD merely give a

rough overview about the particle size distribution of oleosomes. Moreover, since LD generates volume-weighted particle sizes, a skew of the distribution and thus a trend to larger average diameters is likely. The presence of a few individual larger voluminous particles might outweigh the effect of very smaller particles on the distribution. Thus, additionally light microscopical (LM), NMR via self-diffusion and small angle neutron scattering (SANS) measurements were performed. The physical principle of neutron scattering is similar to light and X-ray scattering techniques. In order to larger structures, such as colloids, small scattering angles are required, which is achieved by SANS. SANS is typically based on coherent elastic scattering events.[152] Since the data analysis of SANS experiments is complex and crucial, the obtained results are discussed in detail in the following chapter (cf. 9).

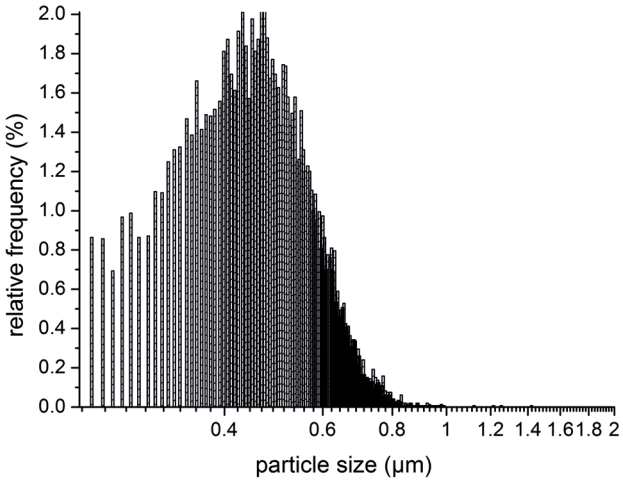

Figure 8.3.: Relative frequency distribution of number-weighted particle sizes of oleosomes obtained by LM imaging.

Apart from the fact that number-weighted average particle sizes are obtained and that the resolution (here 0.3 µm) is limited, the use of LM facilitates the characterisation of particle's shapes and the detection of aggregated particles. By this, it can be evaluated if larger particles detected by LD evolve from destabilisation phenomena, such as flocculation or coalescence, or impurities. Software-supported counting of particle sizes of

oleosomes from LM images revealed a number-weighted average diameter D(v, 0.5) of 0.48 µm (see Table 8.2). Fig. 8.3 represents the relative frequency distribution of number-weighted particle sizes of oleosomes obtained by LM imaging. As it is shown in this figure, merely an infinitesimal amount of oleosomes is larger than 1 µm. The relatively large portion of very small oleosomes, ranging from 0.2 to 0.4 µm, presumably results from falsifications caused by imaging analysis, since every particle size below 0.3 µm is beyond the instrumental resolution ability. Since focusing is only feasible in one plane of the sample, particles in a lower plane were recorded as well and could not be readily erased by the grey-scale correction performed via imaging analysis. With regard to larger particles, the distinct difference between LD and LM might be explainable by the detectable amount of particles within one measurement run, which is for LM of the order of millions smaller than for LD. Nevertheless, it is likely that the redispersion of oleosomes to the required concentration following flotation-centrifugation extraction was, despite extensive vortexing, insufficient and residues of aggregated oleosomes remained.

Particle size measurements applying the NMR method allow to analyse the oleosomes in a higher concentration, thus avoiding the measurement error when the sample is diluted. The NMR method is based on the restriction of the self-diffusion of the soybean oil by the walls of the oleosome.[68] By a time-depending measurement of the diffusion path of the oil in the oleosome, its diffusion coefficient ($9.057\text{x}10^{-13}$ m^2/s) was determined and implemented in to the Stokes-Einstein equation [50, 168] (Eq. 8.1):

$$D = \frac{k_B T}{6\pi\eta_{H2O} r_H}, \tag{8.1}$$

where D is the diffusion coefficient, k_B the Boltzmann constant ($1.38\text{x}10^{-23}$ J/K), T the temperature (temperature during measurement was 25 °C), η_{H2O} the dynamic viscosity of water ($0.891\text{x}10^{-3}$ kg/m·s) and r_H the hydrodynamic radius. Solving this equation for r_H, the measurements revealed that the oleosomes have an average diameter of 0.54 µm.

Particle sizing using different techniques has shown that no absolute value for the average particle size of oleosomes can be obtained. However, LD using the LS 13320, LM and NMR measurements reveal sizes that are relatively close to each other, assuming that the average particle size of oleosomes is most likely lying between 0.38 and 0.54 µm. According to

Table 8.2.: Average particle size of oleosomes obtained by different particle sizing techniques

Method	LD [a] (Horiba LA-950)	LD [a] (LS 13320)	LM	NMR
Particle size (µm)	0.17[c]	0.38[b], 0.41[c]	0.48	0.54

[a] Average particle diameter (D(v, 0.5)) determined by using a real part of refractive index of [b]1.47 and [c]1.6, as well as an attenuation coefficient of 0.01, respectively.

their size, oleosomes can be classified as mini- or submicron-emulsion (0.1 to 1 µm) that is thermodynamically unstable but kinetically stable.[161] Usually, the production of such submicron emulsions requires high energy input commonly achieved by using colloid mills, high pressure homogenizer, microfluidiser or sonicators.[74] Thus, soybean oleosomes provide a beneficial alternative to labour-intensive prepared emulsions as they are already available in form of a natural protein-stabilised emulsion.

9. Small angle neutron scattering

Neutron scattering is a non-invasive and non-destructive method that yields information about the structure and dynamics of the analysed material. Applying neutron methods to complex food-based systems, bulk information about the whole material can be gained, even when contained in thick and complicated sample environments. Thus, a deeper understanding of the nature, behaviour and structure-function relationships in such complex materials can be obtained.[114]

With regard to oleosomes, neutron scattering can be regarded as a promising technology to obtain new and more precise information about their structure, since most of the currently available techniques require extensive sample preparation where disruptive effects on their original structure cannot be prevented. Furthermore, structural analysis can be performed while the oleosin is still embedded in its natural environment, the oleosome. Small angle neutron scattering (SANS) measurements were performed at the facilities of the Institute Laue-Langevin, ILL, in Grenoble, France, and of ISIS research centre at the STFC Rutherford Appleton Laboratory in Didcot, United Kingdom.

The aim of the SANS experiments was to extract the shape and structure information of oleosomes from the measured scattering data by comparing the measured scattered intensities to those calculated from a model assuming a certain geometry of the scattering objects. Additionally, the effect of heat treatment and spray drying on the oleosome's integrity in terms of size and structure was investigated. Here, an overview of the selected data, a route proposed for data analysis and an outlook about further work are given. To begin with, a brief explanation of the physical principles of neutron scattering, with focus on SANS, as well as on the applied instruments is provided.

9.1. Principles of SANS

The physical principle of neutron scattering is similar to other scattering techniques, such as light and X-ray scattering. All these techniques have, according to the quantum mechanical duality, in common that their source of radiation has both wave-like and particulate character. However, while, in case of visible light, the scattering results from differences in polarisability and for X-rays from differences in the electronic structure of the atoms, scattering of neutrons depends on the nuclear structure of the atom.[114] They can interact with the nuclei of matter via nuclear interactions. The wavelength λ of neutrons is in the range of 0.1 - 10 Å. Neutrons that arrive at the nucleus of an atom are scattered in any direction with equal probability, meaning scattering is isotropic.[88] The wavelength of the neutron is very large compared to the nuclear interaction range between the neutron and the nucleus. Thus, the nucleus is regarded as a point scatterer. Assuming that scattering occurs at a single fixed nucleus, the incident wave of the neutron is represented by Eq. 9.1:

$$q(x) = e^{i\vec{k}\vec{x}} \tag{9.1}$$

where $e^{i\vec{k}\vec{x}}$ indicates the wavefunction of a plane wave with a unit amplitude. The incident neutron is described by the neutron wavevector, $\vec{k}$, which travels with a magnitude $\frac{2\pi}{\lambda}$ along the neutron's trajectory ($\vec{x}$).[152] The probability that the neutron is found anywhere but has a definite momentum $mv = \frac{hk}{2\pi}$ is reflected by $\vec{r}$, meaning that the squared modulus of the wavefunction is uniform for all positions $\vec{r}$. The wave scattered by the nucleus spreads in form of circles from the scattering centre (r = 0) and the wavefunction (Eq. 9.2) can be written as

$$q(r) = -\frac{b}{r}e^{i\vec{k'}\vec{r}} \tag{9.2}$$

where the factor $1/r$ indicates that the intensity of the neutron beam (here given by the square of the wavefunction) decreases by the inverse square of the distance from the scattering nucleus, here with a wavevector $\vec{k'}$. The constant b measures the strength of the interaction between the neutron and the nucleus and is also referred to as scattering length of the nucleus.[152] The cross section, σ, having the unit barn (10^{-24} cm^2), describes the probability of interaction between the incident neutron and the nucleus, which

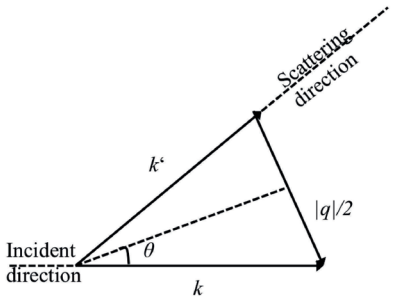

Figure 9.1.: Scattering triangle for an elastic scattering event when an incident neutron is scattered by a nucleus without energy loss. Redrawn from [152].

depends, among others, on the type of target nucleus, the type of nuclear reaction and the energy (speed, temperature) of the incident particle. It is given by $\sigma = 4\pi b^2$ and expresses the ratio between the energy level of the scattered neutrons and the flux of the incident neutrons.[88]

However, matter always consists of atoms, which are, moreover, free to move to some extent. Scattering of neutrons by matter can cause alterations in both the energy and the momentum of the neutrons, as well as the atom. Thus, scattering is either elastic or inelastic. For elastic scattering following vector relationship, here depicted by a scattering triangle (Fig. 9.1) is given by Eq. 9.3:

$$\vec{q} = \vec{k} - \vec{k'} \tag{9.3}$$

which can be calculated (Eq. 9.4) according to the scattering event shown by

$$q = \frac{4\pi \sin\theta}{\lambda}, \tag{9.4}$$

assuming energy conservation that $|\vec{k}| = |\vec{k'}|$. Here, θ is the scattering angle. Furthermore, it is differentiated between coherent and incoherent scattering. The former describes the interference of neutron waves scattered from different nuclei. Coherent scattering depends on the distances between atoms and on the scattering vector $\vec{q}$. From this, information about the structure can be derived. In contrast to that, incoherent scattering involves no interference between waves scattered by different nuclei. For both scattering types, one can distinguish between elastic and inelastic scattering.

While coherent elastic scattering provides information about the equilibrium structure, inelastic coherent scattering refers to the motions of the atoms. In case of incoherent elastic scattering, independent interaction between the incident neutron wave and the nuclei is the same in all directions. In neutron scattering measurements, this event usually contributes to unwanted background effects. Information about atomic diffusion is obtained by incoherent inelastic scattering, which results from interactions of a neutron with the same atom at different times and different positions.[152]

The scattering events described above are based on distances between planes of atoms. For the examination of larger structures, such as colloids or polymers, where the distances are larger than interatomic distances, small scattering angles are required, usually less than 1. This is achieved by a technique also known as small angle neutron scattering (SANS). SANS is typically based on coherent elastic scattering events and is used for measuring structures with dimensions between 10 and 100 Å. The basic scattering equation is given by (Eq. 9.5):

$$I(q) = N(\Delta\overline{\rho}V)^2 P(q)S(q), \tag{9.5}$$

where I is the intensity of the scattered radiation, only dependent on the magnitude of $\vec{q}$, N is the number of molecules/unit volume and V is the molecular volume. The scattering density difference between the scattering particle and the solvent is described by the contrast, $\Delta\overline{\rho} = \langle\rho(r)\rangle - \overline{\rho}_s$. $P(q)$ is the form factor (particle shape) and is calculated as the inverse Fourier transform of $I(q)$. $S(q)$ denotes the structure factor (inter-particle correlation distances) and is negligible for very dilute samples where $S(q) = 1$. The average scattering length density ρ is the sum of all coherent scattering lengths (b) of all atoms over a small volume, which is divided by the total volume.[152, 174] A valuable advantage of SANS is the contrast variation technique, also referred to as contrast matching. Since different isotopes can scatter neutrons differently, which is particularly the case for hydrogen (H) and its heavier isotope, deuterium (D), this phenomenon can be utilised to visualise structural features of hydrogen-containing materials by preparing different ratios of H_2O and D_2O.[114]

9.2. SANS instruments and methodology

9.2.1. SANS experiments at ILL

SANS experiments were performed at the steady-state instrument D22 of the Institute Laue-Langevin, ILL, in Grenoble, France. A principle set-up of the steady state instrument D22 for measuring neutron scattering is shown in Fig. 9.2. Neutrons are continuously produced by fission in a steady-state reactor. A mechanical velocity selector selects the wavelength from a white neutron beam generated by a horizontal cold source in the reactor. An adaptive collimation system determines the size, divergence and intensity of the beam targeting at the sample. A set of mobile apertures is placed right after the collimator, here equipped with a neutron guide of different geometries and directly before the sample, the sample aperture, to restrict the divergence of the beam. Neutrons scattered by the sample can be detected within a wide angular range by varying the distance between the sample and the detector. Since the detectors cannot handle the high intensity of the primary beam, its intensity is reduced by a neutron-absorbing material (*e.g.* cadmium) at the front of the detectors.[62, 71]

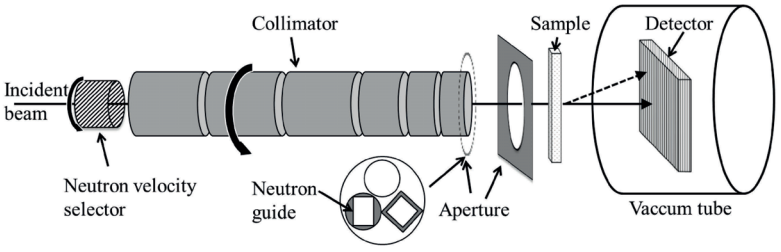

Figure 9.2.: Schematic representation of the steady-state instrument D22 at the Institute Laue-Langevin, ILL, in Grenoble, France (modified according to [71]).

For scattering measurements, the range of scattering vectors $\vec{q}$ from 0.001 to 0.9 $Å^{-1}$ was covered by two different sample-to-detector distances of 5.6 and 17.6 m. The neutron wavelengths were 6.0 and 11.5 Å, respectively. The samples were measured in quartz cells (Hellma, Germany), which had a path length of 1 or 2 mm, depending on the contrast of the buffer solution used for the dilution of the samples. The smearing of the real intensity scattered by the sample induced by the divergence and size of the direct beam, the pixel size of the detector and the wavelength resolution, all depend on the

instrumental settings and were included in the data analysis.

In order to determine the appropriate measurement concentration yielding reasonable scattered intensities while avoiding multiple scattering effects, native oleosomes dispersed in ultra-pure water were diluted with buffer solutions of pH 2 and pH 5 of three different contrasts (0, 40 and 50 % D_2O) to obtain concentrations of 0.65, 1.3 and 2.6 wt%. Measurements were conducted at 25 °C.

Heat treatment of the oleosomes was performed either before or during SANS measurements. In the former case, 1.3 wt% oleosome dispersions of pH 2 with 50 % D_2O were heated at 99 °C for 1 h using a HLC ThermoMixer MKR 13 (Digital Biomedical Imaging Systems AG, Pforzheim, Germany). Prior to measurement, the emulsion was allowed to cool down. For heat treatment during SANS measurements, the samples (oleosome concentration 1.3 wt%, pH 2, 0 and 50 % D_2O) were stepwise heated to temperatures of 50, 55, 60, 65, 70, 80 and 90 °C using a thermostated sample holder. Data was acquired after an equilibration time of 15 min.

For the investigation of spray dried oleosomes, powders of oleosomes encapsulated with maltodextrin (DE 16.5-19.5) were dispersed in buffers of appropriate H_2O/D_2O ratios. Amount of weighted powder and dilutions were calculated as appropriate to obtain oleosome concentrations similar to those used for the native ones. In general, it was assumed that the ratio of the oleosome compounds remained the same during spray drying.

9.2.2. SANS experiments at ISIS

Further experiments were performed using the time-of-flight small angle scattering instrument Sans2d (Fig. 9.3) of the STFC Rutherford Appleton Laboratory near Oxford, United Kingdom. The incident white beam coming from a pulsed neutron source passes through a super-mirror bender, which reduces the fast neutron background, as well as a disk chopper with variable openings used to define the wavelengths. The neutrons fly then through removable guide sections that match the incident collimation length to the sample-detector distance. Neutrons are detected over a wide angular range by movable detectors. In contrast to the steady-state instrument D22, the time-of-flight detection technique allows for measuring in a very large dynamic range of the scattering vector without requiring any reconfiguration of the instrument.[71, 107]

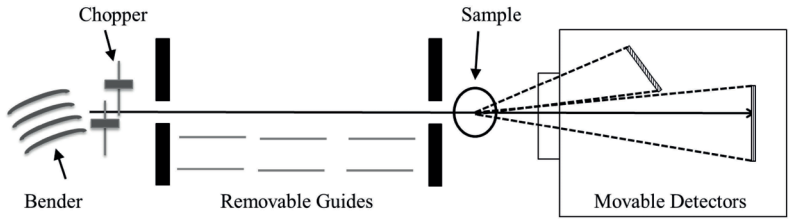

Figure 9.3.: Schematic representation of the time-of-flight instrument Sans-2d at the STFC Rutherford Appleton Laboratory near Oxford, United Kingdom (modified according to [107]).

SANS measurements were conducted at two different sample-to-detector distances of 4 and 12 m, thereby covering a broad q range of $0.004 \leq q \geq 0.747$ Å^{-1} and $0.0014 \leq q \geq 0.286$ Å^{-1}. Neutron wavelengths varied between 1.75 and 16.5 Å (4 m), as well as 1.5 and 12.5 Å (12 m). All measurements were made using 1 mm and 2 mm quartz cells (Hellma, Germany) and at a temperature of 25 °C. Oleosome emulsions were diluted to obtain a concentration of 4 wt% using buffer solutions of pH 7 at four different contrasts, which have been 0, 12, 40 and 100 % D_2O. Additional, SANS measurements of an intralipid emulsion (CAS 68890-65-3, Sigma Aldrich, Saint Louis, MO/USA), which is phospholipid-stabilised soybean oil, were performed. The concentration of this emulsion was also adjusted to 4 wt% using a buffer solution of pH 7 of two different contrasts (12 and 100 % D_2O). The pure buffer solutions corresponding to the different contrasts used were measured as reference samples.

9.3. Data analysis

The raw data was reduced to transform the recorded scattering into intensity, being a function of the scattering vector $\vec{q}$. Data reduction is in principle device-specific and was performed by the instrument scientist Dr. Andrew Jackson. Additional data corrections were made by subtracting the empty cell and the buffer. In order to extract the parameter of interest, here the particle size and shell thickness, from the obtained SANS data, model calculations were performed. As a first approximation, the oleosomes are assumed to be spherical core-shell particles with a core composed of PL and TAG and a shell consisting of the hydrophilic N- and C-terminal domains (see Fig. 9.4). Therefore, a core-shell sphere model is assumed by taking

into account the instrumental resolution function (smearing), the scattering length densities (SLD) of the solvent, the shell and the core, as well as the polydispersity and the volume concentration of scatterers.

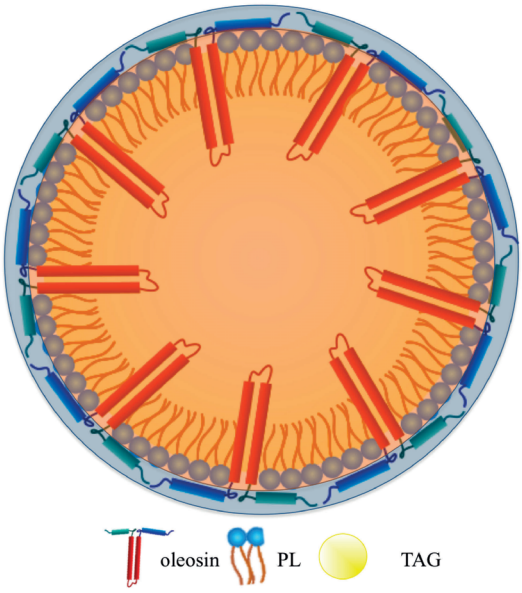

Figure 9.4.: Schematic representation of a soybean oleosome analysed by SANS experiments, which are evaluated by assuming a core-shell model. The shell (blue) is presumably composed of the hydrophilic N- and C-terminal domains of the oleosin and the core (orange) contains the hydrophobic domains of the oleosin, the PL and TAG.

The SLD of the shell is determined by the elemental composition of the primary structure of the hydrophilic domains of the oleosins and the SLD of the core is given by the elemental composition of the TAG included in soybean oil. The contrast variation method, which relies on the different scattering lengths of hydrogen (-0.37×10^{-12} cm^{-2}) and deuterium (0.67×10^{-12} cm^{-2}), was applied to contrast match particular components so that they become invisible to neutrons.[88] By adjusting the ratio of H_2O to D_2O appropriately, either the shell or the core can be visualised in the resulting scattering pattern. Accordingly, the SLD of the solvent used as input parameter to the model has to be recalculated for each used contrast. The same applies to the SLD of the oleosin shell, since the H-atoms of its amino acid residues are exchanged by D-atoms, which changes its SLD differently,

depending on the contrast of the solvent. On basis of these parameters, the particle size and the shell thickness can be calculated provided that the solution concentration, the SLD of all compounds and the polydispersity are well known. However, up to now, no satisfactory fit to all the data could be obtained, indicating that a further refinement of the model is necessary.

9.4. First results

Native oleosome dispersions at different pH-value and at different contrast were measured to gain information about their structure and size. Only scattering data for oleosomes dispersed in buffer solutions of pH 2 were obtained, as samples at pH 5 showed pronounced creaming due to aggregation, resulting in depletion of oleosomes in the detection volume. Measurements at three different concentrations (0.65, 1.3 and 2.6 wt%) revealed no multi-scattering effects, thus all samples are in principle suitable for measurements. Subsequent measurements were performed using only samples with 1.3 wt% oleosomes. In Fig. 9.5, the scattering intensity of native oleosomes (1.3 wt%, pH 2) measured at three different contrasts (0, 40 and 50 % D_2O) using the steady-state instrument D22 at the ILL is shown.

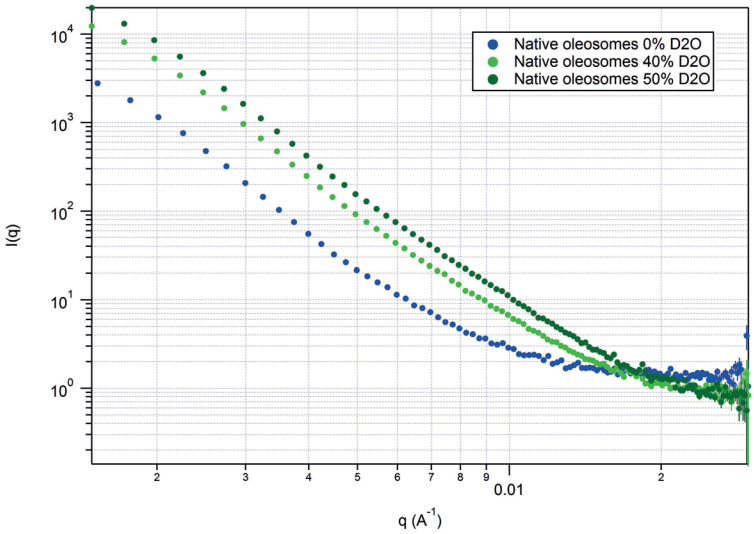

Figure 9.5.: Scattered intensities of native oleosomes (1.3 wt%, pH 2) measured at three different contrasts (0, 40 and 50 % D_2O) using the D22 instrument at ILL.

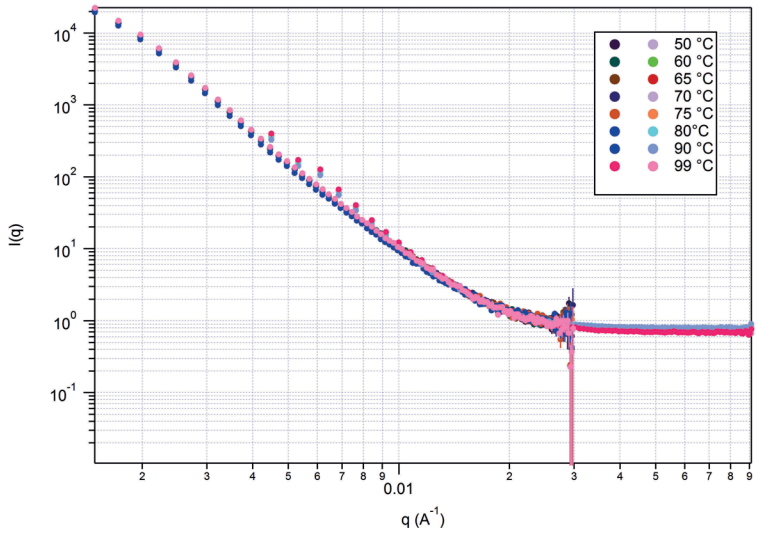

Figure 9.6.: Scattered intensity $I(q)$ of native oleosomes (1.3 wt%, pH 2, 0 % D_2O) stepwise heated up to 90 °C in situ and to 99 °C before measurement. Measurements were performed using the D22 instruments at ILL.

Heat treatment of oleosomes up to temperatures of 99 °C revealed no impact on the structure or size of the oleosomes as the scattering intensity was the same for all measured samples (Fig. 9.6). These findings are in line with the results obtained by particle size distribution and ζ-potential measurements (cf. Sec. 6.2.2).

Measurements of native oleosomes in comparison to redispersed oleosome powders spray dried with 10 wt% MD at either 80 or 180 °C yield significant differences in the scattered intensity, particularly in the range of $0.004 \leq q \leq 0.02\,\text{Å}^{-1}$ (Fig. 9.7). However, no difference is observed for the different drying temperatures. Since up to now no satisfying fit of the scattering data of the native oleosomes was obtained, and thus no information about their size or structure, it is consequently not possible to quantify the differences in the scattering data of native and spray dried oleosomes reliably.

In order to find out more about the general structure of the oleosomes, a comparable system, here the phospholipid-stabilised soybean oil (intralipid) was measured to exclude the effect of the oleosin. Measurements performed at contrasts of 12 % D_2O intended to delete the scattering signal from

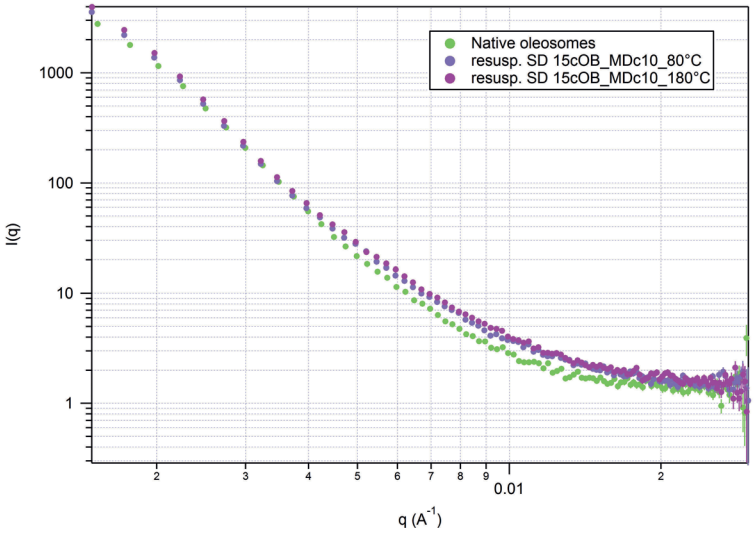

Figure 9.7.: Scattered intensities $I(q)$ of native oleosomes and of MD encapsulated oleosomes (drying temperatures have been 80 and 180 °C) redispersed in buffer solution of pH 7 at 0 % D_2O. In all cases, the oleosome concentration was 1.3 wt% at 0 % D_2O. Measurements were performed using the D22 instrument at ILL.

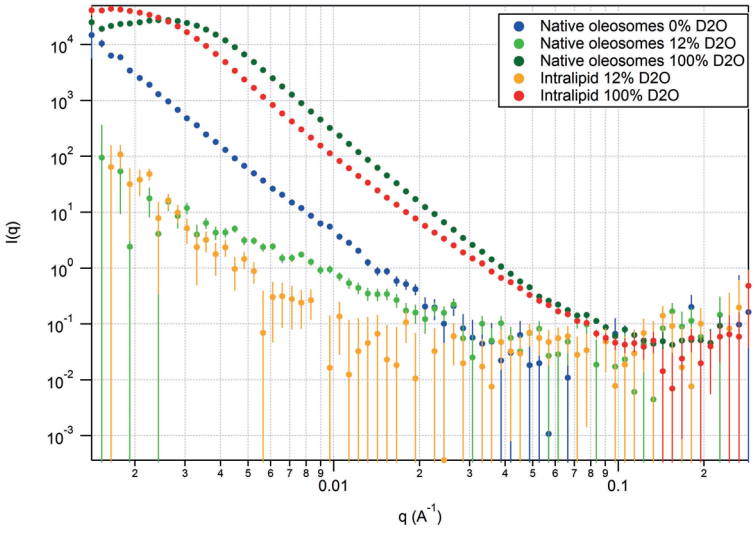

Figure 9.8.: $I(q)$ of native oleosomes and intralipid (phospholipid-stabilised soybean oil), both having a concentration of 4 wt% at three, respectively two contrasts of pH 7. Measurements were performed using the Sans2d instrument at ISIS.

the core and highlight the protein signal and 100 % D_2O reveal significant differences in the scattered intensities of the native oleosomes and the intralipid samples (Fig. 9.8). This indicates that the oleosin contributes to the scattering behaviour of the oleosomes.

9.5. Outlook

Small angle neutron scattering is a non-destructive and non-invasive technique to obtain information about the oleosome structure and size in the bulk. First measurement results have shown that SANS is a promising technique to learn more about the soybean oleosome's structure and particularly about the oleosin as it can be analysed in-situ. This aspect provides a huge advantage towards other measurement techniques, since the long hydrophobic domain of the oleosins impedes their isolation and reliable data analysis when examined ex-situ. However, in comparison to other analytical techniques, SANS requires extensive set-up times and laborious measurements. However, since the allocated beam time was limited and a better part of the available time had to be used for method development, it was not possible within the time frame of this study to acquire a reasonable amount of measurements to gather a comprehensive picture of the oleosome structure. Thus, to complete the model calculations of the already acquired data, additional information about the model parameters is required. Future research will thus involve the investigation of simpler systems like the intralipid in order to better distinguish between the individual oleosome components. Furthermore, measurements of enzymatically modified oleosomes are planned to stepwise analyse the complex architecture of oleosomes, particularly with regard to the oleosin.

10. Conclusion

Spray drying is one of the most widely used drying technologies and is preferably used for the microencapsulation of lipids, containing high amounts of unsaturated fatty acids. In order to achieve a high fat/oil encapsulation efficiency and thus an adequate protection against fat oxidation, the lipids need to be properly embedded into a capsule, isolating them from their surrounding environment. Powder formation and thus the fat/oil encapsulation efficiency depend, amongst others, on the properties of the feed emulsion, the physicochemical properties of the components present and the applied process parameters. The resulting properties of the powder are crucial for its final product quality, particularly for its handling, processing and storage.

Over the last two decades, the food industry has discovered the beneficial use of oleosomes as emulsifying agent and capsule for bioactive ingredients. Soybean oleosomes provide an emulsion of pre-emulsified oil and thus a promising system suitable for encapsulating soybean oil that is rich in unsaturated fatty acids. Oleosomes are ubiquitous in nature and extractable from diverse sources of plant seeds. In particular, soybeans are an important agricultural commodity that could facilitate a reliable and constantly available source of oleosomes. However, the lack of understanding the link between micro- and macroscopic properties in relation to the molecular structure of the oleosomes, impedes the rational structure-based design of oleosome products and thus their commercial use.

The aim of this thesis was to characterise soybean oleosomes in solution and to investigate the role of the oleosin for their stability and function. Stability tests were performed to evaluate the applicability of oleosomes for spray drying. The impact of spray drying on the oleosomes' integrity, meaning physicochemical properties and stability, was investigated by comparing native oleosome emulsions with emulsions of reconstituted oleosomes. In order to obtain a high oil encapsulation efficiency, which implies a high level of intact oleosomes, optimal parameters needed to be established.

Particle size measurements were performed using different particle sizing techniques. Measurements by means of laser diffractometry revealed that the particle size distribution of soybean oleosomes is relatively broad, ranging from 0.2 to 0.8 µm. NMR, light microscopy and laser diffractometry measurements have shown that the average particle diameter of oleosomes cannot be determined unambiguously, thus the average size is between 0.38 and 0.54 µm.

By comparing the molecular composition, the interfacial activity, the surface structure and the colloidal stability of native and enzymatically digested oleosomes, it has been shown that the stability and function of oleosomes predominantly depend on the unique structure of the oleosin. Enzymatic digestion causes degradation of the oleosin structure, which is accompanied by changes in the molecular composition and structure of the oleosome surface. As a result of this, the interaction between oleosomes and thus their aggregation behaviour have changed, decreasing the stability of the oleosome emulsion. The destabilisation is reflected by an increasing polydispersity of the oleosome size, a reduced elasticity of the droplet interfacial layer and a changing ζ-potential. Based on these findings, it is likely that coalescence of the oil droplets has occurred after digestion, which can be attributed to the loss off steric stabilisation via the oleosin's hydrophilic termini.

Axisymmetrical drop shape analysis has shown that native and digested oleosomes reveal a different interfacial behaviour at the air-water interface of a pendant drop. Oleosomes burst at the air-water interface and their components spread on the surface of the droplet. The release of the oleosome components results in an increase of the surface pressure with different rates. Time-dependent changes in the surface pressure are most likely determined by the kinetics of oleosomes rupturing at the interface and by phospholipid phase transitions within the interfacial layer. For digested oleosomes, phospholipids have presumably a dominating influence on the surface pressure, while it is assumed that for intact oleosomes, the interfacial layer is filled with a large amount of oleosin-conjugates [193].

Stability tests of native oleosomes subjected to heat and shear stresses of different magnitude and duration revealed that oleosomes are stable to temperatures up to 100 °C but only to a limited extent to shear stresses. It has been shown that more than 90 % of oleosomes remain intact when subjected to shear stresses induced by atomization at an air flow rate of 439 L/h and a liquid flow rate of either 0.16 or 0.3 L/h. However, with

increasing air flow rate and thus increasing shear stresses acting on the liquid feed stream of oleosomes, the more oleosomes rupture and coalesce.

Spray drying of soybean oleosomes has been performed for the first time. In order to establish a suitable spray drying method for oleosome encapsulation, oleosomes with and without maltodextrin were spray dried at different inlet temperatures and at different ratios of spray air to liquid feed flow rate. Spray drying of pure oleosomes resulted in extensive oleosome rupture and coalescence, yielding oily, highly agglomerated particles that do not correspond with the specifications of a powder product. These effects are more pronounced, the higher the drying temperature is.

With the addition of maltodextrin (DE 16.5-19.5), it has been shown that the rupturing of oleosomes could be reduced and the oil encapsulation efficiency improved. The spray drying efficiency, here in terms of powder collection and thus oil encapsulation efficiency, turned out to depend significantly on the maltodextrin concentration and the process parameters. Five wt% of maltodextrin (MD : oleosin = 1 : 2.4) proved insufficient to obtain an adequate oil encapsulation efficiency. Qualitatively satisfying results, macroscopically indicating a good oil encapsulation efficiency, were obtained when adding 10 wt% maltodextrin (MD : oleosin = 1 : 3.9). In order to quantify these observations, ESCA measurements of oleosomes spray dried without and with 10 wt% maltodextrin were performed and correlated with findings obtained by SEM, CLSM and FTIR measurements.

These measurements have shown that, despite the use of maltodextrin as encapsulant, significant portions of oleosomes has lost their original structure and segregation of oleosome components has occurred during spray drying. Segregation of components has shown to significantly influence the powder morphology and the powder surface composition. Powders produced from pure oleosome emulsions at 180 °C exhibited predominantly phospholipids on their surface but no oleosins. At drying temperatures of 100 °C, the main component present in the outermost surface layer was oil. When the oleosomes were encapsulated with maltodextrin by means of spray drying, minor levels of oleosins and predominantly parts of free soybean oil are accumulated in the outer-most surface layer of the particles, preferentially to maltodextrin.

By comparing particle sizes of soybean oleosomes before and after spray drying, valuable information could be gathered about the reconstitution properties and about how efficiently the original structure of the oleosomes

could be maintained during spray drying. The findings revealed that up to 36 % of oleosomes encapsulated with 10 wt% maltodextrin remained intact when spray drying occurred at an inlet drying temperature of 100 °C. The higher the drying temperature, the more oleosomes rupture and coalesce, resulting in a higher level of free surface oil. Homogenisation tests revealed that the emulsions of redispersed oleosomes could not be further homogenised.

Secondary structure analysis by means of FTIR has shown that structural transformations within the secondary structure of the oleosin were induced by spray drying but have been reversible in the presence of maltodextrin, which is presumably capable of keeping the oleosin solubilised.

In summary, the combination of experimental techniques providing information about oleosin function at different length scales allowed to further confirm the expected role of oleosins for the function and stability of oleosomes. Soybean oleosomes are a protein-stabilised micro-emulsions that is stable over a broad pH-range and up to temperatures of 100 °C, providing a promising emulsifying agent for use in diverse food applications. Thus, the labour-intensive production of stable emulsions, usually requiring high energy-consuming processing, as well as the time-consuming search for emulsifiers of food-grade can be avoided when applying oleosomes in food processing. Moreover, enzymatic digestion of oleosomes inducing drastic changes in their physical character can be beneficially used as valuable tool for food oil refinery. The yields of enzyme-assisted aqueous extraction processes, that are in general economically and environmentally friendly and healthier than common solvent extraction processes, could be improved, when extracting the oil from isolated oleosomes.[122, 178]

Spray drying of pure oleosomes turned out to be impractical as the concentration of oleosin and phospholipids is insufficient to properly encapsulate the soybean oil. In combination with the findings obtained for oleosomes encapsulated with maltodextrin, it has been shown that it is crucially important to maintain the original oleosome structure. Once the unique architecture is destructed and thus the oleosins are separated from the oil core, they are presumably not capable of folding back into the lipid matrix. Thus, they lost their emulsifying and stabilising functions due to the formation of insoluble aggregates. An enrichment of oleosins to improve the encapsulation efficiency is critical as a suitable solubilisation method of isolated oleosins and their reconstitution into the oil matrix remains to be

developed.

Therefore, in order to maintain the valuable function of oleosomes to act as barrier against fat-oxidation and as capsule for lipophilic bioactive ingredients, it would be worthwhile to add a further encapsulant. Maltodextrin is in general favourably used in order to obtain a high oil encapsulation efficiency but it has been shown that the formation of a rigid shell has presumably a negative impact on the oleosomes' integrity. The addition of other proteins could possibly increase the elasticity of the formed shell and thus provide a better encapsulation of oleosomes.

A. Oleosome characterisation

A.1. Interfacial behaviour

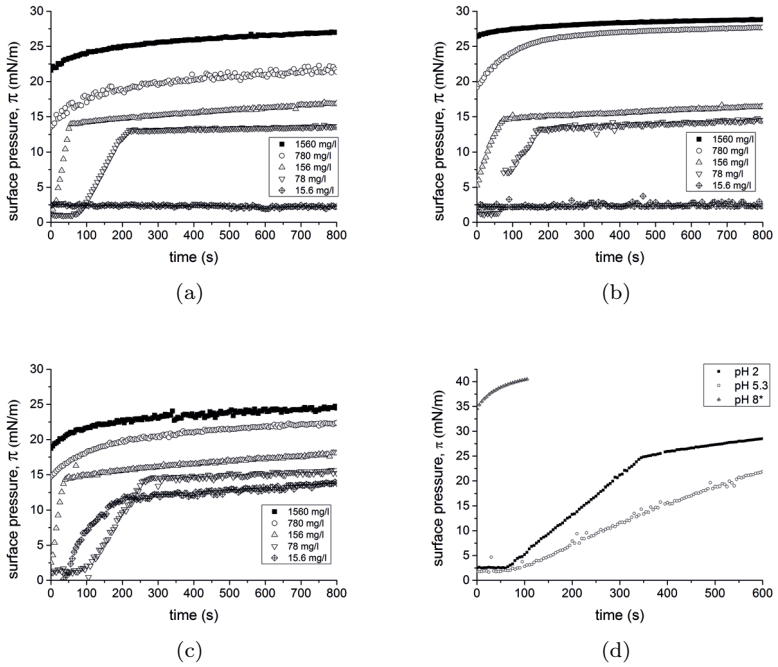

Figure A.1.: Surface pressure (mN/m) of intact (a-c) and digested (d) oleosomes of different concentrations diluted in a buffer solution of varying pH-value. (a) pH 2. (b) pH 5. (c) pH 8. (d) 78 mg/L.

A.2. Secondary structure analysis

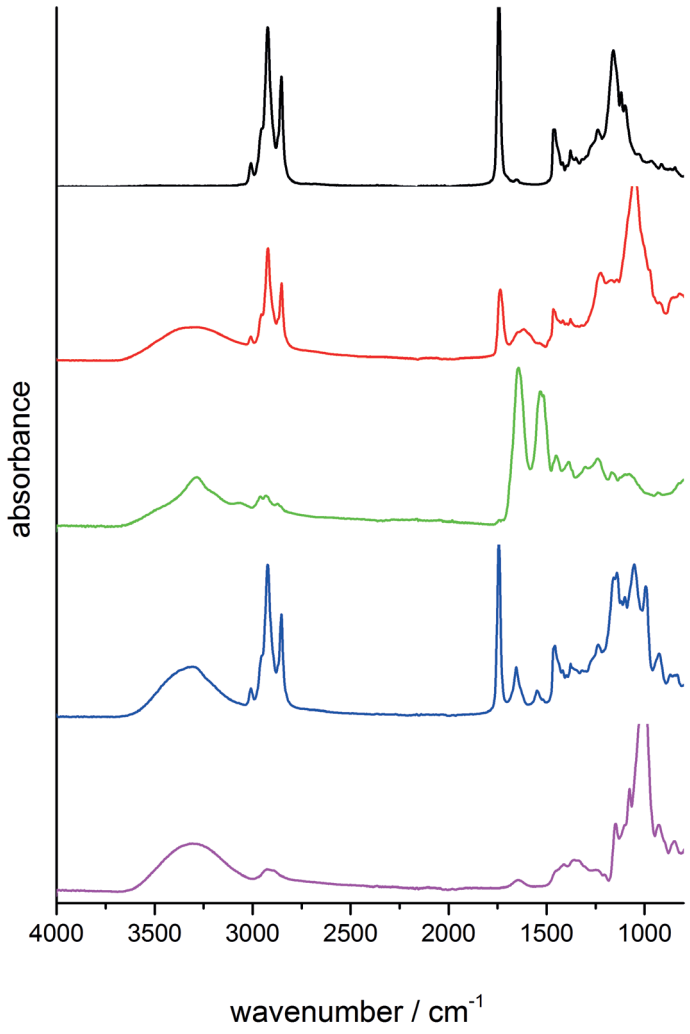

Figure A.2.: Infrared spectra of soybean oil (black), phospholipids/lecithin (red), isolated oleosin (green), native oleosomes (blue) and maltodextrin (pink). Spectra have been determined by transmission measurements.

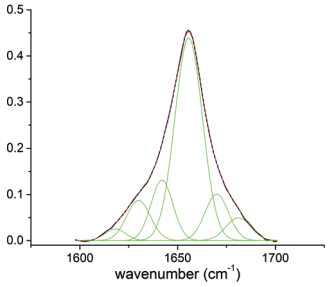

(a)

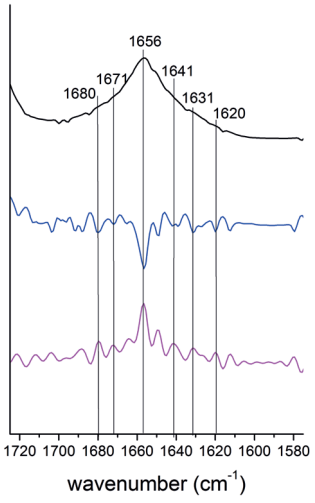

(b)

Figure A.3.: (a) Amide I band of the native oleosomes and (b) the resolved curve bands thereof and the curve fits to them. Measurement occurred in the transmission mode.

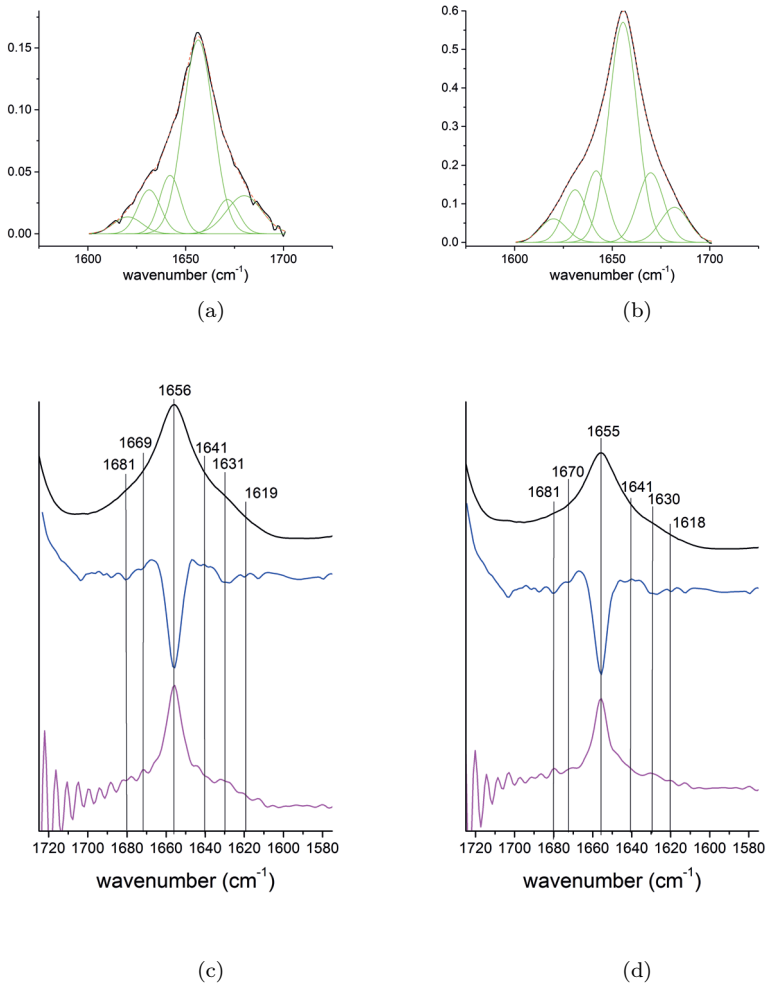

Figure A.4.: a) and b): Amide I band of the redispersed samples (10 wt% MD, 100 and 180 °C) (a)/c), b)/d)), the resolved curve bands (c) and d)) thereof and the curve fits (a)-b)) to them. Measurement occurred in the transmission mode.

B. Powder characterisation

B.1. Influence of process parameters

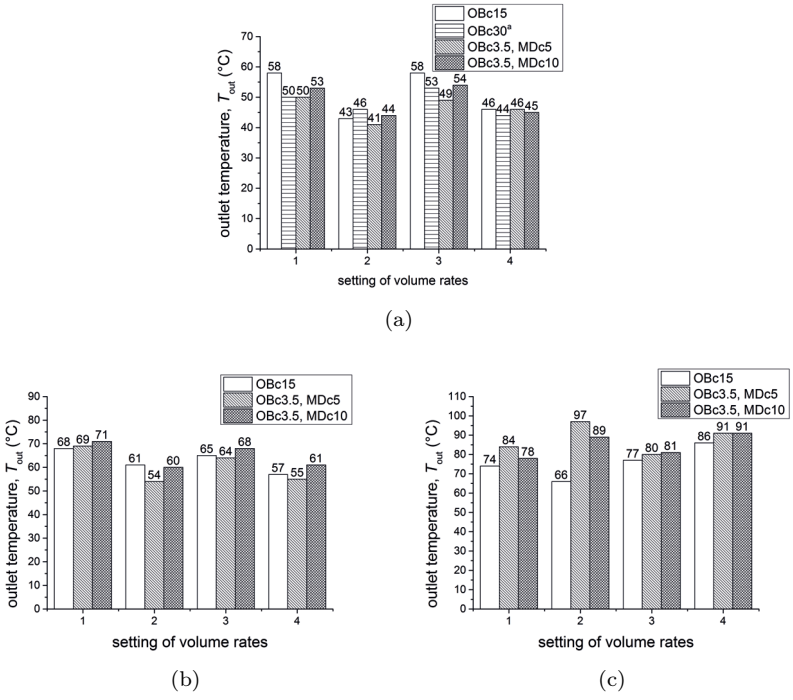

Figure B.1.: Outlet temperature in terms of varying process parameters and different sample composition. a) $T_{\mathrm{in}} = 100$ °C, [a]sample only spray dried at 100 °C b) $T_{\mathrm{in}} = 130$ °C. c) $T_{\mathrm{in}} = 180$ °C.

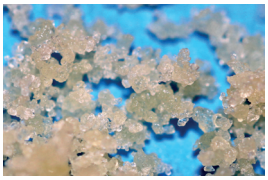

(a) 15 wt% oleosomes, air: 439 L/h, liquid: 0.3 L/h, T_{in} = 100 °C

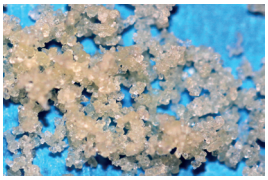

(b) 15 wt% oleosomes, air: 1052 L/h, liquid: 0.3 L/h, T_{in} = 100 °C

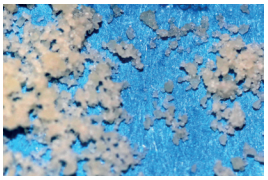

(c) 15 wt% oleosomes, air: 1052 L/h, liquid: 0.16 L/h, T_{in} = 100 °C

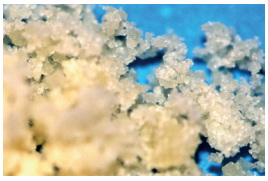

(d) 15 wt% oleosomes, air: 439 L/h, liquid: 0.3 L/h, T_{in} = 130 °C

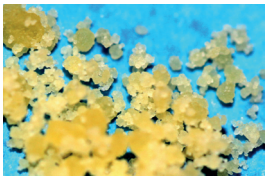

(e) 15 wt% oleosomes, air: 439 L/h, liquid: 0.3 L/h, T_{in} = 180 °C

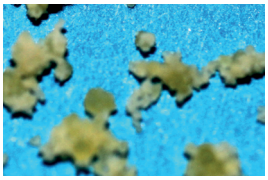

(f) 15 wt% oleosomes, air: 1052 L/h, liquid: 0.3 L/h, T_{in} = 180 °C

(g) 15 wt% oleosomes, air: 1052 L/h, liquid: 0.16 L/h, T_{in} = 180 °C

Figure B.2.: Photographs of spray dried oleosome emulsions.

Bibliography

[1] AG, Büchi Labortechnik, "The B-290 two fluid nozzle," 2014.

[2] Aguilera, J. M., et al. "New dimensions in microstructure of food products," *Food Science and Technology*, *11*:3–9 (2000).

[3] Allison, S. D., et al. "Effects of drying methods and additives on structure and function of actin: mechanisms of dehydration-induced damage and its inhibition," *Archives of Biochemistry and Biophysics*, *358*(1):171–181 (1998).

[4] Andrade, J. D. *Surface and interfacial aspects of biomedical polymers, surface chemistry and physics*, *1*, chapter X-ray photoelectron spectroscopy (XPS), 105–195. New York: Plenum Press, 1985.

[5] Anton, M. "Recent advances concerning the functional properties of egg yolk low-density lipoproteins." *EPC 2006 - 12th Europeean Poultry Conference Verona, Italy, 10-14 September 2006, paper 352*. 2006.

[6] Augustin, M. A. and L. Sanguansri. *Food Materials Science: Principles and Practice*, chapter Encapsulation of Bioactives, 557–601. Springer New York, 2008.

[7] Bae, E. K. and S. J. Lee. "Microencapsulation of avocado oil by spray drying using whey protein and maltodextrin," *Journal of Microencapsulation*, *25*(8):549–560 (2008).

[8] Bair, C. W. and H. E. Synder. "Electron microscopy of soybean lipid bodies," *JAOCS*, -:279–281 (1980).

[9] Baize, J. C. *Global agricultural soy and grain - Outlook and supply situation*. Technical Report, U.S. 2013 Global Soy Trade Exchange, September 2013.

[10] Banga, A. K. *Therapeutic Peptides and Proteins: Formulation, Processing, and Delivery Systems*. Taylor and Francis Group, LLC, Boca Raton, Florida, 2006.

[11] Barlow, D. J. and P. L. Poole. "The hydration of protein secondary structures," *FEBS Letters*, *213*(2):423–427 (1987).

[12] Barth, A. "Infrared spectroscopy of proteins," *Biochimica et Biophysica Acta*, *1767*:1073–1101 (2007).

[13] Barth, W. "Design and layout of the cyclone separator on the basis of new investigations," *Brenn. Wärme Kraft*, *8*:1–9 (1956).

[14] Beer, A. "Bestimmung der Absorption des rothen Lichts in farbigen Flüssigkeiten," *Annalen der Physik und Chemie*, *86*(1):78–88 (1852).

[15] Beverung, C. J., et al. "Protein adsorption at the oilrwater interface: characterization of adsorption kinetics by dynamic interfacial tension measurements," *Biophysical Chemistry*, *81*:59–80 (1999).

[16] Bhandari, B. R. and T. Howes. "Implication of glass transition for the drying and stability of dried foods," *Journal of Food Engineering*, *40*:71–79 (1999).

[17] Bhandari, B. R., et al. *Drying technologies in food procdrying*, chapter Spray drying of food materials and product characteristics, 113–157. Blackwell Publishing Ltd, 2008.

[18] Bhatla, S. C., et al. "Use of oil bodies and oleosins in recombinant protein production and other biotechnological applications," *Biotechnology*, *28*:293–300 (2010).

[19] Blonk, J. C. G. and H. van Aalst. "Confocal scanning light microscopy in food research," *Food Research International*, *26*:297–311 (1993).

[20] Bonazzi, C. and E. Dumoulin. *Modern Drying Technology*, *3*, chapter Quality Changes in Food Materials as Influenced by Drying Processes, 1–20. Wiley-VCH Verlag GmbH & Co. KGaA, 2011.

[21] Bott, S. and H. Hart. "Charakterisierung kleinster Teilchen mit der neuen PIDS-Technologie," *Chemie Technik*, *5*:196–200 (1991).

[22] Buxbaum, E. *Fundamentals of Protein Structure and Function*, chapter Protein structure, 13–38. Springer Science + Buisiness Media B.V., LLC, 2007.

[23] Cabanos, C., et al. "Expression and Purification of Peanut Oleosins in Insect Cells," *Protein Journal*, *30*:457–463 (2011).

[24] Calhoun, W. R., et al. "Measurement of the refractive index of highly turbid media," *Optic Letters*, *35*(8):1224–1226 (2010).

[25] Calvo, P., et al. "Microencapsulation of extra-virgin olive oil by spray-drying: Influence of wall material and olive quality," *European Journal of Lipid Science and Technology*, *112*:852–858 (2010).

[26] Capuano, F., et al. "Properties and exploitation of oleosins," *Biotechnology Advances*, *25*:203–206 (2007).

[27] Carbonaro, M. and A. Nucara. "Secondary structure of food proteins by Fourier transform spectroscopy in the mid-infrared region," *Amino Acids*, *38*:679–690 (2010).

[28] Chen, B., et al. "Physical and oxidative stability of pre-emulsified oil bodies extracted from soybeans," *Food Chemistry*, *132*:1514–1520 (2012).

[29] Chen, X. D. "Heat-Mass Transfer and Structure Formation During Drying of Single Food Droplets," *Drying Technology*, *22*(1-2):179–190 (2004).

[30] Chen, X. D. and N. Ozkan. "Stickiness, Functionality, and Microstructure of Food Powders," *Drying Technology*, *25*:969–979 (2007).

[31] Chen, Y. and T. Ono. "Simple Extraction Method of Non-allergenic Intact Soybean Oil Bodies That Are Thermally Stable in an Aqueous Medium," *Journal of Agricultural and Food Chemistry*, *58*:7402–7407 (2010).

[32] Chen, Y., et al. "Oleosins (24 and 18 kDa) Are Hydrolyzed Not Only in Extracted Soybean Oil Bodies but Also in Soybean Germination," *Journal of Agricultural and Food Chemistry*, *62*(4):956–965 (2014).

[33] Cheng, P., et al. "Automation of Axisymmetric drop shape analysis for measurements of interfacial tensions and contact angles," *Colloids and Surfaces*, *43*:151–167 (1990).

[34] Chiang, C.-J., et al. "Functionalized nanoscale oil bodies for targeted delivery of a hydrophobic drug," *Nanotechnology*, *22*:1–9 (2011).

[35] Chuang, R. L. C., et al. "Characterization of Seed Oil Bodies and Their Surface Oleosin Isoforms from Rice Embryos," *The Journal of Biochemistry*, *120*:74–81 (1996).

[36] Consortium, The UniProt. "Activities at the Universal Protein Resource (UniProt)," *Nucleic Acids Research*, *42*:D191–D198 (2014).

[37] Courthaudon, J. L. and E. Dickinson. "Competitive adsorption of lecithin and α-casein in oil in water emulsions," *Journal of Agricultural and Food Chemistry*, *39*:1365–1368 (1991).

[38] Cullis, P. R. and B. De Kruijf. "Lipid polymorphism and the functional roles of lipids in biological membranes," *Biochimica et Biophysica Acta*, *559*:399–420 (1979).

[39] Cussler, E. L. *Diffusion mass transfer in fluid systems*, *2*. Cambridge University Press, New York, 1997.

[40] Danviriyakul, S., et al. "Physical Stability of Spray-Dried Milk Fat Emulsion as Affected by Emulsifiers and Processing Conditions," *Journal of Food Science: Food Engineeering and Physical Properties*, *67*(6):2183–2189 (2002).

[41] Dauphas, S., et al. "Hen Egg Yolk Low-Density Lipoproteins Film Spreading at the Air-Water and Oil-Water Interfaces," *Journal of Agricultural and Food Chemistry*, *54*:3733–3737 (2006).

[42] Deckers, Harm M., et al., "Oil body based personal care products," 2001.

[43] Deleu, M., et al. "Interfacial properties of oleosins and phospholipids from rapeseed for the stability of oil bodies in aqueous medium," *Colloids and Surfaces, B*, *80*:125–132 (2010).

[44] DeMan, J. M. *Principles of Food Chemistry*, chapter Proteins, 111–152. Aspen Publishers, Inc., 1999.

[45] Dong, A., et al. "Protein Secondary Structures in Water from Second-Derivative Amide I Infrared Spectra," *Biochemistry*, *29*:3303–3308 (1990).

[46] Dong, M. L., et al. "Accurate in situ measurement of complex refractive index and particle size in intralipid emulsions," *Journal of Biomedical Optics*, *18*(8):1–7 (2013).

[47] Drusch, S., et al. "Surface accumulation of milk proteins and milk protein hydrolysates at the air-water interface on a time-scale relevant for spray-drying," *Food Research International*, *47*(2):140–145 (2012).

[48] Drusch, S. and S. Mannino. "Patent-based review on industrial approaches for the microencapsulation of oils rich in polyunsaturated fatty acids," *Food Science and Technology*, *20*:237–244 (2009).

[49] Drusch, S., et al. "Microencapsulation of fish oil with n-octenylsuccinate-derivatised starch: Flow properties and oxidative stability," *European Journal of Lipid*, *108*:501–512 (2006).

[50] Einstein, A. "Über die von der molekularkinetischen Theorie der Wärme geforderte Bewegung von in ruhenden Flüssigkeiten suspendierten Teilchen," *Annalen der Physik*, *17*:549 (1905).

[51] Elversson, J. and A. Millqvist-Fureby. "In situ coating - An approach for particle modification and encapsulation of proteins during spray-drying," *International Journal of Pharmaceutics*, *323*:52–63 (2006).

[52] Fäldt, P. and B. Bergenstahl. "The surface composition of spray-dried protein-lactose powder," *Colloids and Surfaces A: Physicochemical and Engineering Aspects*, *90*(2-3):183–190 (1994).

[53] Fäldt, P. and B. Bergenstahl. "Fat Encapsulation in Spray-Dried Food Powders," *JAOCS*, *72*(2):171–176 (1995).

[54] Fäldt, P. and B. Bergenstahl. "Spray-dried whey protein/lactose/soybean oil emulsions. 1. Surface composition and particle structure," *Food Hydrocolloids*, *10*(4):421–429 (1996).

[55] Fäldt, P. and B. Bergenstahl. "Spray-dried whey protein/lactose/soybean oil emulsions. 2. Redispersability, wettability and particle structure," *Food Hydrocolloids*, *10*(4):431–439 (1996).

[56] Fäldt, P., et al. "The surface coverage of fat on food powders analyzed by ESCA (electron spectroscopy for chemical analysis)," *Food structure*, *12*:225–234 (1993).

[57] Fang, Y. and D. G. Dalgeish. "Dimensions adsorption on the surfaces of oil-in-water emulsions modified by lecithin," *Colloids and Surfaces, B*, *1*:357–364 (1993).

[58] Fisk, I. D. and D. A. Gray. "Soybean (*Glycine max.*) oil bodies and their associated phytochemicals," *Journal of Food Science, C: Food Chemistry*, *76*(9):1349–1354 (2011).

[59] Fisk, I. D., et al. "Entrapment of a volatile lipophilic aroma compound (D-limonene) in spray dried water-washed oil bodies naturally derived from sunflower seeds (*Helianthus annus*)," *Food Research International*, *54*:861–866 (2013).

[60] Frandsen, G. I., et al. "Oil bodies and their associated proteins, oleosin and caleosin," *Physicologia Planatarum*, *112*:301–307 (2001).

[61] Freudig, B., et al. "Dispersion of powders in liquid in a stirred vessel," *Chemical Engineering and Processing*, *38*:525–532 (1999).

[62] Frielinghaus, H. *Neutron scattering lectures of the JCNS Laborator Course held at Jülich*, chapter Nanostructure investigated by small angle neutron scattering, 1–43. Forschungszentrum Jülich, 2012.

[63] Gaiani, C., et al. "Surface composition of dairy powders observed by X-ray photoelectron spectroscopy and effects on their rehydration properties," *Colloids and Surfaces, B*, *49*:71–78 (2006).

[64] Garcia, J. M., et al. "Oil bodies and lipid synthesis in developing soybean seeds," *Phytochemistry*, *27*(10):3083–3087 (1988).

[65] Gaukel, V. and R. Bernewitz. *Emulgiertechnik: Grundlagen, Verfahren und Anwendungen*, chapter Tropfengroessenmessmethoden in der Emulgiertechnik, 56–87. Behr's Verlag, 2005.

[66] Gharsallaoui, A., et al. "Applications of spray-drying in microencapsulation of food ingredients: An overview," *Food Research International*, *40*:1107–1121 (2007).

[67] Goud, K., et al. "Recent Developments in Microencapsulation of Food Ingredients," *Drying Technology: An International Journal*, *23*:1361–1394 (2005).

[68] Goudappel, G. J. W., et al. "Measurement of Oil Droplet Size Distributions in Food Oil/Water Emulsions by Time Domain Pulsed Field Gradient NMR," *Journal of Colloid and Interface Science*, *239*:535–542 (2001).

[69] Gouin, S. "Microencapsulation: industrial appraisal of existing technologies and trends," *Trends in Food Science & Technology*, *15*:330–347 (2004).

[70] Gray, D. A., "Oil body extraction and uses," August 2012. WO 2012/110797 A1.

[71] Grillo, I. *Soft-matter Characterisation*, chapter Small-anlge neutron scattering and applications in soft condensed matter, 707–764. Springer, 2008.

[72] Guzey, D. and D. J. McClements. "Formation, stability and properties of multilayer emulsions for application in the food industry," *Advances in Colloid and Interface Science*, *128-130*:227–248 (2006).

[73] Hashimoto, A. and T. Kameoka. "Applications of Infrared Spectroscopy to Biochemical, Food, and Agricultural Processes," *Applied Spectroscopy Reviews*, *43*:416–451 (2008).

[74] Hebishy, E., et al. "Stability of Sub-Micron Oil-in-Water Emulsions Produced by Ultra High-Pressure Homogenization and Sodium Caseinate as Emulsifier." *AIDIC Conferences Serier11*. 161–170. 2013.

[75] Hede, P. D., et al. "Two-fluid spray atomisation and pneumatic nozzles for fluid bed coating/agglomeration purposes: A review," *Chemical Engineering Science*, *63*:3821–3842 (2008).

[76] Heertje, I., et al. "Observations on Emulsifiers at the Interface between Oil and Water by Confocal Scanning Light Microscopy," *Lebensmittel-Wissenschaft und-Technolologie*, *29*:217–226 (1996).

[77] Herman, E. M. "Immunogold-localization and synthesis of an oil-body membrane protein in developing soybean seeds," *Planta*, *172*:336–345 (1987).

[78] Hevonoja, T., et al. "Structure of low density lipoprotein (LDL) particles: Basis for understanding molecular changes in modified LDL," *Biochemica et Biophysica Ata*, *1488*:189–210 (2000).

[79] Hogan, S. A., et al. "Microencapsulating Properties of Sodium Caseinate," *Journal of Agricultural and Food Chemistry*, *49*:1934–1938 (2001).

[80] Horiba Instruments, Inc. "A Guidebook to Particle Analysis,". www.horiba.com/us/particle, 2012.

[81] Huang, A. H C. "Oil bodies and oleosin in seeds," *Annual Review of Plant Physiology and Plant Molecular Biology*, *43*:177–200 (1992).

[82] Huang, A. H C. "Oleosins and oil bodies in seeds and other organs," *Plant Physiol.*, *110*:1055–1061 (1996).

[83] Israelachvili, J. N. *Intermolecular and surface forces*. Academic Press Limited, London, 1992.

[84] Iwanaga, D., et al. "Stabilization of Soybean Oil Bodies Using Protective Pectin Coatings Formed by Electrostatic Deposition," *Journal of Agricultural and Food Chemistry*, *56*:2240–2245 (2008).

[85] Iwanaga, D., et al. "Extraction and Characterization of Oil Bodies from Soy Beans: A Natural Source of Pre-Emulsified Soybean Oil," *Journal of Agricultural and Food Chemistry*, *55*:8711–8716 (2007).

[86] Jacks, T. J., et al. "Isolation and Physicochemical Characterization of the Half-Unit Membranes of Oilseed Lipid Bodies," *JOACS*, *67*(6):353–361 (1990).

[87] Jackson, M. and H. H. Mantsch. "The use and misuse of FTIR spectroscopy in the determination of protein structure," *Critical reviews in biochemistry and molecular biology*, *30*(2):95–120 (1995).

[88] Jacrot, B. "The study of biological structures by neutron scattering from solution," *Reports on Progress in Physics*, *39*:911–953 (1976).

[89] Jafari, S. M., et al. "Encapsulation efficiency of food flavours and oils during spray drying," *Drying*, *26*:816–835 (2008).

[90] Jayasundera, M., et al. "Surface modification of spray dried food and emulsion powders with surface-active proteins: A review," *Journal of Food Engineering*, *93*:266–277 (2009).

[91] Jolivet, P., et al. "Protein Components of Low-Density Lipoproteins Purified from Hen Egg Yolk," *Journal of Agricultural and Food Chemistry*, *54*:4424–4429 (2006).

[92] Jolivet, P., et al. "Oil body proteins sequentially accumulated throughout seed development in *Brassica napus*," *Journal of Plant Physiology*, *168*:2015–2020 (2011).

[93] Jonasz, Mirsolaw. *Principles, methods and application of particle size analysis*, chapter Size, shape, composition, and structure of microparticles from light scattering, 143–162. Cambridge University Press, New York, 1991.

[94] Jones, J. R., et al. "Effect of processing variables and bulk composition on the surface composition of spray dried powders of a model food system," *Journal of Food Engineering*, *118*:19–30 (2013).

[95] Kaganer, V. M., et al. "Structure and phase-transitions in Langmuir monolayers," *Reviews of Modern Physics*, *71*:779–819 (1999).

[96] Kaiser, P. *Einführung die thermische Verfahrenstechnik*, chapter Trocknung fester Stoffe, 281–314. Walter de Gruyter & Co., 1997.

[97] Kapchie, V. N., et al. "Process Improvement for Semipurified Oleosomes on a Pilot-Plant Scale," *Journal of Food Science C: Food Chemistry*, *76*(6):853–860 (2011).

[98] Karkani, O. A., et al. "Effect of recovery methods on the oxidative and physical stability of oil body emulsions," *Food Chemistry*, *139*:640–648 (2013).

[99] Keck, C. M. *Cyclosporine Nanosuspensions: Optimised Size Characterisation & Oral Formulation*. PhD dissertation, Freie Universität Berlin, 2006.

[100] Kelly, R. N. and F. M. Etzler. *What is wrong with laser diffraction? A critical review of current laser diffraction methods for particle analysis*. Technical Report DIPA2000 Brochure, Donner Technologies, undated.

[101] Kennedy, J. F., et al. *Handbook of starch hydrolysis products and their derivates*, chapter Maltodextrins, 65–83. Springer-Science + Business Media Dordrecht, 1995.

[102] KeShun, L. *Soybeans as functional foods and ingredients*. PhD dissertation, University of Missouri, 2004.

[103] Kim, E. H.-J., et al. "Surface characterization of four industrial spray-dried dairy powders in relation to chemical composition, structure and wetting property," *Colloids and Surfaces B: Biointerfaces*, *26*:197–212 (2002).

[104] Kim, E. H.-J., et al. "On the Mechanisms of Surface Formation and the Surface Compositions of Industrial Milk Powders," *Drying Technology: An International Journal*, *21*(2):265–278 (2003).

[105] King, N. "Dispersibility and reconstitutability of dried milk," *Dairy science abstracts*, *28*(3):105–118 (1966).

[106] Kong, J. and S. Yu. "Fourier Transform Infrared Spectroscopic Analysis of Protein Secondary Structures," *Acta Biochimica et Biophysica Sinica*, *39*(8):549–559 (2007).

[107] Laboratory, ISIS Rutherford Appleton, "ISIS second target station project - Sans2d science Case." pdf file, 2014.

[108] Lacey, D. J., et al. "Secondary structure of oleosins in oil bodies isolated from seeds of safflower (*Carthamus tinctorius L.*) and sunflower (*Helianthus annuus L.*)," *Biochemical Journal*, *334*:469–477 (1998).

[109] Lee, G. *Rational Design of Stable Protein Formulations - Theory and Practice*, chapter Spray-drying of proteins, 135–158. Kluwer Academic/Plenum Press, New York, 2002.

[110] Leprince, O., et al. "Oleosins prevent oil-body coalescence during seed imbibition as suggested by a low-temperature scanning electron microscope study of desiccation-tolerant and -sensitive oilseeds," *Planta*, *204*:109–119 (1998).

[111] Levy, M. Y., et al. "Interactions of a non-ionic surfactant with mixed phospholipid-oleic acid monolayers," *Colloids and Surfaces*, *59*:225–241 (1991).

[112] Li, M., et al. "Expression and Characterization of the N-terminal Domain of an Oleosin Protein from Sunflower," *The Journal of Biological Chemistry*, *268*(23):17504–17512 (1993).

[113] Li, M., et al. "Purification and structural characterisation of the central hydrophobic domain of oleosin," *The Journal of Biological Chemistry*, *277*:37888–37895 (2002).

[114] Lopez-Rubioa, A. and E. P. Gilbert. "Neutron scattering: a natural tool for food science and technology research," *Food Science and Technology*, *20*:576–586 (2009).

[115] Maa, Y. F. and C. C. Hsu. "Effect of high shear on protein," *Biotechnology and Bioengineering*, *51*(4):458–465 (1996).

[116] Maa, Y. F., et al. "Spray-drying of air-liquid interface sensitive recombinant human growth hormone," *Journal of Pharmaceutical Sciences*, *87*(2):152–159 (1998).

[117] Madhu, A. N., et al. "Impact of Freeze and Spray Drying on the Retention of Probiotic Properties of Lactobacillus fermentum: An in vitro Evaluation Model," *International Journal of Microbiological Research*, *2*(3):243–251 (2011).

[118] Marquardt, D. W. "An algorithm for least-square estimation of nonlinear parameters," *Journal of the Society for Industrial and Applied Mathematics*, *11*:431–441 (1963).

[119] Masters, K. *Spray-Drying Handbook* (5th Edition). Longman Scientific & Technical, Essex, 1991.

[120] Masters, K. *Spray drying in Practice*. SprayDryConsult international ApS, Charlottenlund, 2002.

[121] Mauerer, A. *Secondary Structural Changes of Spray Dried Proteins with Fourier Transform Infrared Spectroscopy*. PhD dissertation, Friedrich-Alexander Universität Erlangen-Nürnberg, 2006.

[122] Maurer, S., et al. "The role of intact oleosin for stabilitzation and function of oleosomes," *The Journal of Physical Chemistry B*, *117*:13872–13883 (2013).

[123] Maury, M., et al. "Spray-drying of proteins: effects of sorbitol and trehalose on aggregation and FT-IR amide I spectrum of an immunoglobulin G," *European Journal of Pharmaceutics and Biopharmaceutics*, *59*:251–261 (2005).

[124] McClements, D. J. *Food Emulsion: Principles, Practice and Techniques*. CRC Press. Boca Raton, Florida, 1999.

[125] McClements, D. J. "Protein-stabilized emulsions," *Current Opinion in Colloid & Interface Science*, *9*:305–313 (2004).

[126] McMeekin, T. L., et al. *Amino Acids and Serum Proteins*, chapter Refractive Indices of Amino Acids, Proteins and Related Substances, 54–66. Advances in Chemistry Series; American Chemical Society, Washington D.C., 1964.

[127] Meerdink, G. and K. v. Riet. "Modelling segregation of solute material during drying of liquid foods," *AIChE Journal*, *41*(3):732–736 (1995).

[128] Meeteen, G. H. *The Measurement, Instrumentation, and Sensors: Handbook - VIII Optical Variables Measurement*, chapter Refractive Index Measurement, 61.1 – 61.4. Co-published by CRC press, Florida and Springer, Germany, 1999.

[129] Merkus, H. G. *Particle Size Measurements: Fundamentals, Practice, Quality*, chapter Particle Size, Size Distributions and Shape, 13–43. Springer Science + Buisiness Media B.V., 2009.

[130] Metcalf, H. J. and P. van der Straten. *Laser cooling and trapping*, chapter The dipole force, 123–136. Springer-Verlag New York Inc., 1999.

[131] Mie, G. "Beiträge zur Optik trüber Medien, speziell kolloidaler Metallösungen," *Annalen der Physik*, *330*(3):377–445 (1908).

[132] Millichip, M., et al. "Purification and characterization of oil-bodies (oleosomes) and oil-body boundary proteins (oleosins) from the developing cotyledons of sunflower (*Helianthus annuus L.*)," *Biochemistry*, *314*:333–337 (1996).

[133] Millqvist-Fureby, A., et al. *Food Emulsions and Foam*, chapter Surface activity at the air-water interface in relation to the surface composition of spray dried milk protein-stabilized emulsions, 236–246. London: Royal Society of Chemistry, 1999.

[134] Millqvist-Fureby, A. and P. Smith. "In-situ lecithination of dairy powders in spray-drying for confectionery applications," *Food Hydrocolloids*, *21*:920–927 (2007).

[135] Murray, B. S., et al. "Dilatational rheology of protein + nonionic surfactant films at air-water and oil-water interfaces," *Colloids and Surfaces*, *143*:211–219 (1998).

[136] Murrieta-Pazos, I., et al. "Food powders: Surface and form characterization revisited," *Journal of Food Engineering*, *112*:1–21 (2012).

[137] Nijdam, J. J. and T. A. G. Langrish. "The effect of surface composition on the functional properties of milk powders," *Journal of Food Engineering*, *77*(4):919–925 (2006).

[138] Nikiforidis, C. V., et al. "Exploitation of maize germ for the preparation of a stable oil-body nanoemulsion using a combined aqueous extraction - ultrafiltration method," *Food Hydrocolloids*, *25*:1122–1127 (2011).

[139] Nikiforidis, C. V. and V. Kiosseoglou. "Physicochemical Stability of Maize Germ Oil Body Emulsions As Influenced by Oil Body Surface-Xanthan Gum Interactions," *Journal of Agricultural and Food Chemistry*, *58*:527–532 (2010).

[140] Nikiforidis, C. V., et al. "Oil bodies: An insight on their microstructure - maize germ vs. sunflower seed," *Food Research International*, *52*:136–141 (2013).

[141] Norde, W. *Proteins at solid surfaces*, chapter Physical Chemistry of Biological Interfaces, 115–135. Marcel Dekker, Inc., New York, 2000.

[142] Nylander, T., et al. *Food Emulsifiers and Their Applications*, chapter Protein/Emulsifier Interactions, 89–171. Springer, 2008.

[143] Olivier, T. and B. Moine. *Optics in Instruments: Applications in Biology and Medicine*, chapter Confocal Laser Scanning Microscopy, –. John Wiley &. Sons, Inc., 2013.

[144] Pace, C. N. and M. Fisher. "Globular protein stability: Aspects of interest in protein turnover," *Acta Biologica Et Medica Germanica*, *40*:1385–1392 (1981).

[145] Partanen, R., et al. "Effect of Relative Humidity on Oxidation of Flaxseed Oil in Spray Dried Whey Protein Emulsions," *Journal of Agricultural and Food Chemistry*, *56*:5717–5722 (2008).

[146] Petelska, A. D. and Z. A. Figaszewski. "Interfacial tension of bilayer lipid membrane formed from phosphatidylethanolamine," *Biochimica et Biophysica Acta*, *1567*:79–86 (2002).

[147] Poth, U. *Ullmann's Encyclopedia of Industrial Chemistry*, *11*. Wiley-VCH Verlag GmbH & Co. KGaA, Weinheim, 2012.

[148] Prestrelski, S., et al. "Dehydration induced conformational transitions in proteins and their inhibition by stabilisers," *Biophysical Journal*, *65*:661–671 (1993).

[149] Princen, H. M. "Osmotic Pressure of Foams and Highly Concentrated Emulsions. 1. Theoretical Considerations," *Langmuir*, *2*:519–524 (1986).

[150] Privalov, P. L. and S. J. Gill. "Stability of protein structure and hydrophobic Interaction," *Advances in Protein Chemistry*, *39*:191–234 (1988).

[151] Purkrtova, Z., et al. "Structure and function of seed lipid body-associated proteins," *Comptes Rendus Biologies*, *331*:746–754 (2008).

[152] Pynn, R. *Neutron applications in eartch, energy and environmental sscience, neutron scattering, applications and techniques*, chapter Neutron scattering - A non-destructive microscope for seeing inside matter, 1–29. Springer Science + Buisiness Media, LLC, 2009.

[153] Rawle, A. *Basic Principles of Particle Size Analysis*. Technical Paper, Engima Business Park Grovewood Road Malvern Worcs, WR14 1XZ, U.K.: Malvern Instruments Limited, undated.

[154] Richards, F. M. "Areas, volume, packaging, and protein structure," *Annual Review of Biophysics and Bioengineering*, *6*:151–176 (1977).

[155] Risch, S. J. and G. A. Reineccius. "Spray dried orange oil - effect of emulsion size on flavor retention and shelf stability," *ACS Symposium Series*, *370*:67–77 (1988).

[156] Roux, E., et al. "Oleosins of *Arabidopsis thaliana*: Expression in *Escherichia coli*, Purification, and Functional Properties," *Journal of Agricultural and Food Chemistry*, *52*:5245–5249 (2004).

[157] Sanguansri, L. and M. A. Augustin. *Functional food product development*, chapter Microencapsualation of functional food development, 3–23. John Wiley &. Sons, Blackwell Publishing Ltd, 2010.

[158] Sankarikutty, B., et al. "Studies on microencapsulation of cardamon oil by spray-drying technique.," *Journal of Food Science and Technology*, *25*:352–355 (1988).

[159] Savitzky, A. and M. J. E. Golay. "Smoothing and Differentiation of Data by Simplified Least Squares Procedures," *Analytical Chemistry*, *36*(8):1627–1639 (1964).

[160] Schröder, J., et al. "Effect of Atomizer Geometry and Rheologic l Properties on Effervescent Atomization of Aqueous Polyvinylpyrrolidone Solutions." *ILASS - Europeean 2011, 24th European Conference on Liquid Atomization and Spray Systems, Estoril , Portugal, September 2011*. 2011.

[161] Schuchmann, H. P. *Emulgiertechnik: Grundlagen, Verfahren und Anwendungen*, chapter Grundlagen der Emulgiertechnik, 1–16. Behr's Verlag, 2005.

[162] Sessions, L.G. Alexander R. B., et al. "Characterization and modelling of the hydrophobic domain of a sunflower oleosin," *Planta*, *214*:546–551 (2002).

[163] Sheu, T.-Y. and M. Rosenberg. "Microencapsulation by Spray Drying Ethyl Caprylate in Whey Protein and Carbohydrate Wall Systems," *Journal of Food Science*, *60*(1):98–103 (1995).

[164] Shiga, H., et al. "Encapsulation of shiitake (*Lenthinus edodes*) flavors by spray drying," *Bioscience, Biotechnology, and Biochemistry*, *68*(1):66–71 (2004).

[165] Shimada, T. L. and I. Hara-Nishimura. "Oil-body-membrane proteins and their physiological functions in plants," *Biological & Pharmaceutical Bulletin*, *33*(3):360–363 (2010).

[166] Siloto, R. M. P., et al. "The accumulation of oleosins determines the size of seed oilbodies in Arabidopsis," *The Plant Cell*, *18*:1961–1974 (2006).

[167] Small, D., et al. "The adsorption of biological peptides and proteins at the oil/water interface. A potentially important but largely unexplored field," *Journal of Lipid Research*, *50*:329–334 (2009).

[168] Smoluchowski, M. "Zur kinetischen Theorie der Brownschen Molekularbewegung und der Suspensionen," *Annalen der Physik*, *326*:756–780 (1906).

[169] Soottitantawat, A., et al. "Structural analysis of spray-dried powders by confocal laser scanning microscopy," *Asia-pacific Journal Of Chemical Engineering*, *2*:41–46 (2007).

[170] Soottitantawat, A., et al. "Microencapsulation by Spray Drying: Influence of Emulsion Size on the Retention of Volatile Compounds," *Journal of Food Science*, *68*(7):2256–2262 (2003).

[171] Stojanovic, Z. and S. Markovic. "Determination of Particle Size Distributions by Laser Diffraction," *Technics - New Materials*, *21*:11–20 (2012).

[172] Surewicz, W. K., et al. "Determination of Protein Secondary Structure by Fourier Transform Infrared Spectroscopy: A Critical Assessment," *Biochemistry*, *32*(2):389–394 (1993).

[173] Susi, H. and D. M. Byler. "Resolution-Enhanced Fourier Transform Infrared Spectroscopy of Enzymes," *Methods in Enzymology*, *130*:290–311 (1986).

[174] Svergun, D. I. and M. H. J. Koch. "Small-angle scattering studies of biological macromolecules in solution," *Reports on Progress in Physics*, *66*:1735–1782 (2003).

[175] Tanford, C. *Physical Chemistry of Macromolecules*. John Wiley &. Sons, New York, 1967.

[176] Tesch, S., et al. "Stabilization of emulsions by OSA starches," *Journal of Food Engineering*, *54*(2):167–174 (2002).

[177] Ting, J. T. L., et al. "Oleosin genes in maize kernels having diverse oil contents constitutively expressed independent of oil contents - Size and shape of intracellular oil bodies are determined by the oleosins oils ratio," *Planta*, *199*:158–165 (1996).

[178] Towa, L. T. and V. N. Kapchie. "Pilot Plant Recovery of Soybean Oleosome Fractions by an Enzyme-Assisted Aqueous Process," *Journal of American Oil Chemists' Society*, *88*:733–741 (2011).

[179] Tripp, B. C., et al. "Adsorption of globular proteins at the air/water interface as measured via dynamic surface tension: concentration dependence, mass-transfer considerations, and adsorption kinetics," *Journal of Colloid and Interface Science*, *173*(1):16–27 (1995).

[180] Tzen, J. T. C. "Integral Proteins in Plant Oil Bodies," *International Scholary Research Network ISRN Botany*, *2012*:1–16 (2012).

[181] Tzen, J. T. C., et al. "Lipids, proteins, and structure of seed oil bodies from diverse species," *Plant Physiol.*, *101*:267–276 (1993).

[182] Tzen, J. T. C. and A. H. C. Huang. "Surface Structure and Properties of Plant Seed Oil Bodies," *The Journal of Cell Biology*, *117*(2):327–335 (1992).

[183] van Aken, G. A. and T. van Vliet. "Flow-Induced Coalescence in Protein-Stabilized Highly Concentrated Emulsions: Role of Shear-Resisting Connections between the Droplets," *Langmuir*, *18*:7364–7370 (2002).

[184] Vargo, K. B., et al. "Self-assembly of tunable protein suprastructures from recombinant oleosin," *Processdings of the National Academy of Sciences of the United States of America*, *109*(29):11657–11662 (2012).

[185] Vega, C. and Y. H. Roos. "Spray-Dried Dairy and Dairy-Like Emulsions - Compositional Considerations," *Journal of Dairy Science*, *89*(2):383–401 (2006).

[186] Verger, R., et al. "Action of phospholipase A at interfaces," *Journal of Biological Chemistry*, *248*(11):4023–4034 (1973).

[187] Wabel, C. *Influence of lecithin on structure and stability of parental emulsions*. PhD dissertation, Friedrich-Alexander-University, July 1998.

[188] Walton, D. E. and C. J. Mumford. "Spray Dried Products - Characterization Of Particle Morphology," *TransIChemE*, *77*:21–38 (1999).

[189] Walzel, P. "Liquid atomization," *International Chemical Engineering*, *33*(1):46–60 (Jan 1993).

[190] Wang, L., et al. "Analysis of Cyclone Collection Efficiency." *ASAE Annual International Meeting*, number 034114 in An ASAE Meeting Presentation, edited by food The Society for engineering in agricultural and biological systems. 1–10. 2003.

[191] Wang, S. and T. Langrish. "A review of process simulations and the use of additives in spray drying," *Food Research International*, *42*:13–25 (2009).

[192] Waschatko, G., et al. "Soy milk oleosome behaviour at the air-water interface," *Faraday Discussions*, *158*:157–169 (2012).

[193] Waschatko, G., et al. "Soybean oleosomes behavior at the air-water interface," *The Journal of Physical Chemistry B*, *116*:10832–10841 (2012).

[194] Webb, P. A. *A Primer on Particle Sizing by Static Laser Light Scattering*. Technical Workshop Series: Introduction to the Latest ANSI/ISO Standard for Laser Particle Size Analysis, Micromeritics Intrument Corp., January 2002.

[195] White, D. A., et al. "Sunflower-seed oil body emulsions: Rheology and stability assessment of a natural emulsion," *Food Hydrocolloids*, *22*:1224–1232 (2008).

[196] Wilde, P. J. and D. C. Clark. "The competitive displacement of β-lactoglobulin by Tween 20 from oil-water and air-water interfaces," *Journal of Colloid and Interface Science*, *155*:48–55 (1993).

[197] Wu, N., et al. "Stabilization of soybean oil body emulsions using *iota*-carrageenan: Effects of salt, thermal treatment and freeze-thaw cycling," *Food Hydrocolloids*, *28*:110–120 (2012).

[198] Wu, N., et al. "Stabilization of soybean oil body emulsions using kappa, gamma, lambda-carrageenan at different pH values," *Food Research International*, *44*:1059–1068 (2011).

[199] Xu, R. *Particle Characterization: Light Scattering Methods*, chapter Light Scattering, 56–110. Springer Netherlands, 2002.

[200] Yuliani, S., et al. "Application of microencapsulated flavor to extrusion product," *Food Reviews International*, *20*(2):163–185 (2004).

[201] Zeleny, L. and M. H. Neustadt. "Rapid determination of soybean-oil content and of iodine number of soybean oil," *U.S. Departement of Agricultural Bulletin, Washington D.C.*, *748*:1–23 (1940).